

THERMAL BARRIER COATING LIFE PREDICTION MODEL DEVELOPMENT FIRST ANNUAL REPORT

(NASA-CR-175087)	THERMAL BARRIER COATING	N86-22713
LIFE PREDICTION MODEL DEVELOPMENT	Annual	
Report (Pratt and Whitney Aircraft)	92 p	
HC A05/MF A01	CSSL 11G	Unclas
		G3/27 05923

By K.D. Sheffler and J.T. DeMasi

UNITED TECHNOLOGIES CORPORATION
Pratt & Whitney Group
Engineering Division

Prepared for
NATIONAL AERONAUTICS AND SPACE ADMINISTRATION

NASA LEWIS RESEARCH CENTER
21000 BROOKPARK ROAD
CLEVELAND, OHIO 44135

CONTRACT NAS3-23944



1. REPORT NO. CR-175087	2. GOVERNMENT AGENCY	3. RECIPIENT'S CATALOG NO.	
4. TITLE AND SUBTITLE Thermal Barrier Coating Life Prediction Model Development		5. REPORT DATE November 1985	
		6. PERFORMING ORG. CODE	
7. AUTHOR(S) Jeanine T. DeMasi, Kieth D. Sheffler		8. PERFORMING ORG. REPT. NO.	
9. PERFORMING ORG. NAME AND ADDRESS UNITED TECHNOLOGIES CORPORATION Pratt & Whitney Engineering Division		10. WORK UNIT NO.	
		11. CONTRACT OR GRANT NO. NAS3-23944	
12. SPONSORING AGENCY NAME AND ADDRESS National Aeronautics and Space Administration Lewis Research Center 21000 Brookpark Road, Cleveland, Ohio 44135		13. TYPE REPT./PERIOD COVERED Annual Report (First)	
		14. SPONSORING AGENCY CODE	
15. SUPPLEMENTARY NOTES Project Manager: Dr. Robert A. Miller NASA Lewis Research Center, Cleveland, Ohio			
16. ABSTRACT This report summarizes the activities performed during the first year of a two phase program aimed at developing a life prediction model for thermal barrier coatings. The objective of this program is to establish a methodology to predict thermal barrier coating life in an environment simulative of that experienced by gas turbine airfoils. Specifically, work is being conducted to determine failure modes of thermal barrier coatings in the aircraft engine environment. Analytical studies coupled with appropriate physical and mechanical property determinations are being employed to derive coating life prediction model(s) on the important failure mode(s). An initial review of experimental and flight service components indicates that the predominant mode of TBC failure involves thermomechanical spallation of the ceramic coating layer. This ceramic spallation involves the formation of a dominant crack in the ceramic coating parallel to and closely adjacent to the metal-ceramic interface. Initial results from a laboratory test program designed to study the influence of various "driving forces" such as temperature, thermal cycle frequency, environment, coating thickness, etc. on ceramic coating spalling life suggest that bond coat oxidation damage at the metal-ceramic interface contributes significantly to thermo-mechanical cracking in the ceramic layer. Low cycle rate furnace testing in air and in argon clearly shows a dramatic increase of spalling life in the non-oxidizing			
17. KEY WORDS (SUGGESTED BY AUTHOR(S)) Thermal Barrier Coating Failure Mechanisms Life Prediction		18. DISTRIBUTION STATEMENT PRECEDING PAGE BLANK NOT FILMED	
19. SECURITY CLASS THIS (REPT) Unclassified	20. SECURITY CLASS THIS (PAGE) Unclassified	21. NO. PGS	22. PRICE *

* For sale by the National Technical Information Service, Springfield, VA 22161

16. ABSTRACT (continued)

environment. At temperatures on the order of 2000°F or 2100°F, elevated temperature pre-exposure of TBC specimens in air causes a proportionate reduction of cyclic thermal spalling life, whereas pre-exposure in argon does not.

FOREWORD

The First Annual Report contained in this document covers the activities performed during the first year of the NASA HOST Program, "Thermal Barrier Coating Life Prediction Model Development", under Contract NAS3-23944. The objective of this effort is to develop and verify Thermal Barrier Coating life prediction technology for gas turbine hot section components. The NASA program manager is Dr. Robert A. Miller. The program is being conducted in the Pratt & Whitney Materials Engineering and Research Laboratory under the direction of Mr. H. Alan Hauser. The Pratt & Whitney Project Manager is Dr. Keith D. Sheffler and the principal investigator is Jeanine DeMasi. Mr. Frederick Kopper serves as the analytical manager and is directly responsible for analytical modeling efforts. A substantial portion of the modeling effort is being conducted under sub-contract at the Southwest Research Institute, San Antonio, Texas, under the direction of Dr. Thomas A. Cruse. Substantial program contributions in the areas of structural interpretation and test instrumentation were made by Mr. Neal P. Anderson, Mr. Merritt Wight, Mr. Russell Shenstone, Mr. Glenn Allen, and Mr. Kenneth Johnson. Special thanks to Mr. Raymond Skurzeuski, Mr. Claude Clavette, Mr. Frederick Wiese and Mr. Arnold LaPete for their efforts in specimen preparation and testing.

TABLE OF CONTENTS

<u>Section</u>	<u>Page</u>
FOREWORD	v
1.0 SUMMARY	1
2.0 INTRODUCTION	2
3.0 PHASE I - FAILURE MODES ANALYSES AND MODEL DEVELOPMENT	4
3.1 Task I - Failure Mechanism Determination	4
3.1.1 Task IA Experimental Design	6
3.1.2 Task IB.1 Conduct Critical Experiments	9
3.1.2.1 Furnace Exposure Tests	16
3.1.2.2 Cyclic Thermal Exposure Tests	29
3.1.2.3 Cyclic Hot Corrosion Testing	45
3.1.3 Task IB.2 Determine Physical/Mechanical Properties	57
3.1.3.1 Experimental Procedure for Physical Property Tests	60
3.1.4 Task IC Predominant Mode Determinations	62
3.1.4.1 Task IC. 1 Develop Preliminary Life Prediction System	63
3.1.4.2 Task IC. 2 Verification Tests	69
4.0 CONCLUSIONS	75
APPENDICES	
Appendix A Cyclic Burner Rig Test Details	76
Appendix B Corrosion Burner Rig Test	78
REFERENCES	80
DISTRIBUTION LIST	83

LIST OF ILLUSTRATIONS

<u>Figure</u>	<u>Title</u>	<u>Page</u>
1	Thermal Barrier Coating System Microstructure	5
2	Typical Thermal Barrier Coating Engine Failure Mode	12
3	Task I Test Plan to Evaluate Thermal Barrier Coating Failure Life	13
4	Burner Rig Coating Evaluation Specimen	14
5	Task I Furnace Exposure Test Plan to Evaluate Thermal Barrier Coating Static Failure Life	16
6	Task I Furnace Test Results; Weight Change Versus Cycles for 2100°F, Air, 10 Hour Cycle	19
7	Task I Furnace Test Results; Weight Change Versus Cycles for 2100°F, Air, 80 Hour Cycle	19
8	Task I Furnace Test Results; Weight Change Versus Cycles for 2100°F, Argon, 80 Hour Cycle	20
9	Task I Furnace Test Results; Weight Change Versus Cycles for 2200°F, Air, 10 Hour Cycle	21
10	Task I Furnace Test Results; Weight Change Verses Exposure Time for Fractional Exposure Test, 2100°F, Air, 15 Hour Cycle	21
11	X-Ray Diffraction Results of Furnace Exposed Test Specimens	25
12	Light Photomicrograph of Post-Test Microstructure. Furnace Exposure in Argon of 2100°F with 80 Hours Inspection Intervals. (1040 hrs/13 Cycles)	25
13	Light Photomicrograph of Post-Test Microstructure. Failed After Furnace Exposure in Air at 2100°F with 80 Hours Inspection Intervals. (240 hrs/3 cycles)	25
14	Light Photomicrograph of Post-Test Microstructure. Failed After Furnace Exposure in Air at 2100°F with 10 Hours Inspection Intervals. (160 hrs/16 cycles)	26
15	Light Photomicrograph of Post-Test Microstructure. Failed After Furnace Exposure in Air at 2200°F with 10 Hours Inspection Intervals. (60 hrs/6 cycles)	26
16	Light Photomicrograph of Post-Test Microstructure After Furnace Exposure in Air. (90 hrs/2100°F/1 cycle 60%)	27

LIST OF ILLUSTRATIONS (Continued)

<u>Figure</u>	<u>Title</u>	<u>Page</u>
17	Light Photomicrograph of Post-Test Microstructure After Fractional Furnace Exposure in Air (135 hrs/2100°F/1 cycle 90%)	27
18	Light Photomicrograph of Post-Test Microstructure After Fractional Exposure in Air (150 hrs/2100°F/150 hrs/1 Cycle)	28
19	Task I Clean Fuel Cyclic Burner Rig Test Program	29
20a	Light Photomicrograph of Baseline; Pre-Test Microstructures	35
20b	Light Photomicrograph of Baseline Microstructure, 2000°F/Short Cycle/Fast Heat-Up Rate, (Condition D2)	35
21a	Light Photomicrographs of Baseline Microstructure 2100°F/Short Cycle/Fast Heatup Rate(Condition D1) Pre-Test	36
21b	Light Photomicrographs of Baseline Microstructure 2100°F/Short Cycle/Fast Heatup Rate (Condition D1)Post-Test	36
22a	Light Photomicrograph of Pre-Burner Rig Test (D2) Microstructure Pre-Exposed Specimen (Air/2000°F/100 hrs)	37
22b	Light Photomicrograph of Post Burner Rig Test (D2) Microstructure for Pre-Exposed Specimen (2000°F/100hrs)	37
23a	Light Photomicrograph of Pre-Burner Rig Test (D1) Microstructure for Pre-Exposed Specimen (Air/2100°F/40hrs)	38
23b	Light Photomicrograph of Post-Burner Rig Test (D1) Microstructure for Pre-Exposed Specimen (Air/2100°F/40hrs)	38
24a	Light Photomicrograph of Pre-Burner Rig Test (D1) Microstructure for Pre-Exposed Specimen (Argon/2100°F/40 hrs)	39
24b	Light Photomicrograph of Post-Test Burner Rig Test (D1) Microstructure for Pre-Exposed Specimen (Argon, 2100°F/4hrs)	39
25a	Light Photomicrograph of Pre-Burner Rig Test (D2) Microstructure for Argon Pre-Exposed Specimen(Ar/2000°F/100 hrs)	40
25b	Light Photomicrograph of Post-Burner Rig Test (D2) Microstructure for Pre-Exposed Specimen (Ar/2000°F/100 hrs)	40
26a	Light Photomicrograph of Pre-Test Microstructures for Thin Specimen (D1) Test	41
26b	Light Photomicrograph of Post-Test Microstructures for Thin Specimens (D1) Test; 2100°F/Short Cycle/Fast Heatup	41

LIST OF ILLUSTRATIONS (Continued)

<u>Number</u>	<u>Title</u>	<u>Page</u>
27a	Light Photomicrograph of Pre-Test Microstructures for Thick Specimen (D1) Test	42
27b	Light Photomicrograph of Post-Test Microstructures for Thick Specimen (D1) Test; 2100°F/Short Cycle/Fast Heatup	42
28a	Light Photomicrograph of Pre-Test Microstructure for Thick Ceramic Specimen (D2) Test	43
28b	Light Photomicrograph of Post-Test Microstructure for Thick Ceramic Specimen (D2) Test; 2000°F/Short /Fast Heatup Rate	43
29a	Light Photomicrograph of Pre-Test Microstructure for Thin Ceramic Specimen (D2) Test	44
29b	Light Photomicrograph of Post-Test Microstructure for Thin Ceramic Specimen (D2) Test; 2000°F/Short Cycle/Fast Heatup Rate	44
30	Task I Hot Corrosion Test Program	45
31	Cyclic Hot Corrosion Test Specimen Showing Multi-level Flaking of the Ceramic	46
32a	Pre-Test Hot Corrosion Test Specimen; 35 ppm Artificial Sea Salt, 1650°F, 1 Hour Cycle	48
32b	Post-Test Hot Corrosion Test Specimen; 35 ppm Artificial Sea Salt, 1650°F, 1 Hour Cycle	48
33a	Pre-Test Hot Corrosion Test Specimen; 35 ppm Artificial Sea Salt, 1650°F, 1 Hour Cycle	49
33b	Post-Test Hot Corrosion Test Specimen; 35 ppm Artificial Sea Salt, 1650°F, 1 Hour Cycle	49
34	Cyclic Hot Corrosion Test Specimen Surface After 450 Hrs/ 1650°F - High Corrodent Level Test	50
35	Cyclic Hot Corrosion Test Specimen After 450 Hrs/1650°F High Corrodent Level Test in Area Near Failure	51
36	Cyclic Hot Corrosion Test Specimen After 1000 hrs at 1650°F	53
37	Light Photomicrograph of Test Specimen After 1000 hrs at 1650°F, Long Cycle, 10 ppm H_2SO_4 , 1.3% SO_3 Condition J	56
38	Bulk Four Point Bend Specimen Geometry Utilized for Determination of Elastic Constants, Stress Rupture, Creep, and Isothermal LCF Tests	58

LIST OF ILLUSTRATIONS (Continued)

<u>Number</u>	<u>Title</u>	<u>Page</u>
39	Thermal Conductivity Test Specimen	58
40	Thermal Expansion Test Specimen Geometry	58
41	Bulk Ceramic Microstructure Used for Physical/Mechanical Property Tests	59
42	Single Rotating, Internally-Cooled Tube Tests Specimen Geometry	64
43	Thermal Barrier Coating Thermal Analysis Mesh	64
44	Modified Thermal Barrier Coating Life Model	65
45	Finite Element Breakup	65
46	Results from Initial Marc Finite Element Heat Transfer Analysis Conducted on Test Specimen	66
47	Instrumented Test Specimen	67
48	D1 Cycle Thermocouple Data	69
49	D1 Test, Coated Specimen Temperature at Interface	70
50	D1 Test, Uncoated Specimen Surface Temperature	71
51	Cyclic Burner Rig Test at 2100°F, Short Cycle, Fast Heatup Rate (Condition D1) Data Match - Boundary Conditions in Marc Analysis	72
52	Cyclic Burner Rig Test at 2100°F, Short Cycle, Fast Heatup Rate (Condition D1) Data Match - Uncoated	73
53	Cyclic Burner Rig Test at 2100°F, Short Cycle, Fast Heatup Rate (Condition D1) Data Match - Coated Specimen	74
A-1	Diagram of Thermocoupled Specimen Used for Burner Rig Testing.	77
A-2	Schematic Diagram of Cyclic Burner Rig Test Apparatus for Task I	77
B-1	Schematic Diagram of Ducted Burner Rig Test Apparatus for Task I Hot Corrosion Exposure. Test specimens are enclosed to allow precise control of SO ₃ and other contaminants.	79

LIST OF TABLES

<u>Table</u>	<u>Title</u>	<u>Page</u>
I	Composition of Program Materials	4
II	Evaluated Engine Exposed PWA264 Coated Components	10
III	Metallic and Ceramic Powder Analysis	14
IV	Low Pressure Chamber Spray Conditions	15
V	Air Plasma Spray Conditions	15
VI	Inspection Interval for Task 1B Furnace Tests	16
VII	Summary of Air and Argon Furnace Exposure Test Results	18
VIII	Metallographic Evaluation Summary of Post-Test, Furnace Exposed Specimens	24
IX	X-Ray Diffraction Analysis of Some Representative Post-Test Burner Rig Specimens	32
X	Comparison of 2000°F and 2100°F Short Cycle Burner Rig Test Results	33
XI	Burner Rig (D2) Test Results: 2000°F/Short Cycle/Fast Heatup	33
XII	Burner Rig (D1) Test: 2100°F/Short Cycle/Fast Heatup	34
XIII	Cyclic Hot Corrosion Results (Test H); 1650°F/Long Cycle/ 35 ppm Artificial Sea Salt 1.3% 5O ₃	46
XIV	Artificial Sea Salt Composition	47
XV	X-Ray Diffraction Analyses of Some Representative Cyclic Hot Corrosion Post-Test Specimens (High Corrodent Level)	55
XVI	X-Ray Diffraction Analyses of Some Representative Cyclic Hot Corrosion Post-Test Specimens (Low Corrodent Level)	56
XVII	Coating Property Tests	57
XVIII	Thermal Conductivity of the Ceramic Coating	59
XIX	Specific Heat of the Ceramic Coating	60
XX	Thermal Expansion of the Ceramic Coating	60

1.0 SUMMARY

The goals of this program are to identify and understand TBC failure modes, generate quantitative TBC life data, and develop and verify a TBC life prediction model.

The coating being studied on this program is a two layer thermal barrier system incorporating a nominal ten mil outer layer of seven percent yttria partially stabilized zirconia plasma deposited over an inner layer of highly oxidation resistant low pressure plasma sprayed NiCoCrAlY bond coating. This coating, designated PWA264, currently is in flight service on turbine vane platforms in JT9D and PW2037 engines and is bill-of-material on turbine vane airfoils in the advanced PW4000 and IAE V2500 engines.

Effort currently is in progress on the first task of this program, which involves the identification and understanding of TBC failure modes. Five modes of coating damage are being considered in this study: 1) Thermomechanical ceramic failure, 2) Oxidative bond coat failure, 3) Hot corrosion, 4) Foreign Object Damage (FOD), and 5) Erosion.

An initial review of experimental and flight service components indicates that the predominant mode of TBC failure involves thermomechanical spallation of the ceramic coating layer. This ceramic spallation involves the formation of a dominant crack in the ceramic coating parallel to and closely adjacent to the metal-ceramic interface.

Initial results from a laboratory test program designed to study the influence of various "driving forces" such as temperature, thermal cycle frequency, environment, coating thickness, etc. on ceramic coating spalling life suggest that bond coat oxidation damage at the metal-ceramic interface contributes significantly to thermomechanical cracking in the ceramic layer. Low cycle rate furnace testing in air and in argon clearly shows a dramatic increase of spalling life in a non-oxidizing environment. Elevated temperature pre-exposure of TBC specimens in air causes a proportionate reduction of cyclic thermal spalling life, whereas pre-exposure in argon does not.

2.0 INTRODUCTION

Ceramic coatings have been utilized in aircraft gas turbine engines for over twenty years, primarily as an add-on technique to increase the durability of already reliable coatings. More recently, thermal barrier coating usage was extended to protect selected high pressure turbine components as well as combustors and augmentors. For these early turbine applications, no specific design methodology was needed, and coating lives (ceramic spalling resistance) were determined adequate (or not) based on experimental engine testing. Future applications for thermal barrier coatings, which emphasize performance improvement (as apposed to durability extension), will require more sophisticated design tools and lifetime prediction methods.

The objective of this program is to establish a methodology to predict thermal barrier coating life in an environment simulative of that experienced by gas turbine airfoils. Specifically, work is to be conducted to determine failure modes of thermal barrier coatings in the aircraft engine environment. Analytical studies coupled with appropriate physical and mechanical property determinations will be employed to derive coating life prediction model(s) for the important failure mode(s).

The program to accomplish these objectives is divided into two phases. Phase I (36 months) will be directed towards identification and modeling of the predominant failure mode(s), including verification. Phase II (24 months), which will proceed at the option of the government following the conclusion of Phase I, will develop and verify an integrated design capable life prediction model accounting for all important contributions to coating failure.

Phase I, which currently is in progress, includes the following three technical tasks, plus a fourth reporting task.

- o Task I - The objective of this task is to identify the relative importance of various TBC degradation and failure modes. Specific modes to be addressed include degradation resulting from static and cyclic thermal exposure and hot corrosion.
- o Task II - The objective of this task is to design, conduct and analyze experiments to obtain data for major mode life prediction model development. Design of the experiments will be based on results of Task I. Test parameters will be varied as appropriate to failure mode(s) being modeled to cover the range of parameters anticipated on thermal barrier coated turbine components. Transient thermal and stress analyses will be conducted for each test condition. The analytical results will be used to construct life prediction model(s) for the predominant mode(s).
- o Task III - The validity of models developed in Task II will be assessed through a series of approved benchmark engine mission simulation tests. The basis for judgment of model validity shall be how closely the model predicts TBC life for each benchmark engine simulation test. Recommendations for further research or refinement required to arrive at a fully satisfactory engine life prediction methodology shall be made if necessary.

Phase II, if exercised, will include the following five technical tasks, plus a sixth reporting task.

- o Task V - The objective of this task is to develop fracture and continuum mechanics life prediction models based on the design and performance of approved experiments to determine mechanical/material properties and analyze loads resulting from the coating deposition process and those that arise in service.
- o Task VI - The objective of this task is to develop oxidation and hot corrosion failure models both under steady state and simulated engine conditions. Mechanical property implications of bond coat oxidation shall be determined to permit incorporation of oxidation response into an integrated life prediction model. A semi-empirical hot-corrosion model will be developed to include effects of corrodent infiltration and the dilation pressure produced by phase changes of the corrodent during temperature cycling.
- o Task VII - The objective of this task is to design and conduct a series of experiments to develop a data base from which the erosion and foreign object damage models can be developed. Erosion test results will be extrapolated to construct a correlation model to predict TBC erosion life at typical operating conditions. The correlation shall include the velocity, temperature, erodent intensity, impingement angle and temperature-dependent ceramic properties. The degree to which the occurrence of an FOD incident reduces the life of the TBC will be predicted through development of a debit based life prediction model.
- o Task IX - The objective of this task is to integrate the appropriate combinations of models into a comprehensive, design capable, causal, life prediction model. This model shall incorporate the sub-models having the best predictive capability for each failure mode. A modular structural design shall be used in constructing the integrated model for flexibility and ease of incorporation in available thermal and structural computer programs. The integrated models developed and a test plan for their verification shall be subject to NASA Project Manager approval before initiating Task X.
- o Task X - The objective of this task shall be to verify the models proposed under simulated engine conditions including benchmark engine mission simulation tests. Based on these results a model or series of models will be recommended for adequate TBC life prediction as used in design engineering. The utility of the model shall be demonstrated by evaluating its applicability to design of a new hot section component. This demonstration will involve application of the model to an advanced turbine blade design to assess how overall life could be improved by the use of a TBC system. The blade design developed under NASA contract NAS3-23057 entitled "Preliminary Design of a Supersonic Aircraft High Pressure Turbine Program" shall be used. The study shall include the determination of the life fractions for each failure mode. Also, trade-off studies will be carried out to determine changes in the life distribution if the TBC was modified to eliminate certain failure modes.

3.0 PHASE I - FAILURE MODES ANALYSES AND MODEL DEVELOPMENT

The objectives of this phase are to identify thermal barrier coating degradation modes which lead to coating failure, to determine the relative importance of these degradation modes in aircraft engine applications, and to develop and verify life prediction model(s) for the predominant modes(s) of engine failure.

These objectives are being accomplished in three tasks. The objective of the first task is to identify and determine the relative importance of TBC failure modes, including development and verification of preliminary correlative life prediction model(s) for the predominant mode(s) of failure. The objective of the second task is to refine the model(s) developed in Task I, including generation of a substantial body of experimental failure data for model calibration. Additional data will be generated in the third task to verify the model(s) developed in Task II. A fourth reporting task also is included in Phase I of the program. Detailed discussion of effort in the first task, which currently is in progress, is included in the following sections.

The thermal barrier coating being evaluated in this program is designated PWA 264. It consists of an air plasma sprayed 7 w/o Y_2O_3 - partially stabilized ZrO_2 layer and a low pressure chamber sprayed metallic inner layer. The ceramic outer layer is nominally 0.010 \pm 0.002 inches thick, and is approximately 80% dense. The NiCoCrAlY inner layer is nominally fully dense and is 0.005 \pm 0.001 inches thick with appropriate surface roughness. The TBC coating system is shown in Figure 1. The substrate alloy being used for this program is PWA 1455. Its composition as well as the NiCoCrAlY bond coat composition is shown in Table I.

TABLE I
COMPOSITION OF PROGRAM MATERIALS
(Weight Percent)

	<u>Ni</u>	<u>Co</u>	<u>Cr</u>	<u>Al</u>	<u>Mo</u>	<u>Ta</u>	<u>Hf</u>	<u>Ti</u>	<u>B</u>	<u>C</u>	<u>Y</u>
PWA 1455	Remainder	10.0	8.0	6.0	6.0	4.25	1.15	1.0	0.015	0.1	-
PWA 1376	Remainder	22	18	12	-	-	-	-	-	-	0.4

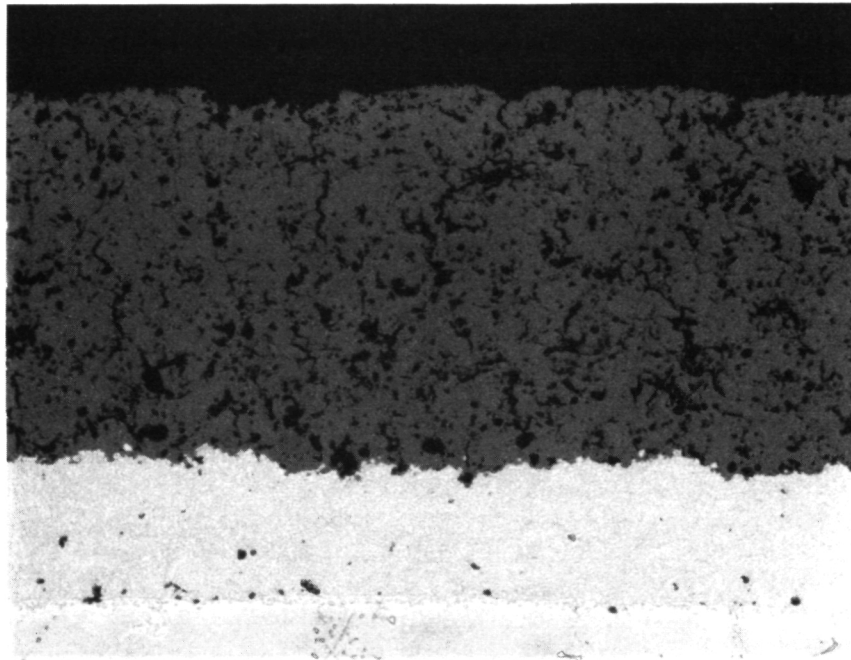
3.1 Task I - Failure Mechanism Determination

The objectives of this task are to identify thermal barrier coating degradation modes which lead to coating failure, to determine the relative importance of these modes in aircraft engine applications, and to develop and verify preliminary correlative life prediction model(s) for the predominant failure mode(s).

The approach to accomplish these objectives includes an initial review of the thermal barrier coating literature and of Pratt & Whitney engine experience with thermal barrier coated turbine components to identify potential modes of thermal barrier coating degradation and to determine which of these modes appear to predominate in engine service. This review has been completed,

ORIGINAL PAGE IS
OF POOR QUALITY

and results have been used to establish a laboratory simulative engine test program which currently is in progress. Results of this test program will be used to critically assess the relative importance of various degradation modes as they relate to coating service life, and to develop and calibrate a preliminary correlative life prediction model. This effort will be followed by additional laboratory testing to verify the preliminary model and to provide a basis for model refinement in Task II.



Pre-Test

200X

Figure 1 Thermal Barrier Coating System Microstructure

3.1.1 Task IA- Experimental Design

The objectives of this subtask, which has been completed, were to review the TBC literature and Pratt & Whitney experience with thermal barrier coated turbine components, and based on this review, to establish an experimental program to determine the relative importance of various TBC degradation mechanisms as they relate to coating service life.

Early work on thermal barrier coatings describes numerous material and process developments, and identifies several potential degradation and failure modes (Refs. 1-14). These modes include thermomechanically induced structural failure of the ceramic coating layer, oxidative degradation of the underlying metallic bond coating, thermochemically (hot corrosion) induced ceramic degradation, foreign object damage (FOD), and erosion.

Examination of experimental and flight serviced engine components indicates the first of these degradation modes to be the predominant cause of coating failure, resulting in spallation of the ceramic coating layer due to formation of a dominant crack in the ceramic parallel and adjacent to the metal-ceramic interface (Figure 2). Laboratory test results reported in the literature suggest that this thermomechanical spallation mode is accelerated by time/temperature dependent interfacial oxidation of the metallic bond coat (Refs. 15-16). The examination of engine exposed components indicates that hot corrosion, FOD, and erosion do not represent life-limiting modes of degradation in engine service. Based on these observations, an experimental program was designed to separately assess and quantify the relative contributions of mechanical and oxidation degradation to TBC failure. While hot corrosion was not identified as a major failure mode in commercial engine service, experimental tests were included in the program to identify the threshold contaminant level for corrosion damage, thus providing a basis for prediction of flight environments where this degradation mode might be important. Details of findings from the literature and engine component review and of the experimental program designed to assess critical mode importance, are provided in the following paragraphs.

In reviewing the available literature, laboratory data and engine hardware, there was general agreement that the major TBC failure mode is thermomechanical ceramic coating spallation due to dominant crack propagation parallel to but not coincident with the ceramic-metal interface. Crack driving forces are presumed due to thermal expansion differences between the ceramic and metal components of the system, with the coefficient of thermal expansion of the ceramic being significantly lower than that of the underlying metallic system. It is also hypothesized that the stresses resulting from thermal expansion mismatch during thermal cycling are augmented by oxidation of the NiCoCrAlY bond coat, which has an irregular roughened surface topology (Refs. 15, 16, 17, 18). Miller and Lowell (see Ref. 15) were the first to discuss the role of the irregular bond coat/ceramic interface on oxidation related failure. A preliminary thermal barrier coating oxidation/thermal stress life prediction model has been proposed by Miller (see Ref. 18).

Despite the observation that the predominant thermal barrier coating failure mode involves thermomechanical spalling, resulting from thermal cycle induced stresses, some laboratory evidence exists to indicate a time and environmental dependence of the mechanical failure mode. Early evidence of time dependence was provided by McDonald & Hendricks (Ref. 19), who showed, at least for some compositions, a substantial decrease in the number of thermal cycles caused ceramic spallation failure as cycle duration increased from 7 minutes to 60 minutes. Similar results have been obtained at Pratt & Whitney. Gedwill (Ref. 20) confirmed this effect with a more durable coating of similar composition. Miller & Lowell (see Ref. 15) postulated time dependent changes of "stress free temperature," resulting from time dependent bond coat flow, as being responsible at least in part for interaction between thermal exposure and thermal cycling effects, but also noted that exposure in an oxidizing atmosphere was much more damaging than exposure on a non-oxidizing environment. Early results from Pratt & Whitney also indicate a cyclic life reduction for both oxidizing and non-oxidizing pre-exposure, with the oxidizing atmosphere being much more deleterious.

Andersson (Ref. 21) analyzed the stresses of typical thermal barrier coated heat engine components and found that the stresses are tensile in directions parallel to metal-ceramic interface for elevated temperature steady state operating conditions and during the cool down portion of the cycle, and in tangential compression during the heatup portion of the cycle.

The stresses induced in coatings are hypothesized to be dependent not only on material properties but also heat flux or degree of thermal loading. The latter was addressed by Miller and Berndt (Ref. 22). They reported that "good" $ZrO_2-8 Y_2O_3$ coatings have remarkable tolerance to an extremely high heat flux plasma torch test.

The geometry of the component and the coating thickness are also important life variables. For thinner coatings (≈ 5 mils) the stresses due to temperature gradients in the coating have been shown to be less severe so that increased service life can be expected (Ref. 23). Normal stresses are introduced in the coating of a curved surface by the tangential compressive stresses present resulting in ceramic spallation. In coated airfoil applications this is seen at the leading and trailing edges where the convex radii of curvature are minimized.

Ceramic thermal stability is an important characteristic effecting coating life. Thermal stability refers to the ability of ceramic layer to endure prolonged high temperature exposure without the occurrence of damaging morphological, chemical, or phase changes. Ceramic sintering is a thermally activated processes which can also limit cycle life. However, it has not been observed in laboratory/engine testing. Phase studies have determined that the presence of large amounts of monoclinic phase correlate to poor performing coatings (Refs. 24,25,26 also Ref 8).

Room temperature x-ray diffraction studies of 7YSZ coatings indicate a two phase structure consisting primarily of the cubic and metastable tetragonal phases together with 0 to 5% monoclinic. Because of the extremely rapid cooling rates associated with deposition of the ceramic coating layer, the tetragonal phase formed in the coating contains a relatively high percentage of Y_2O_3 , and is not readily transformed to monoclinic. With prolonged exposure at elevated temperature in the cubic plus tetragonal phase field, yttrium diffusion occurs and the high Y_2O_3 tetragonal phase transforms to cubic plus low Y_2O_3 tetragonal, with the low Y_2O_3 tetragonal phase being readily transformed to monoclinic upon cooling (Refs. 24, 25, see also Ref. 27).

Stecura (28) studied TBC systems and hypothesized that compositional changes in various bond coats and substrates play a more important role in coating durability than does the coefficient of thermal expansion of the substrate material. It was hypothesized that yttrium, aluminum and chromium in the bond coat critically affect the TBC life. Aluminum, chromium and yttrium oxides are formed at the interface during thermal testing. Yttrium diffuses toward the bond coat-ceramic interface, chromium diffuses towards the substrate and molybdenum into the bond coat. These events are considered to have an adverse effect on coating life. It has been shown that yttria in the bond coat moves coating failure location from the bond coat-substrate interface to just above the ceramic bond coat interface (see Ref. 16). It is hypothesized that the location of major crack initiation, whether within the bond coat oxide layer or in the ceramic, is dependent on the stress state at the roughened interface which is at the very least changed by oxide growth.

Other degradation modes noted in several studies include secondary failure modes i.e., hot corrosion, erosion, FOD. Results from several laboratories (Refs. 29-34), have demonstrated an apparent susceptibility of thermal barrier coatings to failure in hot corrosion environments. The responsible mechanism appears to involve infiltration of the porous ceramic with liquid corrodent deposited on the coating surface at intermediate exposure temperatures, and subsequent "mechanical" spalling resulting from alternate freezing and thawing of the infiltrated corrodent (see Refs. 34,32,30,14).

Some evidence has been reported which supports "thermochemical" ceramic spallation in hot corrosion environments; i.e., the infiltrated (Na_2SO_4) reacts with the ceramic at high SO_3 pressures (Refs. 35,36, also Refs. 34,30), resulting in destabilization of ZrO_2 . This degradation is attributed to acid leaching of yttrium from the ceramic.

Thermal barrier coating degradation and failure modes and mechanisms observed in prior Pratt & Whitney laboratory tests were found to be in general agreement with analysis from the literature. The major mode of failure in PWA264 is spallation of the ceramic layer resulting from in-plane cracking adjacent to but not coincident with the metal ceramic interface. Prior or concurrent bond coat oxidation appears to play a major role in cyclic thermal stress induced spallation cracking. The Task IB testing is designed to identify the relative importance of these two degradation modes and to provide the quantitative data required to develop a preliminary model which will predict spalling life under varying exposure conditions.

While the Task IA study included reviews of TBC literature and prior laboratory experience, primary emphasis was placed on the evaluation of failure mode as observed on ground based experimental engine and field service exposed components. Engine exposed PWA 264 coated parts have been evaluated from the commercial engines; JT9D-7R4G2, -7R4D -7R4D1, 7R4E1, 7R4H and PW2037, and the military engines; F-100, ATEGG (F-100) and TF-30. Details of the reviewed parts are documented in Table II. Where available, components representing the unexposed coating in each of the engine exposed components also have been examined to identify changes which occurred in coating structure during engine test. Significant observations from this review of engine exposed components are as follows:

- a) Ceramic sintering was not observed in any case
- b) Oxidation of the low pressure chamber sprayed PWA276 bond coat contributed to coating failure to a lesser degree than as seen in the laboratory
- c) Coating failure due to oxidation of substandard, air plasma sprayed bond coat was a major life limiting factor found in PW2037 first vane platform
- d) Geometry effects were considered to play a significant role in coating degradation.

Examination of numerous engine tested components indicates that thermal barrier failures are almost exclusively of the "thermomechanical" type shown in Figure 2. In only one case has engine component thermal barrier coating failure been attributable directly to bond coat oxidation alone. That particular failure occurred on a vane airfoil which was operated under unusually severe thermal conditions and was, for reasons of processing convenience, coated with an air sprayed bond coat.

3.1.2 Task IB. 1 Conduct Critical Experiments

The objective of this subtask is to conduct a series of critical experiments and tests designed in Task IA to determine the relative importance of various thermomechanical and thermochemical coating degradation modes. Failure life data from these tests also will be used to develop a preliminary life prediction model in Task IC. The test program includes clean fuel and salted burner rig tests as well as static furnace testing of thermal barrier coated specimens to establish the relative importance of thermal stress cycling versus thermal and thermochemical degradation in determining thermal barrier coating life. The overall Task I test plan is shown in Figure 3.

The specimen to be used for all static and cyclic exposure testing in this task is illustrated in Figure 4. For cyclic burner rig testing, this specimen is thermal barrier coated on all surfaces except for the butt end, where coating is optional but not required. For static furnace exposure testing, the application of a tapered coating to only the cylindrical portion of the bar was employed to minimize the possibility of premature coating failure at the edge of the ceramic layer.

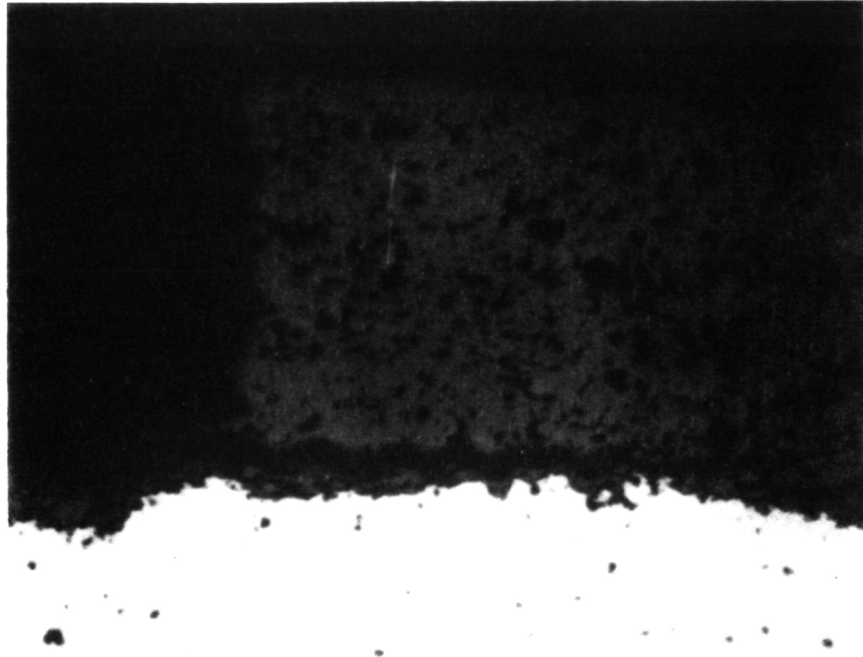
Prior to use in this task, all raw materials were thoroughly characterized and tested to ensure acceptability. Table III presents ceramic and metallic powder analysis which include: chemistry, particle size distribution and x-ray diffraction results.

Table II
EVALUATED ENGINE EXPOSED PWA 264 COATED COMPONENTS

Date	Engine Type	Part Name	Engine #	Operator	Material	Remarks
12/02/83	2037	1st Vane Paired Platform	X-666-1C	P&W	647/264 modified bond coat	265.89 hrs/1500 cycles endurance testing. APS/LPCS bond coat - APS severely oxidized. Spalling at A.P.S. - LPCS bond coat interface. Ceramic thick in some areas.
09/01/82	2037	1st Vane platform N/C	X-664-1A			36.97 hrs/136 cycles endurance testing. Limited spallation of the ceramic on O.D. T.E., ceramic microstructure meets specifications.
09/01/82	2037	1st Vane platform N/C	X-664-1A			36.97 hrs/136 endurance. Limited spallation of the ceramic on O.D. T.E., ceramic microstructure meets specifications.
01/10/84	2037	1st Vane Paired platform	X-662-6			Ceramic Spallation on ID platform bond coat oxidation of the A.P.S. layer.
05/10/84	2034	1st Turbine Vane platform	X-671-5		647/264	485 cycles limited ceramic spallation. Ceramic structure meets specification.
10/25/82	TF30	2nd Vane	P-559-4 1B		633/264	1000 F.H./2171 A/B squirts. Ceramic thickness; 16-20 mils. Spallation around most of C.V. side of airfoil, C.C. L.E. In plane cracking. Metal bond coat has thin oxide layer ceramic microstructure meets specifications.
10/25/82	TF30	2nd Vane	P-559-4 1B	P&W (FAA)	633/264	1000 F.H./2171 A/B squirts. Spallation at L.E.
01/17/83	F-100 (ATEGG)	1st Vane	P-686-2		1422/264	910 TAC cycles/53.7 hot time. Spallation at I.D. L.E. only; due to specimen geometry and thermal cycling stress. Coating structure meets specifications. Bond coat has very thin oxide layer.
01/17/83	F-100 (ATEGG)	1st Blade	P-686-2		1422/264	910 TAC cycles/53.7 hot time. Spallation at I.D. L.E. only due to specimen geometry and Thermal cycling stress. Coating microstructure meets specifications. Bond coat has very thin oxide layer.
05/18/83	F100	1st Vane	-		1480/264 modified bond coat	2000 TAC cycles ceramic spalled L.E.; bond coat failures.
04/20/82	JT9D-7R4D	1st Vane platform	X-491-45	P&W	647/264	246.9 hrs/1500 cycles spalled after engine run. Spalling location - corners of platforms. Ceramic structure meets specifications. Very thin oxide layer/thin Beta depleted zone. Some segmentation and in plane cracking in ceramic. *(Rec'd vacuum H.T./1975°F F/4 hrs.)

TABLE II
EVALUATED ENGINE EXPOSED PWA264 COATED COMPONENTS

Date	Engine Type	Part Name	Engine #	Operator	Material	Remarks
04/20/82	JT9D-7R4D	1st Vane platform	X-491-45	P&W	647/264	246.9 hrs/1500 cycles spalled after engine run. Spallation location - corners of platforms. Ceramic structure meets specifications. Some segmentation and in plane cracking in ceramic. Ceramic Thickness 16-18 mils. *rs.)
04/21/82	JT9D-7R4D	1st Vane platform	X-491-45			Ceramic not distressed after engine run. Ceramic structure meets specifications (Rec'd Ar H.T./1975°F/4hrs). Ceramic thickness 8 mils.
04/19/82	JT9D-7R4G2	Wide Chord 1st Vane Platform	X-579-29			FAA 1000 cycle Test (Bond Coat - A.P.S./L.P.C.S.) A.P.S. portion is severely oxidized. In plane cracking of the ceramic. Ceramic structure meets specification.
05/82	JT9D-7R4G2	Wide Chord 1st Vane Platform	X-579-29A			114 hrs./19 cycles, substantial spallation on OD/ID. Good ceramic porosity but layered in - plane cracking. Spallation due to oxidizable inclusions; ZrCN ₂ (Starck #5399 + Union Carbide 1365-1).
01/12/83	2037	1st Vane (Paired) Platform	X-666-1C			265.89 hrs/1500 cycles endurance testing. Limited spallation on O.D. T.E. and I.D.L.E. due to F.O.D. - (not apparent from microstructure). Spallation adjacent to areas where ceramic thickness 7 mils. Some in plane cracking. A.P.S./L.P.C.S. bond layer-thick A.P.S. 5 mils. Microstructure adjacent to spalled areas was acceptable.
01/07/83	2037	1st Vane Paired platform/airfoil coated also	X-667-1A		647/264 (modified bond coat)	325.3 hrs/1500 cycles endurance testing. Spallation on O.D.T.E. and I.D.L.E. (A.P.S./L.P.C. - bond coat) also hidden pressure airfoil. Metallic thickness specifications not met. Spallation - chipping documented as FOD. Some areas of thick ceramic.
01/12/83	2037	1st Vane Paired platform/airfoil coated also	X-667-1A			325.3 hrs/1500 cycles endurance testing. Spallation on O.D.T.E. and I.D.L.E. (A.P.S./L.P.C. - bond coat) also hidden pressure airfoil. Metallic thickness specifications not met. Spallation - chipping documented as FOD. Some areas of thick ceramic. Note: Layer of engine debris
09/06/83	2037	1st Vane Paired platform/airfoil coated also	X-667-1A,B 2,3, X-670-2A			593.6 hrs/1947 cycles endurance testing. Spallation limited but did occur in bond coat at APS/LPCS bond coat interface due to bond coat oxidation. Some in plane cracking some cracking at bond coat - ceramic interface also ceramic thick in some areas. O.D., I.D., T.E. hidden pressure airfoil. FOD.
04/11/84	JT9D-7R4E1	1st Vane Platform	716102	Airbus A-310	264	2355 hrs/411 cycles coating looks excellent.
04/13/84	JT9D-7R4D	1st Vane Platform	709643	TW	264	227 hrs/868 cycles coating looks excellent.
5/1/85	JT9D-7R4D	1st Vane	708603	SR	264	9300 hrs/2328 cycles coating looks excellent.
10/25/85	JT9D-7R4D1	1st Vane Platform	707714	SR	264	4978 hrs/4109 cycles coating looks excellent.



200X

Figure 2 Typical Thermal Barrier Coating Engine Failure Mode

T E M P E R T U R E	E X P O S U R E	S T A T I C				C Y C L I C				F R A C T I O N A L E X P O S U R E					
		F U R N A C E		B U R N E R R I G		F U R N A C E		B U R N E R R I G		F U R N A C E		B U R N E R R I G			
		OXIDIZING	NON-OXIDIZING	OXIDIZING	HOT CORROSION	OXIDIZING	NON-OXIDIZING	OXIDIZING	HOT CORROSION	OXIDIZING	NON-OXIDIZING	OXIDIZING	HOT CORROSION		
		CYCLE LENGTH	HEATING RATE	CORRODENT LEVEL	SHORT	LONG	SHORT	LONG	SHORT	LONG	SHORT	LONG	SHORT	LONG	
			F A S T	L O W	H I G H	F A S T	L O W	H I G H	F A S T	L O W	H I G H	F A S T	L O W	H I G H	
1650															
2000															
2100		A ₁	A ₂												
2200		B													

CYCLIC OXIDATION BURNER RIG TEST SPECIMEN SET FOR CONDITIONS D1, D2, E & F-12 SPECIMENS PER TEST

4 10 MIL VIRGIN CERAMIC ("BASELINE" COATING)

2 5 MIL VIRGIN CERAMIC

2 15 MIL VIRGIN CERAMIC

2 10 MIL AIR PRE-EXPOSED FOR APPROXIMATELY 1/2 ESTIMATED BURNER RIG HOT TIME LIFE

2 10 MIL Ar PRE-EXPOSED FOR APPROXIMATELY 1/2 ESTIMATED BURNER RIG HOT TIME LIFE

CYCLE LENGTH

SHORT: 6 MINUTE CYCLE = 4 MINUTES IN THE FLAME + 2 MINUTES FORCE AIR COOLED

LONG: 60 MINUTE CYCLE = 57 MINUTES IN THE FLAME + 3 MINUTES FORCE AIR COOLED

CYCLE RATE

FAST: NOMINAL 60 SECOND HEAT-UP TO MAXIMUM TEMPERATURE

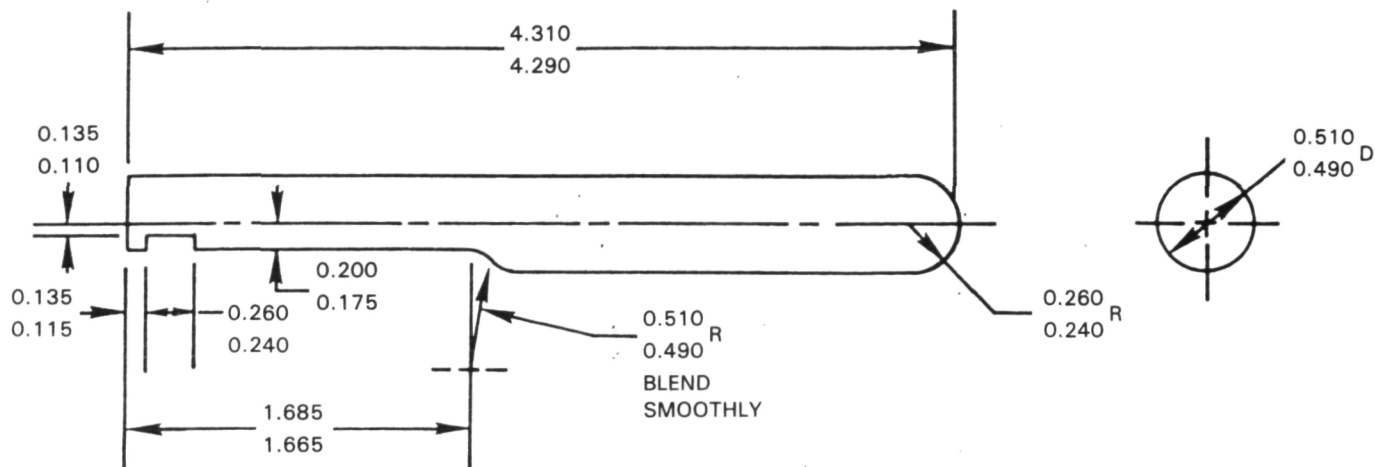
SLOW: NOMINAL 180 SECOND HEAT-UP TO MAXIMUM TEMPERATURE

CORRODENT LEVEL

LOW: 10 PPM % SYNTHETIC SEA SALT

HIGH: 35 PPM % SYNTHETIC SEA SALT

Figure 3 Task I Test Plan to Evaluate Thermal Barrier Coating Failure Life



All Dimensions Shown In Inches

Figure 4 Burner Rig Coating Evaluation Specimen

TABLE III
METALLIC AND CERAMIC POWDER ANALYSIS

Material	Chemical Analysis	Particle Size Analysis	
		Cumulative % Finer	Microns
NiCoCrAlY (Alloy Metals Lot #6192)	21.60 w/o Co	100%	176
	17.50 w/o Cr	100%	125
	13.00 w/o Al	100%	88
	0.66 w/o Y	100%	62
	Bal. - Ni	93%	44
		72.2%	31
		41.5%	22
		21.9%	16
		11.8%	11
		5.5%	7.8
		.2.3	5.5
		0.7%	3.9
		0.0%	2.8
7 w/o Y ₂ O ₃ - ZrO ₂ (Zircoa Lot #30656)	7.2 w/o Y ₂ O ₃	100%	176
	1.7 w/o HfO ₂	94.7%	125
	0.1 w/o CaO	86.1%	88
	0.2 w/o TiO ₂	63.7%	62
	0.1 w/o Fe ₂ O ₃	39.4%	44
	0.3 w/o Al ₂ O ₃	29.0%	31
	Bal. -ZrO ₂	11.8%	22
		5.3%	16
		2.7%	11
		1.3%	7.8
		0.5%	5.5
		0.5%	3.9
		0%	2.8

X-RD Results
80-85 v/o fcc ZrO₂
20-15 v/o monoclinic
ZrO₂

Following raw material qualification, all burner rig standard erosion bars used in Task I testing were LPCS with NiCoCrAlY metallic bond coat (AMI #6192). Low pressure chamber spray conditions and parameters are presented in Table IV. Sample tip sections were taken from selected specimens from each batch of bars for verification of thickness and microstructure.

The test bars were air plasma sprayed with $ZrO_2-7w/o Y_2O_3$. Air plasma spray deposition parameters are given in Table V. A statistical program designed to randomize coating sequence, and hence any uncontrolled variability of deposition parameters, was used to coat and select test bars.

To document uniformity of structure, a pre-test sample was obtained from every specimen tested in this program. Selected samples (about 10%) were examined metallographically using a statistically designed selection plan. The balance of the samples are available for metallographic examination if needed.

TABLE IV
LOW PRESSURE CHAMBER SPRAY CONDITIONS

Standard erosion bar specimens coated using a Electroplasma High Energy Gun.

Gun Voltage (V)	58
Gun Current (A)	1500
Standoff (in.)	15
Workpiece Temperature	1500-1700°F

Helium and Argon arc gases used

TABLE V
AIR PLASMA SPRAY CONDITIONS

Standard erosion bar specimens coated using a Plasmadyne SG-100 Gun.


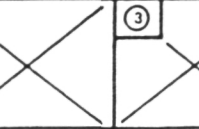
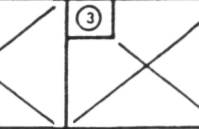
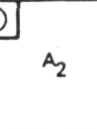
Gun Voltage (V)	42
Gun Current (A)	900
Standoff (in.)	3
Workpiece Temperature	500°F

Helium and Argon arc gases used.

3.1.2.1 Furnace Exposure Tests

Tests were performed to determine the influence of static thermal exposure on TBC degradation and failure. Specimens were furnace exposed for various times of less than 1000 hours in various combinations of oxidizing and non-oxidizing environments and at a minimum of two (2) temperatures, as described below.

As shown in Figure 5, a partial factorial experiment was conducted to study the effects of time, temperature, and environment on static coating failure. Baseline tests designated "A" were conducted at an intermediate temperature (on the order of 2100°F) in oxidizing and non-oxidizing environments. These tests involved furnace exposure of a minimum of two thermal barrier coated specimens per test condition for times sufficient to cause failure of the ceramic coating or a maximum of 1000 hours. Failure in this context is defined as development of "delamination" cracking over a significant area. In order to observe delamination damage, specimens were infrequently cycled to room temperature. Cycle frequency/inspection interval is presented in Table VI.

TEMPERATURE	OXIDIZING ATMOSPHERE		NON-OXIDIZING ATMOSPHERE	
	STATIC FAILURE	FRACTIONAL EXPOSURE	STATIC FAILURE	FRACTIONAL EXPOSURE
HIGH 2200	① B	② 	③ 	④ 
INTERMEDIATE 2100	⑤ A ₁	⑥ C	⑦ A ₂	⑧ 

MINIMUM OF TWO (2) COUPONS PER BLOCK

TEST CONDITIONS SHOWN THUS:  NOT TO BE EVALUATED

Figure 5 Task I Furnace Exposure Test Plan to Evaluate Thermal Barrier Coating Static Failure Life

TABLE VI
INSPECTION INTERVAL FOR TASK IB FURNACE TESTS

<u>Test Code</u>	<u>Condition</u>	<u>Inspection Interval</u>
A1.A	2100°F/Air	10 hrs.
A1.B	2100°F/Air	80 hrs.
A2	2100°F/Argon	80 hrs.
B	2200°F/Air	10 hrs.

Examination involved visual observation to look for areas of delaminated ceramic. To determine the influence of temperature on static coating failure life in air, an additional furnace exposure test designated "B" was conducted at a higher temperature, on the order of 2200°F. To evaluate progressive damage accumulation, a fractional exposure test designated "C" was conducted in the oxidizing environment at the intermediate test temperature. This fractional exposure test involved metallographic examination of specimens successively removed at approximate decile fractions of the "static failure" life as defined in the corresponding "A" test. The primary goal of the examination was to find evidence of incipient delamination cracking; in addition, specimens were examined to determine oxide scale growth at the interface between the metal and ceramic coating layers and beta phase depletion in the metallic coating layer.

All planned furnace exposure tests have been completed and a summary of the results is presented in Table VII. The results showed that all specimen failures occurred upon cool-down initiating at the tip area where there is a radius change. Weight gain measurements were made at each inspection interval for every specimen; these measurements are plotted in Figures 6-10. Although the tapered coating scheme prevented premature coating failure, the design allowed for exposed substrate; thus the weight gain data will give only a rough indication of the amount of oxide accumulated.

Ceramic spallation is clearly influenced by the temperature, exposure environment and shock frequency. The results show that thermal exposure in Ar does not cause coating failure for an extended period of time. The Argon environment significantly reduces the weight gain (oxidation) rate as compared to an air environment so that exposure time and cycle life increase dramatically without causing ceramic spallation.

For furnace exposure conducted in air, frequent thermal cycling seems to slightly decrease the total exposure time to failure. This is demonstrated in the 2100°F air tests with 10 hour and 80 hour inspection intervals. A possible explanation is that the additional stresses imposed on the system due to oxidation of the bond coat eventually become too great to be accommodated by the strain tolerant microstructure of the ceramic, leading to earlier failure upon cool-down.

The high temperature (2200°F in air) furnace exposure results show a significant decrease in TBC life. This life decrease presumably results from larger thermal stresses due to an increased ΔT through the ceramic upon cooling, coupled with the additional stresses associated with more rapid bond-coat oxide development.

Thermal exposure effects including oxidation, beta (NiAl) depletion, bond coat substrate interdiffusion, ceramic structure, and ceramic phase distribution currently are being studied. Microprobe analysis is being conducted to analyze any time dependent chemical changes occurring in the substrate-bond coat-ceramic system. X-ray diffraction results have been conducted for representative furnace exposed specimens and the results are presented in Figure 11.

TABLE VII
SUMMARY OF AIR AND ARGON FURNACE EXPOSURE TEST RESULTS

<u>Specimen I.D. #</u>	<u>Code/Condition</u>	<u>Exposure Time/(hrs) # of Cycles</u>	<u>Results</u>	<u>Metallographic Observations</u>
TP07 TP08	A1.A/Air-2100°F (10 hr inspection)	140/14 160/16	Failed	Major crack just above interface within ceramic oxide layer
TP01 TP02	A1.B/Air-2100°F (80 hr inspection)	240/3 160/2	Failed	Major crack just above interface within ceramic
TP05 TP06	A2/Ar-2100°F (80 hr. inspection)	1040/13	No Failures	Incipient cracking near interface noted
TP03 TP04	B/Air-2200°F (10 hr inspection)	40/4 60/6	Failed	Major crack just above interface within ceramic
TP16	C/Air-2100°F Fractional	90/1	No Failures	(60%)No major cracking; some incipient cracking near the ceramic oxide interface
TP19	C/Air-2100°F Fractional	135/1	No Failures	
TP20	C/Air-2100°F Fractional	150/1	No Failures	Incipient failure observed at suspected bond coat defect; Major cracking extending from "blister" through aligned Kirkendall voids
TP21	C/Air-2100°F Fractional	165/1	Failed	Major cracking/delamination
TP22	C/Air-2100°F Fractional	180/1	Failed	Major cracking/delamination
TP23	C/Air-2100°F (10hr inspection)	120/12	Failed	Incipient cracking at the tip
TP24	C/Air-2100°F (10hr inspection)	150/15	Failed	Major cracking with some delamination at tip

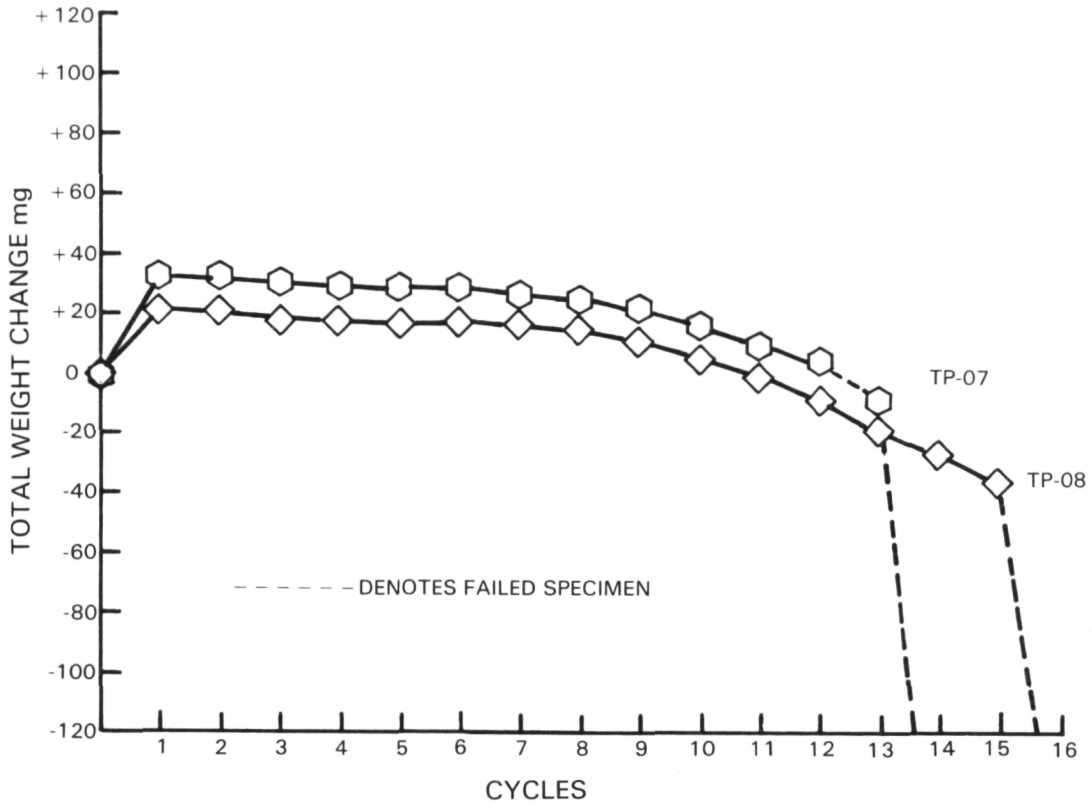


Figure 6 Task I Furnace Test Results; Weight Change Versus Cycles for 2100°F, Air, 10 Hour Cycle

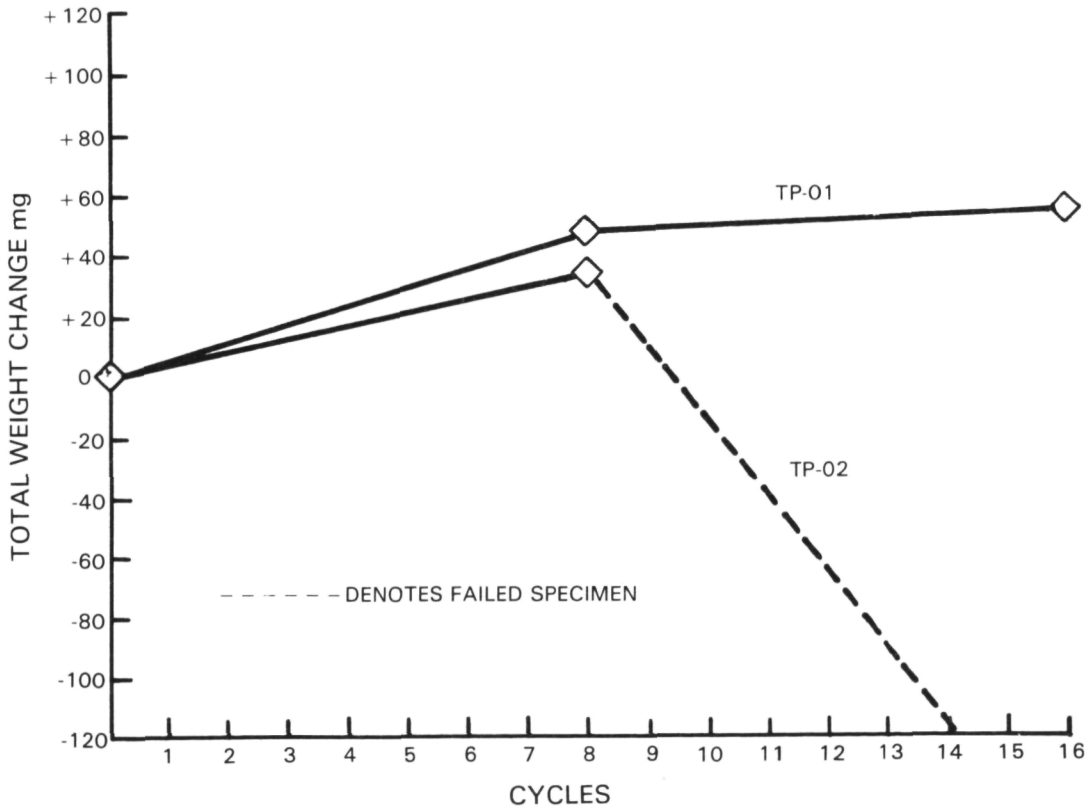


Figure 7 Task I Furnace Test Results; Weight Change Versus Cycles for 2100°F, Air, 80 Hour Cycle

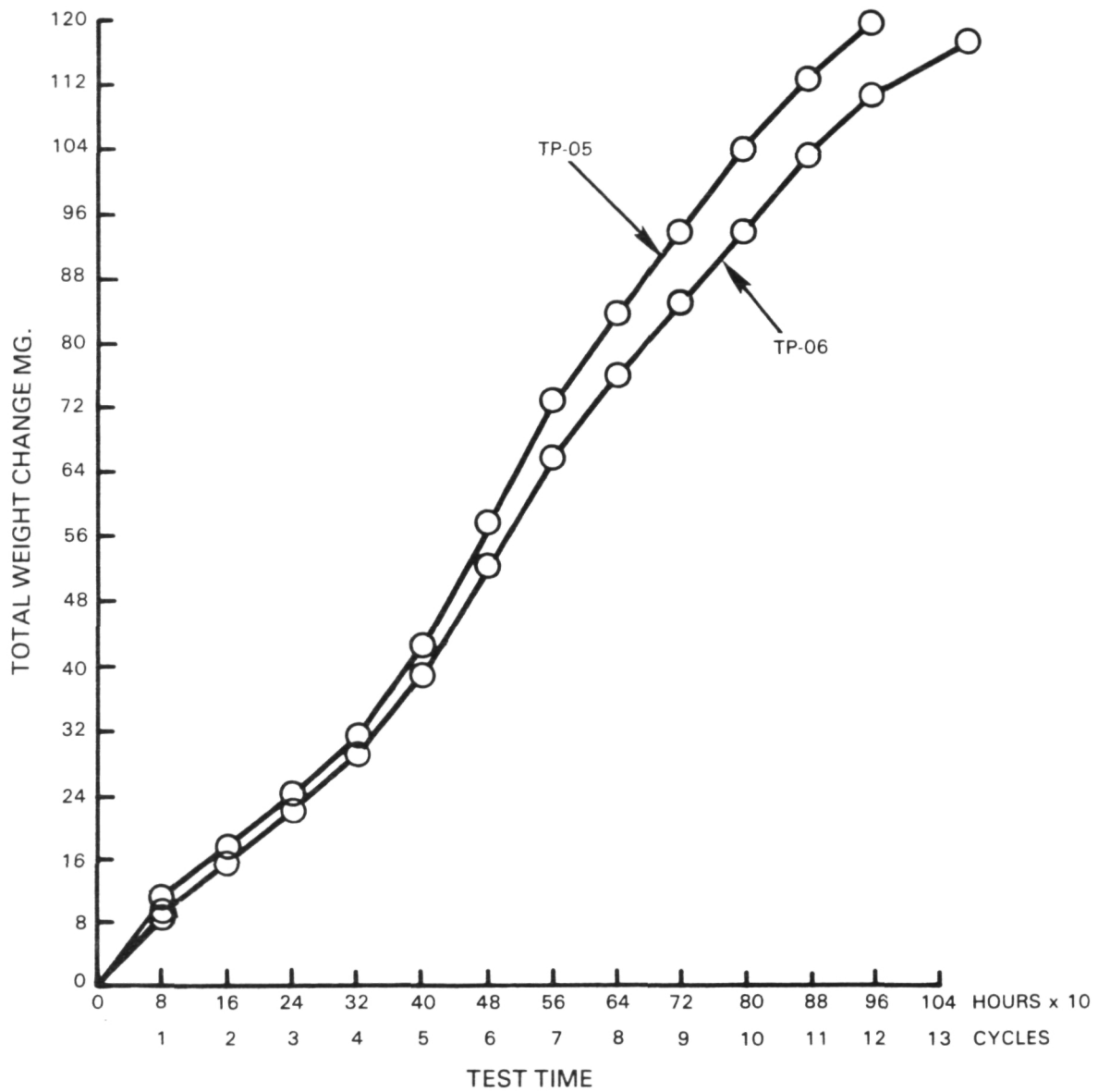


Figure 8 Task I Furnace Test Results; Weight Change Versus Cycles for 2100°F, Argon, 80 Hour Cycle

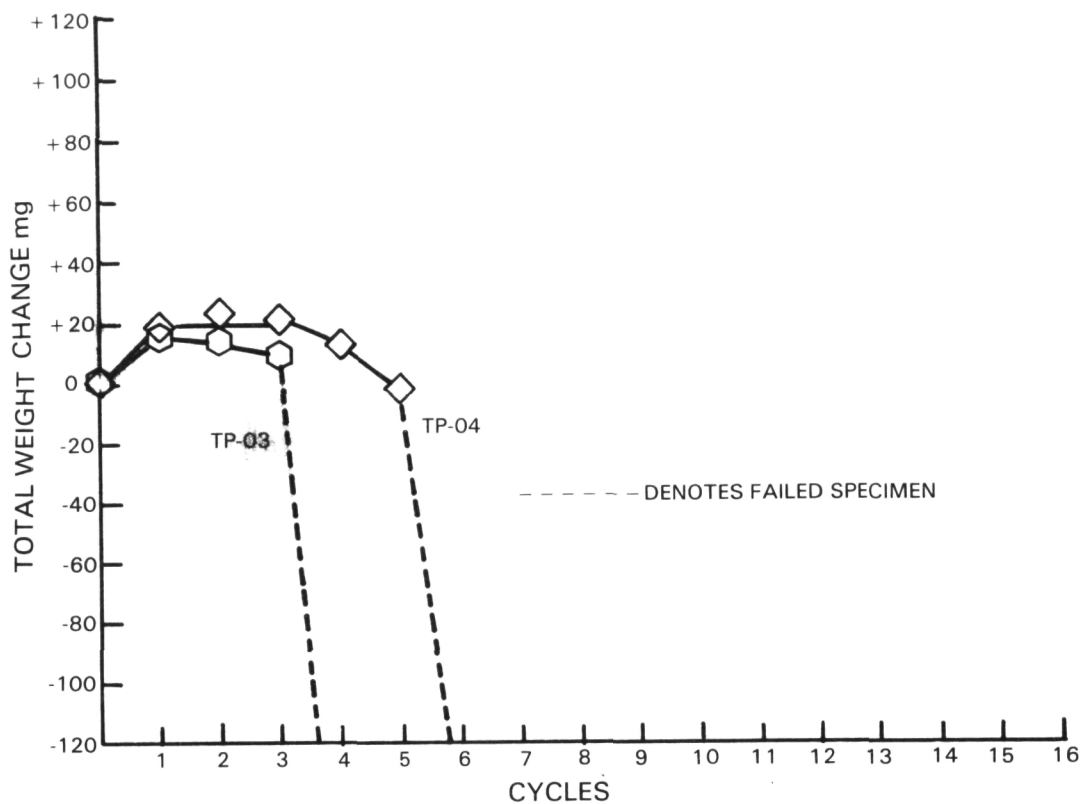


Figure 9 Task I Furnace Test Results; Weight Change Versus Cycles for 2200°F, Air, 10 Hour Cycle

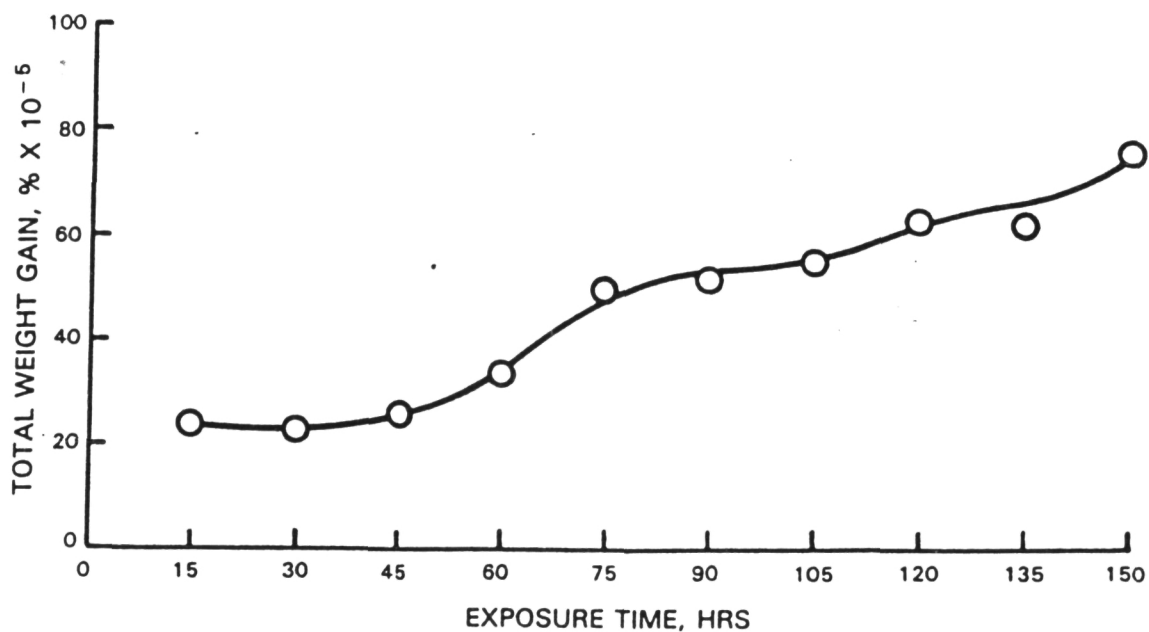


Figure 10 Task I Furnace Test Results; Weight Change Verses Exposure Time for Fractional Exposure Test, 2100°F, Air, 15 Hour Cycle

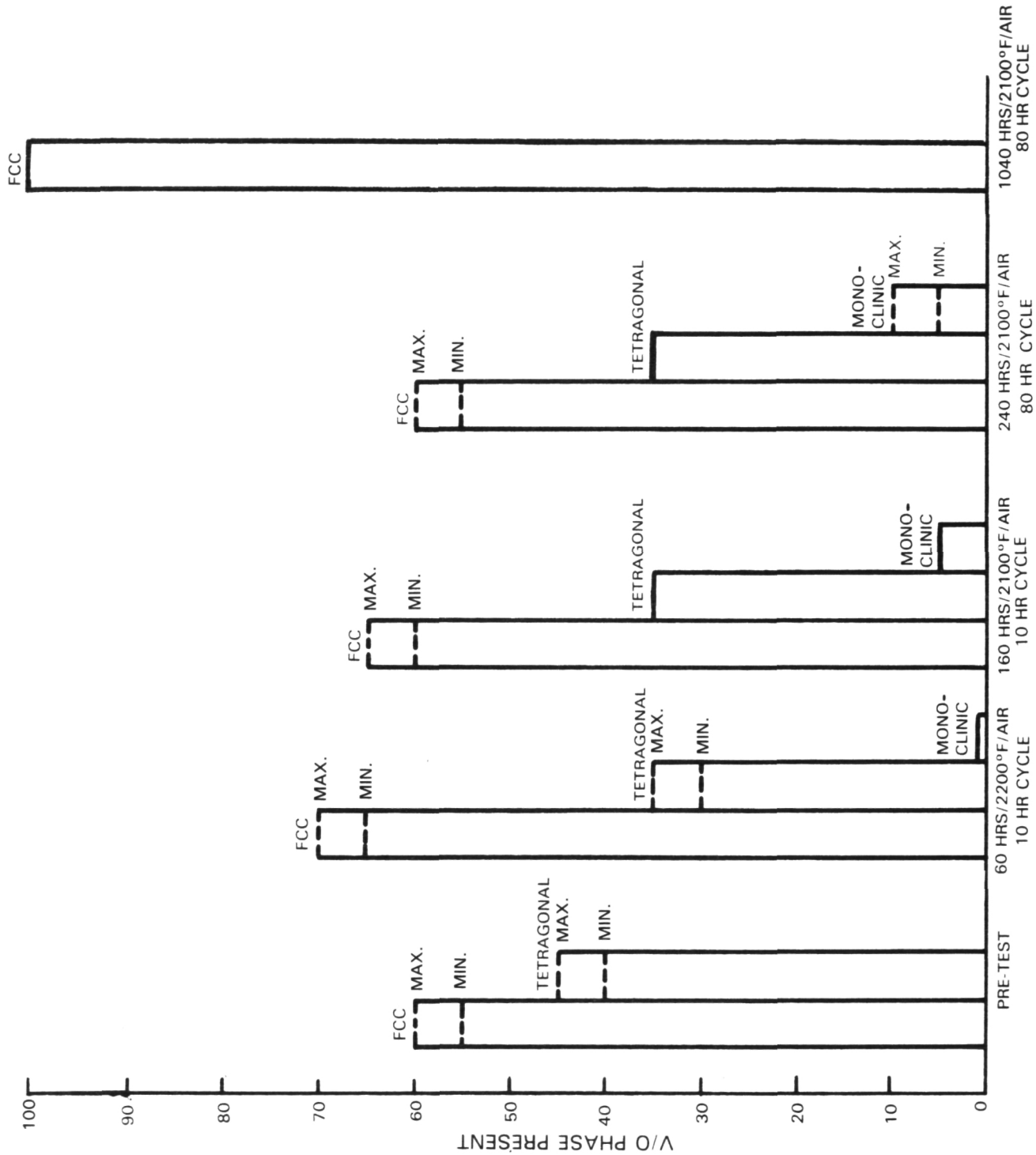


Figure 11 X-Ray Diffraction Results of Furnace Exposed Test Specimens

In the air exposed specimens, the v/o of monoclinic ZrO_2 increases with increasing exposure time. In individual comparisons between these tested specimens and the pre-test specimen, there is an apparent decrease in the tetragonal phase which accompanies the increase in the monoclinic phase and a slight increase in the FCC phase, suggesting that existing metastable tetragonal phase is undergoing transformation. In looking at the two specimens tested at 2100°F (different cycle lengths; 80 hrs. and 10 hrs.), one failing at 160 hours and the other at 240 hours, there appears to be not only an increase in the v/o monoclinic phase with time but an associated decrease in the v/o FCC phase and no change in the v/o tetragonal phase with increasing time.

Homogenization resulting from heat treatment may have resulted in an increase in both the low Y_2O_3 transformable tetragonal and the high Y_2O_3 cubic phase. Upon cooling, the transformable tetragonal then would transform to the monoclinic phase, while the cubic phase is retained. X-ray diffraction analysis of the Ar exposed specimen revealed 100% FCC ZrO_2 . This result suggests that the phase changes occurring can be controlled by the heat treat atmosphere (Reference 37).

Table VIII presents a summary of the metallographic evaluation of selected post-test furnace exposed specimens which are shown in Figures 12-18. Thermal barrier coating failure was observed to be associated with increased time at temperature which resulted in increased beta depletion, average oxide thickness, interdiffusion zone width and average void size. An increase in Kirkendall void population is seen with the high exposure temperature. Although thermal exposure in Argon did not result in TBC failure, the microstructure shown in Figure 12 reveals major crack formation or pullout due to weakening of that area at the typical failure site.

Figures 16 and 17 represent the "fractional" exposure test specimen microstructures after exposure for 60% and 90% of the total exposure time. These specimens were cycled once upon removal from the furnace and show less microcracking than the cycled specimens. Figure 18 shows the post-test specimen microstructure in cross-section through the blister after exposure for 100% of the total test time and after 150 hrs. It is highly probable that this was caused by an initial bond coat defect.

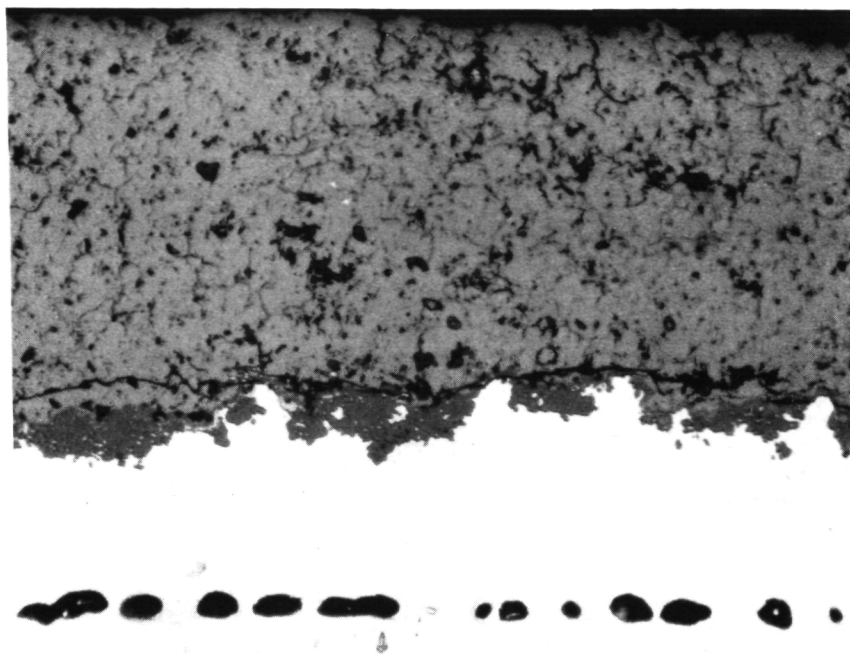
Two additional specimens were tested at 2100°F in air for 165 hours and 180 hours with one thermal cycle achieved upon removal from the furnace. Both of these specimens showed ceramic distress. A "cyclic" fractional exposure test was conducted where test time was 150 hrs at 2100°F with 10 hour inspection intervals. As noted in Table VII, cracking occurred at the tip location for the 80% (120 hrs) specimen and major cracking and delamination was observed for the 100% (150 hrs) specimen. These observations along with the incipient cracking noted for other specimens at fractions of total test life may suggest that an accumulated damage or progressive failure mode exists, at least for lower stress level testing; i.e., conditions where thermal transients are not severe.

Analysis of the completed test results will continue as necessary to further understanding of TBC failure mechanism as related to life prediction.

TABLE VIII
METALLOGRAPHIC EVALUATION OF SELECTED FURNACE EXPOSURE SPECIMENS AFTER EXPOSURE

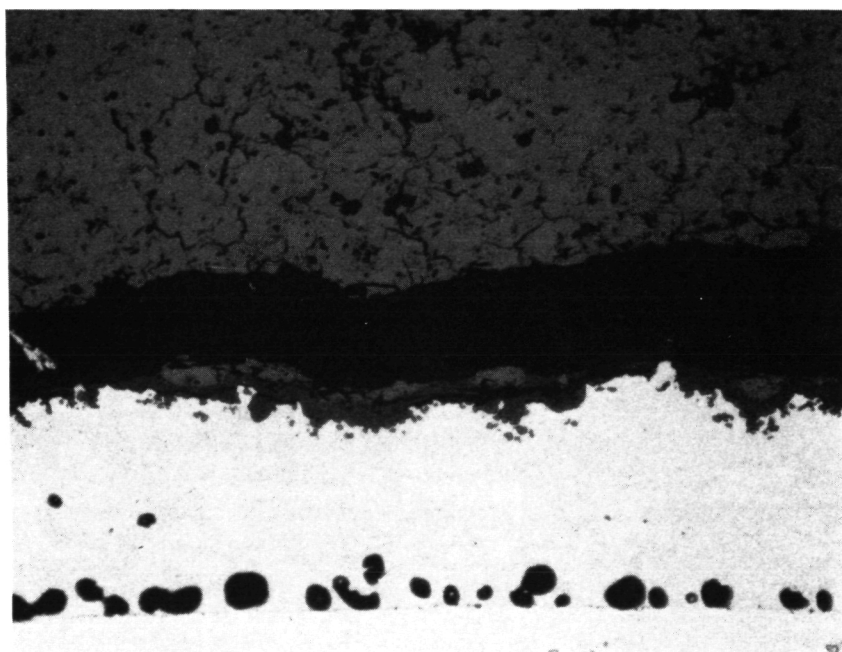
Specimen I.D.#	Test Code/ Conditions	Average Oxide Thickness(mils)	Beta (NiAl) Depletion	Interdiffusion Zone (mils)	Average Void Width (Mils)
TP01	A1.A/240 hrs in Air 2100°F/3 80 hr. inspections	0.25 - 0.50	100%	4	0.50 - 1.00
TP08	A1.B/160 hrs in Air 2100°F/16 10 hr. inspections	0.25 - 0.50	100%	3	0.50
TP05	A2/1040 hrs. in Ar 2100°F/13 80 hr. inspections	1.0 - 1.25 *very irregular discontinuous	100%	7	0.75 - 100
TP04	B/60 hrs Air 2200°F/6 10 hr. inspection	0.25	Overall 60 - 70% 40-50 depleted MCrAlY to ceramic 10-25% depleted MCrAlY to substrate interface	4.5 - 5.0	0.50 - 0.75 *void population is high
TP16	C/90 hrs. in Air 2100°F 60%	0.25 - 0.50	Overall 80 - 100% 60 - 70% depleted MCrAlY to ceramic interface 10-20% depleted MCrAlY to substrate interface	2.5 - 3	0.25 - 0.75
TP19	C/135 hrs. in Air 2100°F 90%	0.25 - 0.50	100%	2.5 - 3.0	0.25 - 0.50
TP20	C/150 hrs. in Air 2100°F	0.25	100%	2.5 - 3.0	0.25 - 0.50

ORIGINAL PAGE IS
OF POOR QUALITY



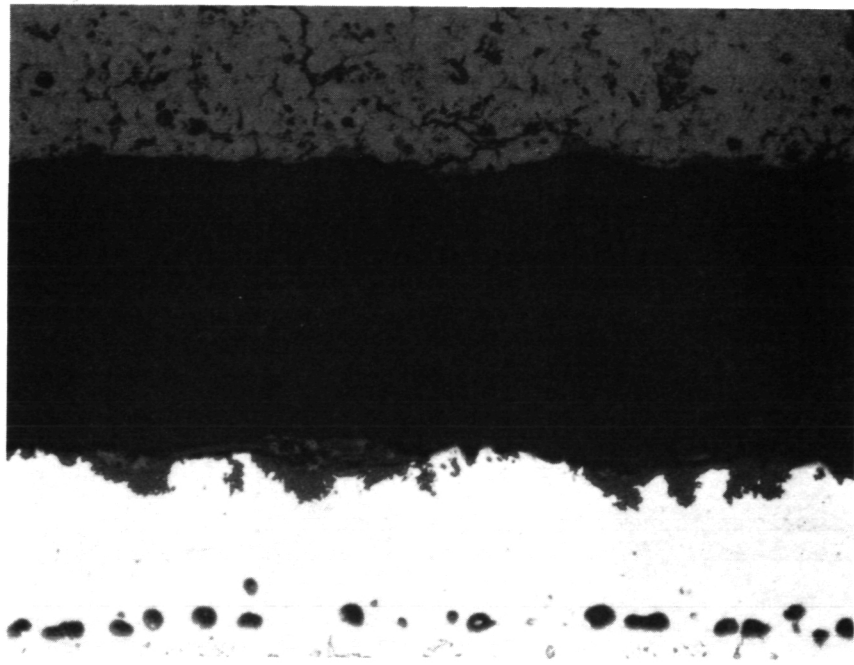
200X

Figure 12 Light Photomicrograph of Post-Test Microstructure. Furnace Exposure in Argon of 2100°F with 80 Hours Inspection Intervals. (1040 hrs/13 Cycles)



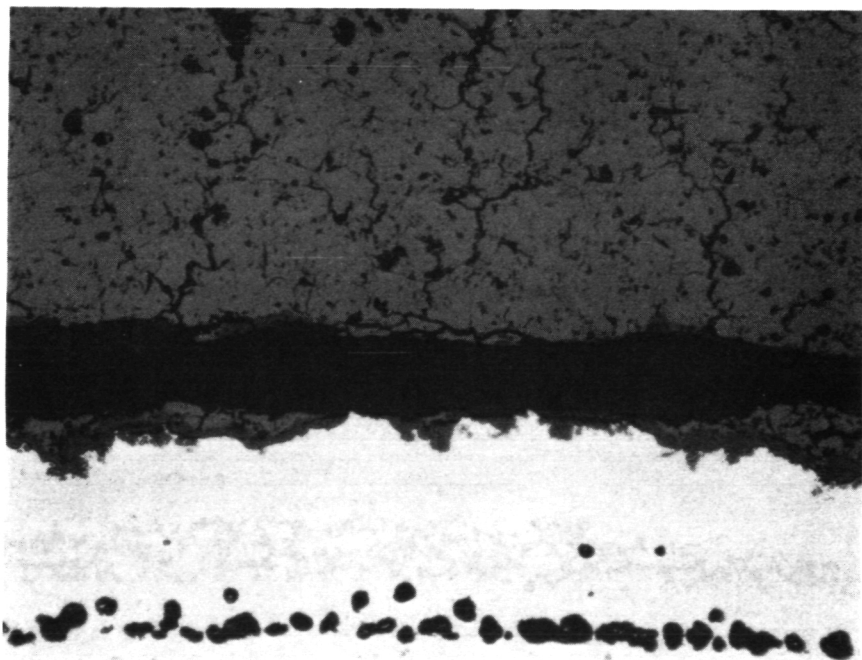
200X

Figure 13 Light Photomicrograph of Post-Test Microstructure. Failed After Furnace Exposure in Air at 2100°F with 80 Hours Inspection Intervals. (240 hrs/3 cycles)



200X

Figure 14 Light Photomicrograph of Post-Test Microstructure. Failed After Furnace Exposure in Air at 2100°F with 10 Hours Inspection Intervals. (160 hrs/16 cycles)



200X

Figure 15 Light Photomicrograph of Post-Test Microstructure. Failed After Furnace Exposure in Air at 2200°F with 10 Hours Inspection Intervals. (60 hrs/6 cycles)

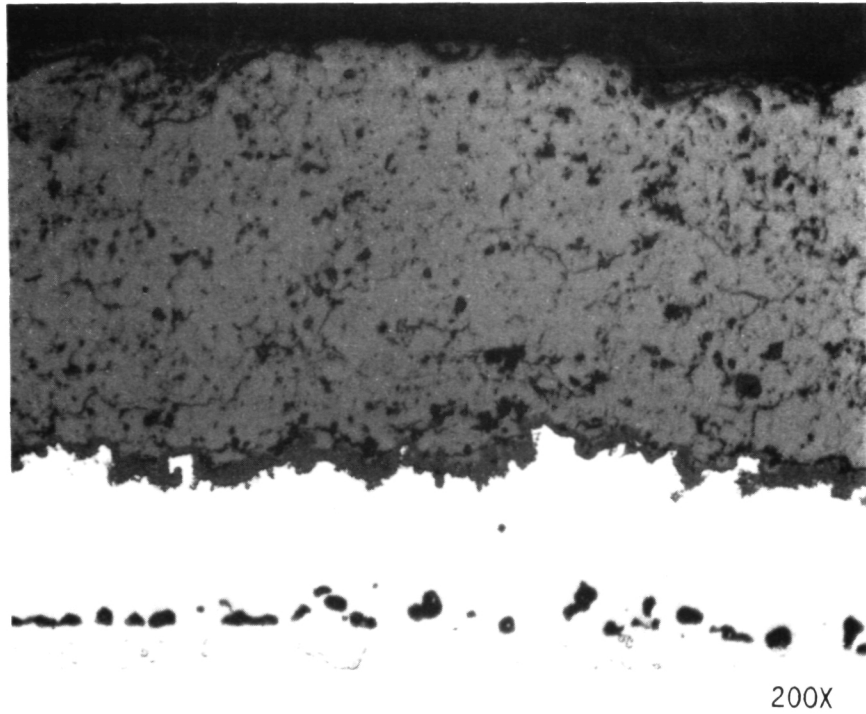


Figure 16 Light Photomicrograph of Post-Test Microstructure After Furnace Exposure in Air. (90 hrs/2100°F/1 cycle 60%)

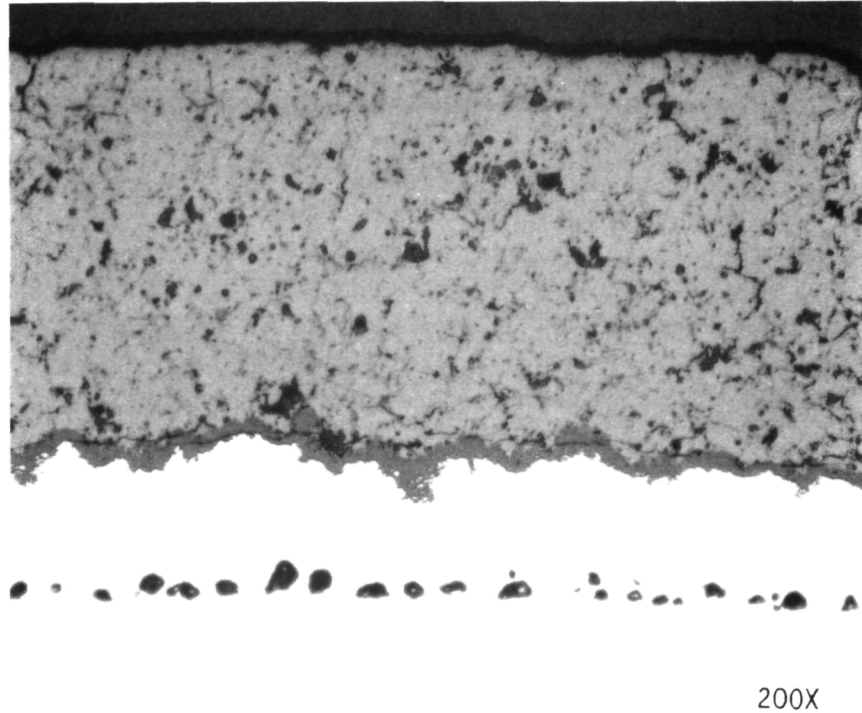


Figure 17 Light Photomicrograph of Post-Test Microstructure After Fractional Furnace Exposure in Air (135 hrs/2100°F/1 cycle 90%)

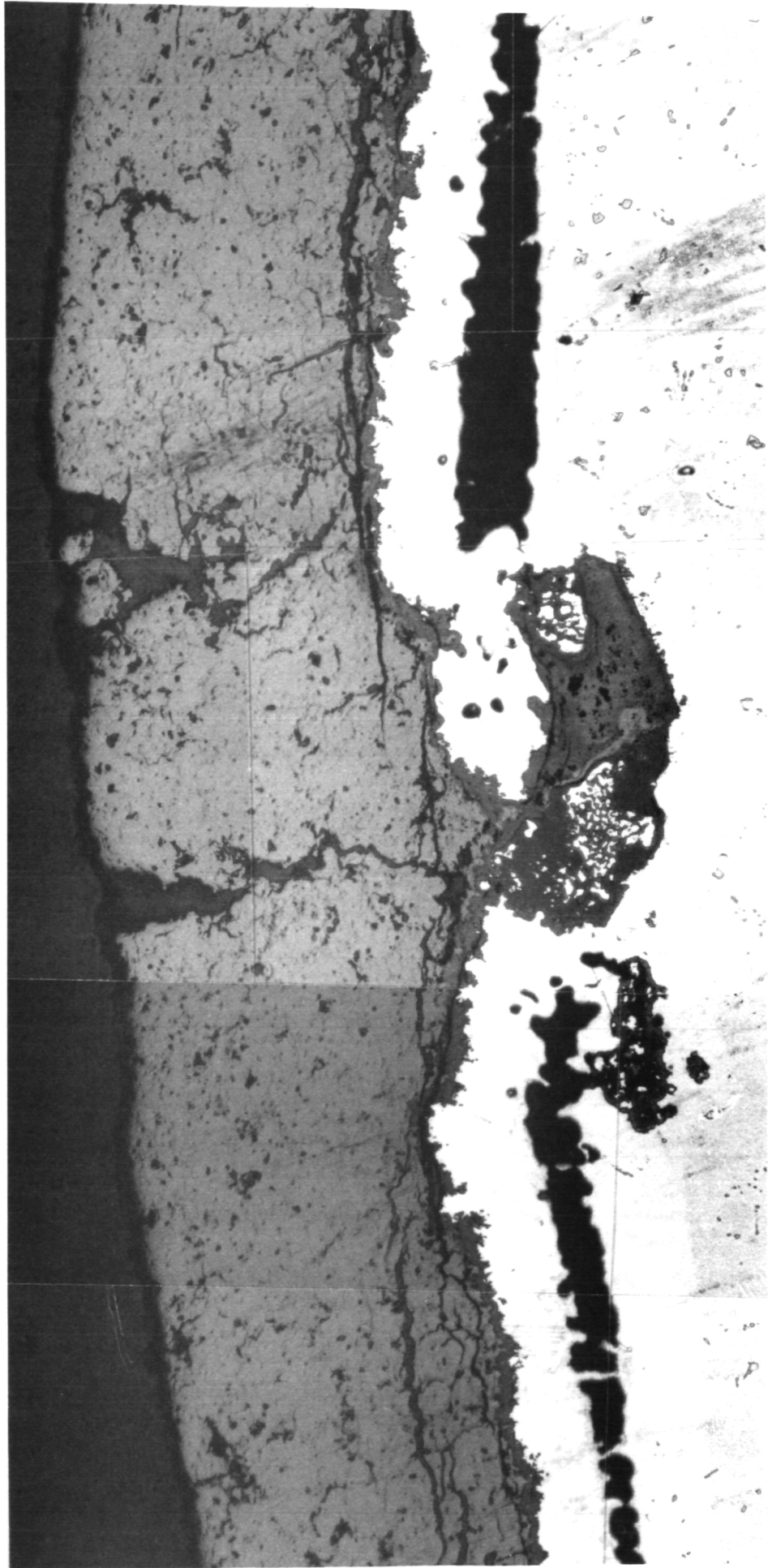


Figure 18 Light Photomicrograph of Post-Test Microstructure After 150 Hrs Fractional Exposure at 2100°F in Air

3.1.2.2 Cyclic Thermal Exposure Tests

A partial factorial test program shown in Figure 19 is presently being conducted to determine coating cyclic thermal failure life and provide preliminary information concerning interactions between static and cyclic thermal failure modes. A minimum of five (5) clean fuel cyclic burner rig tests of 1000 hours maximum duration are being conducted to expose a minimum of sixty-four (64) thermal barrier coated specimens to a minimum of four different combinations of burner rig test parameters.

MAXIMUM CYCLE TEMPERATURE	TRANSIENT HEATING RATE	SHORT CYCLE		LONG CYCLE	
		CYCLE TO FAILURE	FRACTIONAL EXPOSURE	CYCLE TO FAILURE	FRACTIONAL EXPOSURE
2100	FAST	⑨ D ₁	⑩ G	⑪ F	⑫
	SLOW	⑬ E	⑭	⑮	⑯
2000	FAST	⑰ D ₂	⑱	⑲	⑳
	SLOW	㉑	㉒	㉓	㉔

CONDITION D,E,F – 12 SPECIMENS PER TEST:

- | | |
|--|---|
| 4 – 10 MIL VIRGIN CERAMIC ("BASELINE" COATING) | } 40 HR AT 2100 °F FOR 2100°F TESTING
100 HR AT 2000°F FOR 2000 °F TESTING |
| 2 – 5 MIL VIRGIN CERAMIC | |
| 2 – 15 MIL VIRGIN CERAMIC | |
| 2 – 10 MIL AIR PRE-EXPOSED CERAMIC | |
| 2 – 10 MIL ARGON PRE-EXPOSED CERAMIC | |

CONDITION G:

FRACTION EXPOSURE TEST, DESCRIBED IN TEXT

Figure 19 Task I Clean Fuel Cyclic Burner Rig Test Program

The test method which is being used to measure cyclic coating life involves uncooled cyclic burner rig testing as described in Appendix A. The Jet A fueled burner employed in this test simulates the clean fuel combustor environment in which most hot section components operate. The primary method of temperature control in this test involves optical measurement of specimen surface temperature. To ensure consistent test conditions, a thermocoupled specimen is employed at all times during testing to monitor/calibrate test temperature. To provide specimen temperature distributions required for subsequent preliminary life prediction modeling (Task IC), instrumented specimens have been tested, as needed, (described in Appendix B) to characterize specimen temperature distributions for each of the test conditions studied.

Baseline cyclic life of the TBC is determined as a function of maximum surface temperature by exposure of a minimum of three baseline coated burner rig test specimens to each of the two sets of test conditions identified as "D" in Figure 19. Cycle duration in this test was on the order of 6 minutes, with approximately 4 minutes flame immersion (1 minute to temperature + 3 minutes at temperature) and 2 minutes forced air cooling. Each specimen was cycled to failure or a maximum of 1000 hours of total test time, with failure being defined as spallation of the TBC over approximately 50% of the specimen hot zone which amounts approximately to a 1/2" X 1/2" size patch.

To provide information on the influence of transient heating rate on thermal barrier coating spalling life, a minimum of three specimens is being tested to failure or 1000 hours at a transient heating rate which is less than that used for the baseline cyclic failure tests; i.e., it will take 3 minutes to get up to temperature. Results of these tests, identified as "E" in Figure 19 will be used in Task IC and subsequent life prediction modeling analyses.

Two approaches are employed to evaluate interaction(s) between thermal exposure and cyclic degradation modes. The first of these involves cyclic exposure as defined above with a longer cycle duration (identified as "long cycle" in Figure 19). The long cycle is on the order of 60 minutes, involving approximately 57 minutes flame immersion (1 minute to temperature + 56 minutes at temperature) and 3 minutes forced air cooling. A minimum of three "baseline" thermal barrier coated specimens has been cycled to failure (or 1000 hours) at the condition identified as 'F' in Figure 19.

A second approach to evaluate interactions between cycling and thermal exposure involves cyclic testing of furnace pre-exposed specimens at the same cyclic conditions as the baseline specimens. The test plan involves pre-exposure of test specimens in air and in argon to approximately one-half of the estimated respective total hot times which will be accumulated to failure for the baseline coating in the corresponding test. Pre-exposure durations were selected on the basis of prior experience. The actual pre-exposure "life fraction" was calculated from baseline test results after testing was completed. A minimum of four pre-exposed specimens, two each exposed in oxidizing and non-oxidizing environments, is being tested at each of the test conditions identified as in Figure 19.

To determine the influence of ceramic thickness on coating life, two specimens coated with a nominal 5 mil thick ceramic and two specimens coated with a nominal 15 mil thick ceramic were included in each of the four burner rig tests indentified as 9, 11, 13, and 17 in Figure 19.

To provide information concerning the nature and rate of accumulation of coating damage, a fractional exposure test, identified as "G" is being conducted. In this test, specimens are exposed to decile fractions of the cyclic failure life and examined metallographically to identify possible progressive damage mode(s) which cause ceramic spalling failure. A minimum of two specimens is being cycled to each of the approximately 10%, 20%, 30%, 40%, 50%, 60%, 70%, 80%, and 90% fractions of the average cyclic failure life defined in the "D₁" test. A minimum of two additional specimens is being cycled to failure to verify prior failure life data.

The designed test program above is nearing completion. The 2100°F (D1) and 2000°F (D2) short cycle, fast heat up rate tests have been completed while the 2100°F, short cycle slow heat up rate (Test E) and the 2100°F, long cycle fast heat up rate (Test F) tests are approaching completion. The fractional exposure test, G, has been initiated with defined parameters based on D1 test results. Table X presents a comparative summary of results obtained to date for the 2000°F and 2100°F (D2 and D1) test with Table XI and XII showing the individual test results.

The failure mode for all specimens was typical of the component failure mode shown in Figure 2; that is, a dominant crack propagates parallel to but not coincident with the bond coat ceramic interface resulting in spallation of the coating leaving a thin layer of remnant ceramic remaining adherent to the bond coat.

Post-test analysis has shown that increased test time results in: 1) increased MgCrAlY oxide scale thickness; 2) increased beta-depletion and/or coarsening; 3) some increase in Kirkendall void population and size at the interface and 4) no significant phase changes in the ceramic as seen in Table IX for representative test specimen X-ray diffraction analysis of the two tests in which no significant v/o monoclinic ZrO_2 is noted.

The data shows clearly that the coating life is dependent on test temperature, pre-exposure environment and ceramic thickness. Decreasing the test temperature from 2100°F to 2000°F yields 2.5 X the coating durability of the higher temperature test. Figures 20 and 21 (a and b) show pre- and post-test baseline specimens for the 2000 and 2100°F burner rig test, respectively (Note the Kirkendall porosity differences between both post-test specimens). Also, for both cases, air pre-exposure reduces coating burner rig test life dramatically; i.e., 50 - 70% reduction. Figures 22 and 23 (a and b) show the pre-test and post-test microstructure for the air pre-exposed at 2000°F/100 hrs and 2100°F/40 hrs specimens respectively.

Argon pre-exposure specimens showed no test life debit at 2100°F and a 47% improvement over baseline specimens in the 2000°F test, D2, was seen. Preliminary metallographic observation indicates only subtle differences in the pre-test structures of the 2100 and 2000°F specimens; i.e., less Kirkendall porosity in the 2000°F specimen. This data therefore suggest "inert" pre-exposure does not affect coating life. Figures 24 and 25 (a and b) show the pre-test (post-argon exposure) and post-test microstructures for both the 2000°F and 2100°F test specimens. In comparing the air and Ar pre-exposed microstructures, the presence of an interdiffusion layer at the area adjacent to and below the bond coat-substrate interface is now marked by Kirkendall void alignment. This suggests that the bond coat and substrate composition has changed. It is possible that the increase in coating life with the Ar pre-exposed specimens is due to these compositional changes which may result in changes in the bond coat strength properties. In the air pre-exposed specimens any benefits obtained due to compositional changes is overridden by the thick oxide developed at the interface.

TABLE IX

X-RAY DIFFRACTION ANALYSIS OF SOME REPRESENTATIVE POST TEST
D1 AND D2 SPECIMENS

Specimen/ Location	v/o FCC ZrO ₂	v/o Tetragonal ZrO ₂	v/o Monoclinic ZrO ₂	Failure Time (hours)
<u>2100°F Test (D1)</u>				
Standard Pre-test	60-55 (a ₀ =5.122A)	40-45 (a ₀ =5.1172A c ₀ =5.1646)A	Not detected	N/A
Standard/adjacent to spall	60-65 (a ₀ =5.13263A)	35-30	5	175
Standard/180° from spall	55-60 (a ₀ =5.13575A)	45-40	1	
Thick/adjacent to spall	60-65 (a ₀ =5.13762A)	40-35	Not detected	104
Thick/adjacent to spall(other side)	60-65 (a ₀ = 5.14152A)	40-35	--	
Air pre-exposed/ adjacent to spalled area	60-65 (5.13907A)	35-30	5	
Air pre-exposed/ 180° from spalled area	55-60 (5.13910A)	45-40	Not detected	50
<u>2000°F Test(D2)</u>				
Argon pre-exposed/ adjacent to spalled area	60-65	35-30	1 (Possibly mono- clinic ZrO ₂ or hexagonal Y ₂ O ₃)	679
Thin ceramic/ adjacent to spall	50-55	50-45	Not detected	557
Thick ceramic/ adjacent to Spall (other side)	55-60	45-40	Not detected	443
Air pre-exposed/ adjacent to spalled area	65-70	35-30	1	194

TABLE X
 COMPARISON OF 2000°F and 2100°F SHORT CYCLE BURNER RIG TEST RESULTS
 (Total Hours to Failure/Cycles to Failure/Estimated Hours of Hot Time to Failure)

Test Code/ Condition	Standard "Baseline" Average	Thin Average	AR Pre-Exposed Average	Thick Average	Air Pre-Exposed Average
D1/2100°F I.D., Short Cycle - Fast Heat Up	185/1850/92	238/2380/118	210/2100/145	132/1320/66	50/500/65
D2/2000°F I.D., Short Cycle - Fast Heat Up	471/4710/235	525/5250/263	639/6390/420	470/4700/235	205/2050/102

TABLE XI

D1 TEST: 2100°F - I.D./SHORT CYCLE (4 minutes in the
 Flame + 2 minutes FAC)/FAST HEAT-UP

<u>Specimen Condition</u>	<u>Failure Time (hours)</u>	
Air Pre-Exposed 40 hours/2100°F	50 50	Avg = 50
Ar Pre-Exposed 40 hours/2100°F	75 67 279 279 279 279 221 199 199 271	Avg = 210
Thick Ceramic Nominal 15 mils	104 160	Avg = 132
"Baseline" (10 mil ceramic, no pre-exposure)	182 172 213 175 172 193 182 198	Avg = 185
Thin Ceramic Nominal 5 mils	243 232	Avg = 238

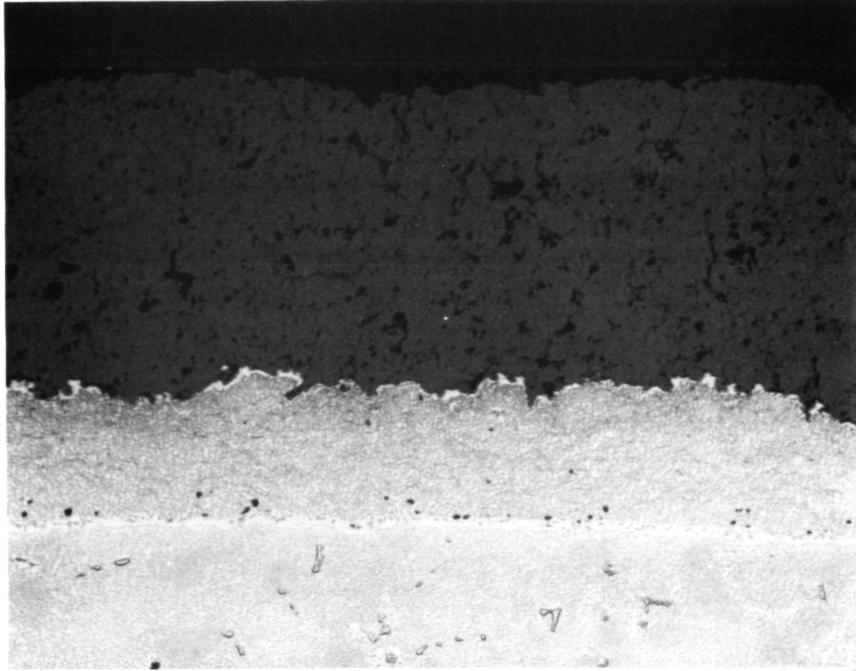
TABLE XII
 D2 TEST: 2000°F - I.D./ SHORT CYCLE (4 minutes in the
 Flame + 2 minutes FAC)/FAST HEAT-UP

<u>Specimen Condition</u>	<u>Failure Time (hours)</u>	
Air Pre-Exposed (100 hours/2000°F)	194 } 215 }	Avg = 250
Ar Pre-Exposed 100 Hours/2000°F	679 } 708 }	Avg = 693
Thick Ceramic (15 Mils)	515 } 425 }	Avg = 470
Thin Ceramic (5 Mils)	557 } 492 }	Avg = 525
"Baseline" (10 mil ceramic, no pre-exposure)	386 } 443 } 435 } 557 } 536 }	Avg = 471

Figures 26 and 27 (a and b) are the pre-test and post-test microstructures for thin and thick specimens tested at 2100°F respectively and Figures 28 and 29 (a and b) are shown for the 2000°F burner rig test. Nominal 15 mil thick ceramic specimens exhibited a significant life debit as compared with baseline specimens in the 2100°F burner rig test; however, this life debit was less dramatic at 2000°F testing.

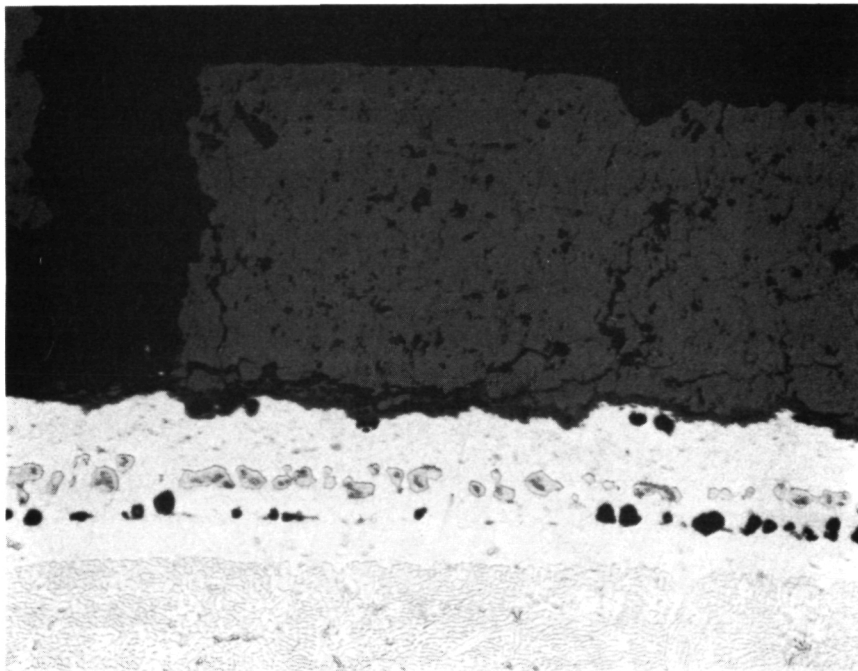
The 2100°F short cycle, 180 sec. transient heating rate test (Condition E) currently is in progress. Generally, specimens in this test are exhibiting failure times somewhat shorter, 70% of previous baseline specimens, than the fast heatup rate test (D1). This was not expected since these specimen see both reduced transient severity and less hot time. Rationalization of this unexpected result must await analytical effort which may show a reason.

The 2100°F long cycle, 60 sec. heating rate test is in progress and nearing completion. Baseline specimens are showing approximately 50% of the baseline test life for previous testing conducted at this temperature but with a short cycle. In terms of hot time/accumulated time-at-temperature, as well as failure ranking, results correlate to previous testing, with Ar pre-exposed specimens showing 1.3 X the coating life of the baseline specimens.



200X

Figure 20a Light Photomicrograph of Pre-Test Microstructure (D2 Test)



200X

Figure 20b Light Photomicrograph of Baseline Post-Test Microstructure (D2 Test After 435 hrs at 2000°F/ Short Cycle/ Fast Heatup)

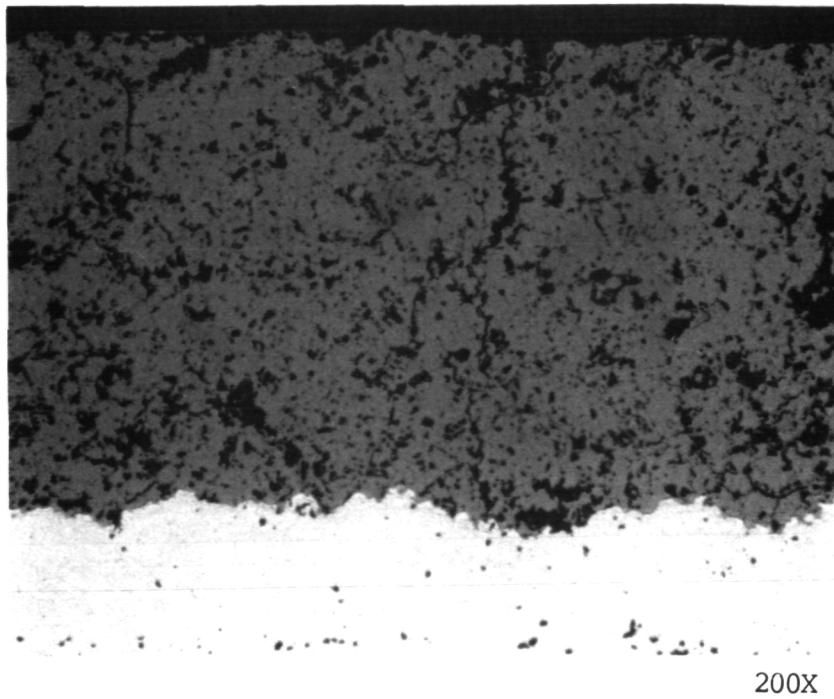


Figure 21a Light Photomicrograph of Baseline Pre-Test Microstructure (D1 Test)

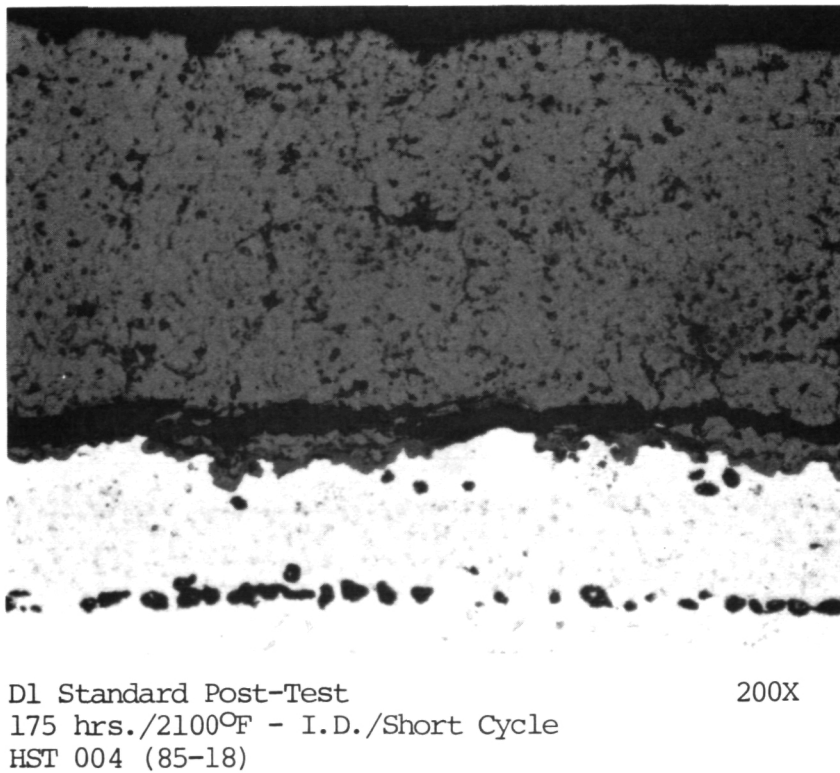
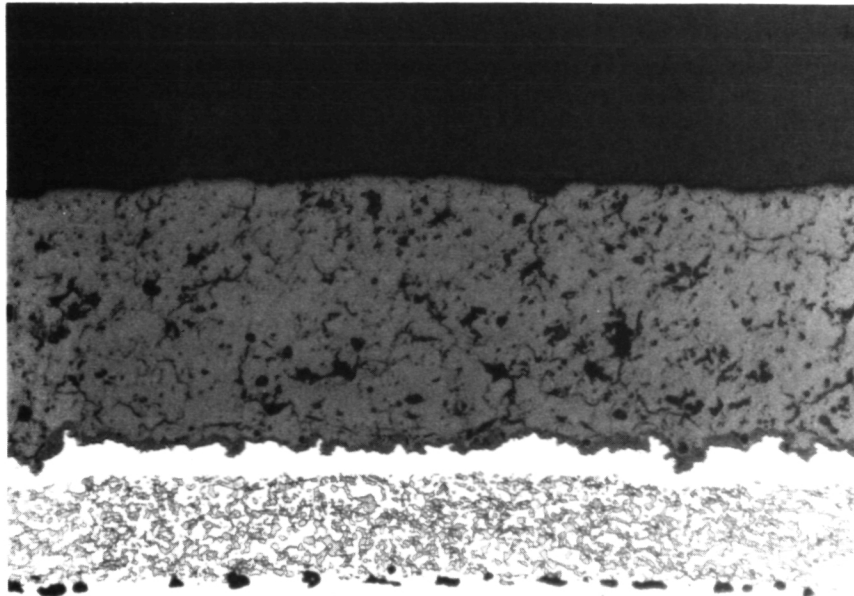


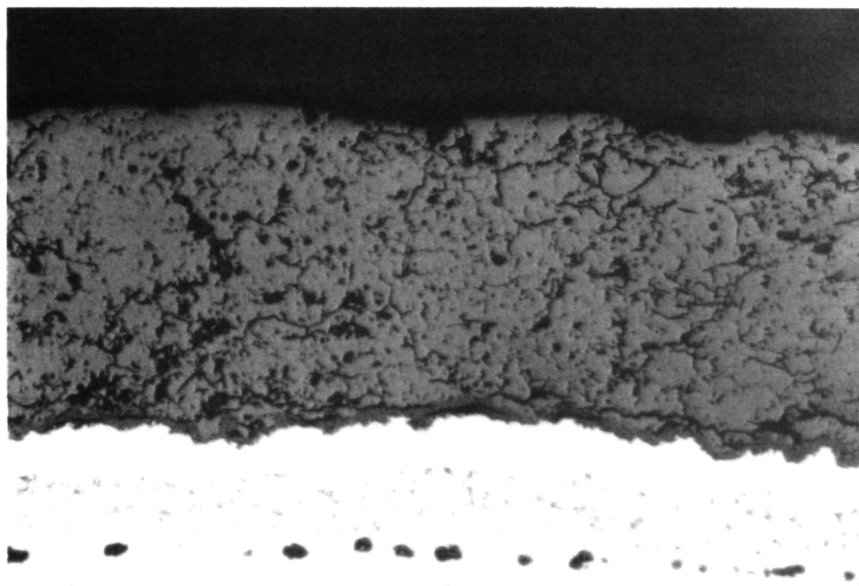
Figure 21b Light Photomicrograph of Baseline Microstructure After 175 hrs at 2100°F/Short Cycle/Fast Heatup

ORIGINAL PAGE IS
OF POOR QUALITY



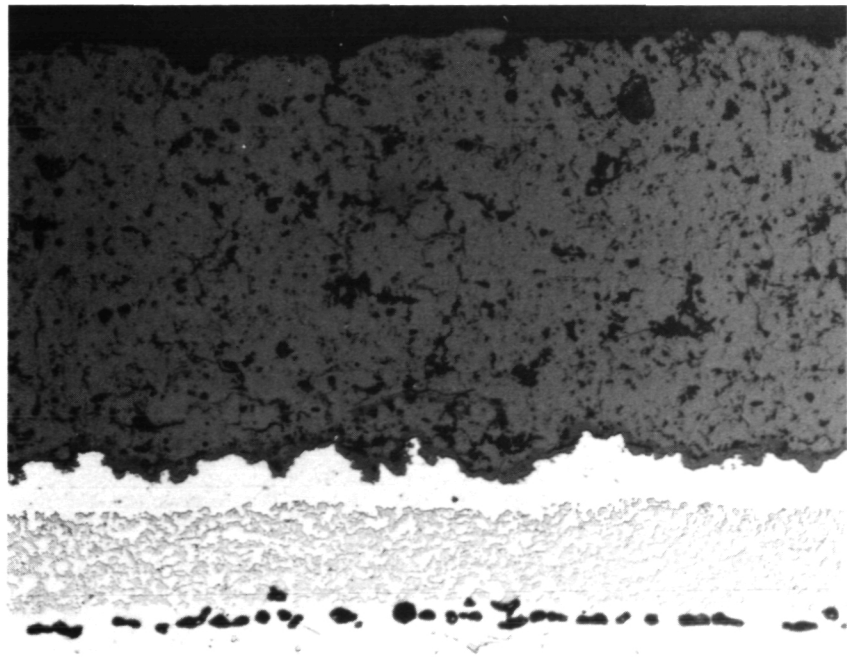
200X

Figure 22a Light Photomicrograph of Pre-Burner Rig Test (D2) Microstructure for Pre-Exposed Specimen (Air/2000°F/100 hrs)



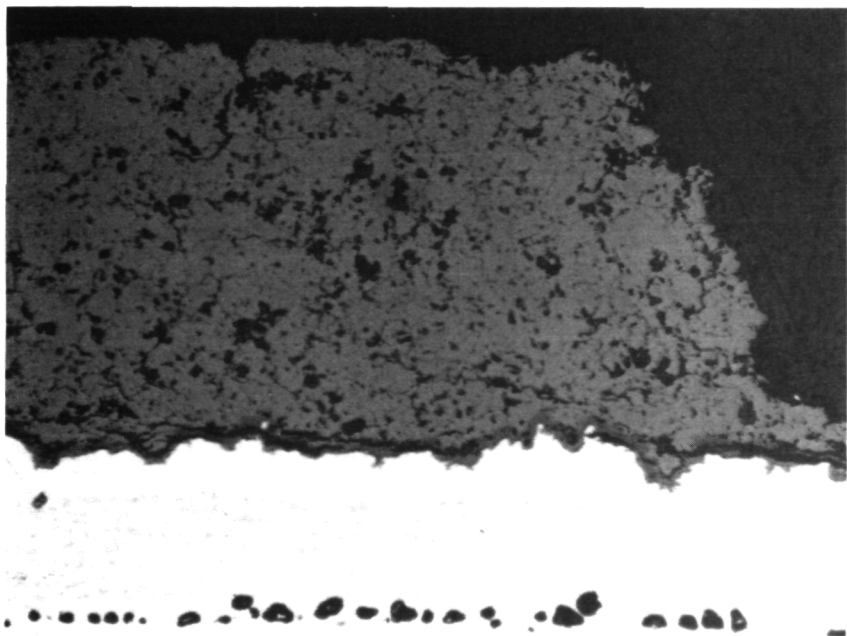
200X

Figure 22b Light Photomicrograph of Post Burner Rig Test (D2) Microstructure for Pre-Exposed Specimen (Air/2000°F/100 hrs) After 215 hrs at 2000°F/Short Cycle/Fast Heatup



200X

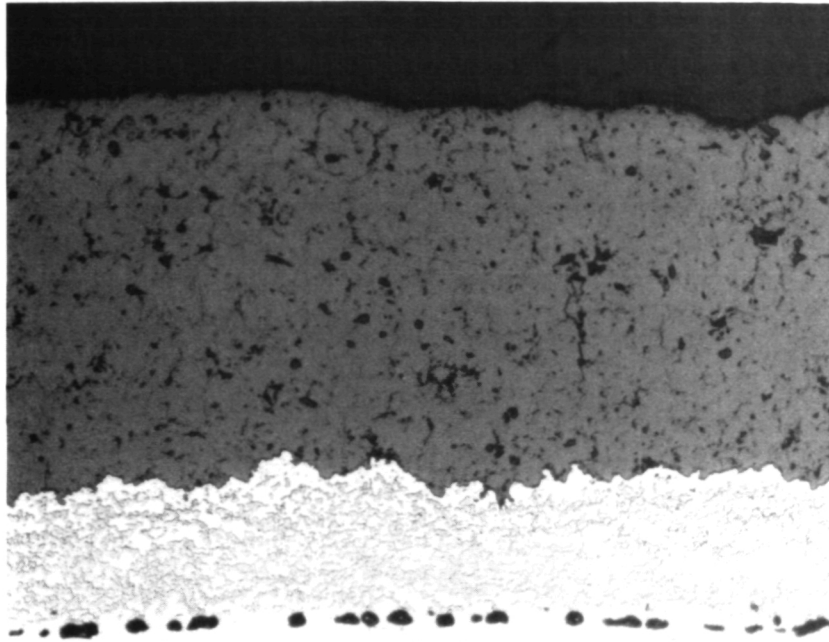
Figure 23a Light Photomicrograph of Pre-Burner Rig Test (D1) Microstructure for Pre-Exposed Specimen (Air/2100°F/40hrs)



200X

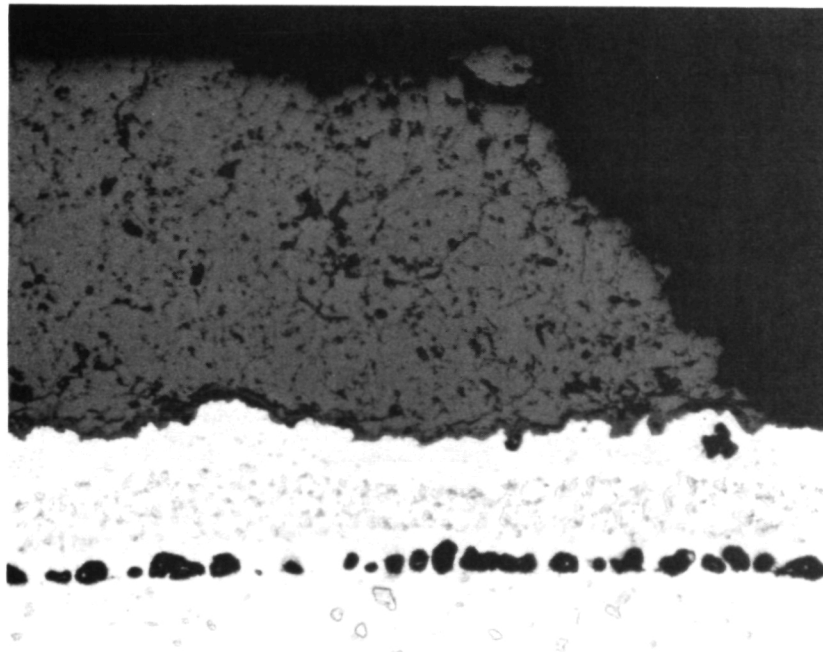
Figure 23b Light Photomicrograph of Post-Burner Rig Test (D1) Microstructure Pre-Exposed Specimen (Air/2100°F/40 hrs) After 50 hrs at 2100°F/Short Cycle/Fast Heatup

ORIGINAL PAGE IS
OF POOR QUALITY



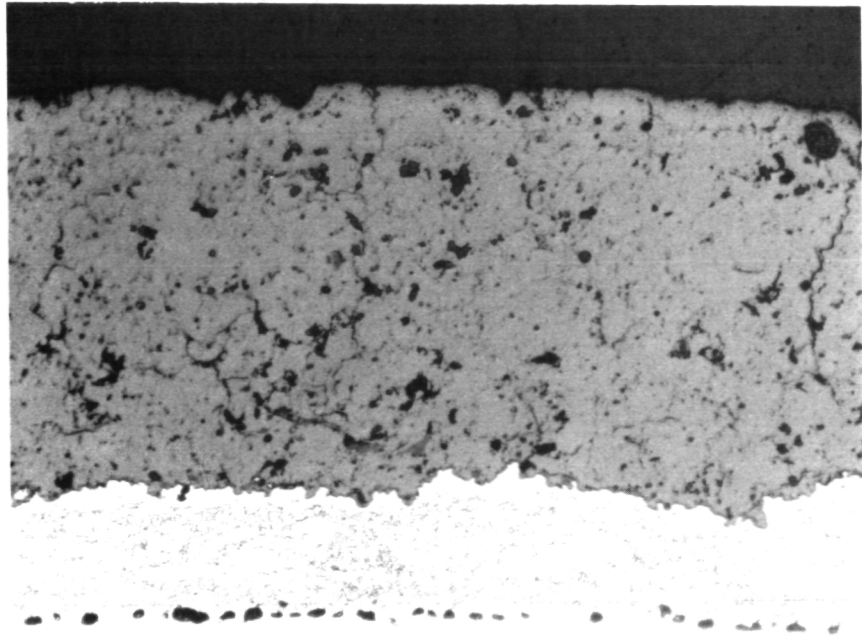
200X

Figure 24a Light Photomicrograph of Pre-Burner Rig Test (D1) Microstructure for Pre-Exposed Specimen (Argon/2100°F/40 hrs)



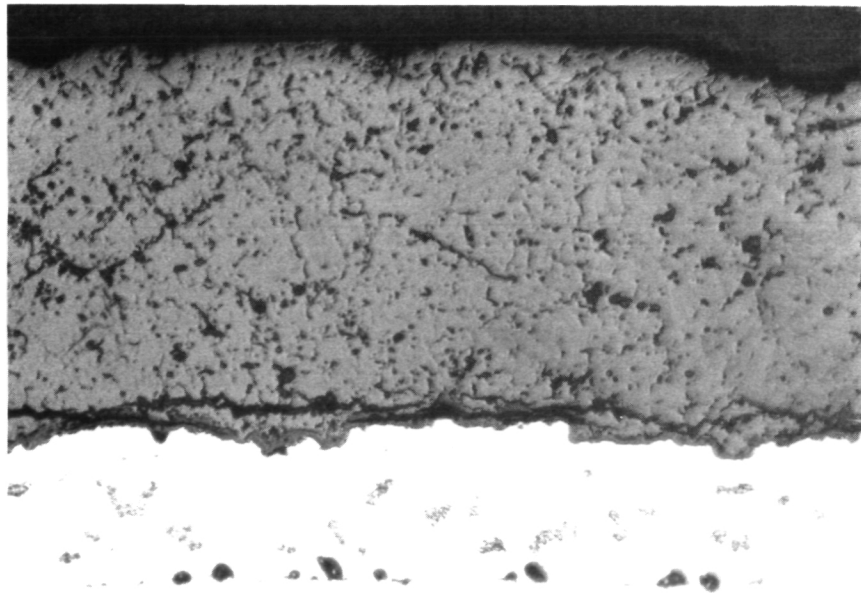
200X

Figure 24b Light Photomicrograph of Post Burner Rig Test (D1) Microstructure for Pre-Exposed Specimens (Argon/2100°F/40hrs) After 67 hrs at 2100°F/Short Cycle/Fast Heatup



200X

Figure 25a Light Photomicrograph for Pre Burner Rig Test (D2) Microstructure for Pre-Exposed Specimen (Ar/2000°F/100 hrs)



200X

Figure 25b Light Photomicrograph of Post Burner Rig Test (D2) Microstructure for Pre-Exposed Specimen (Ar/2000°F/100 hrs) After 708 hrs at 2000°F/Short Cycle/Fast Heatup

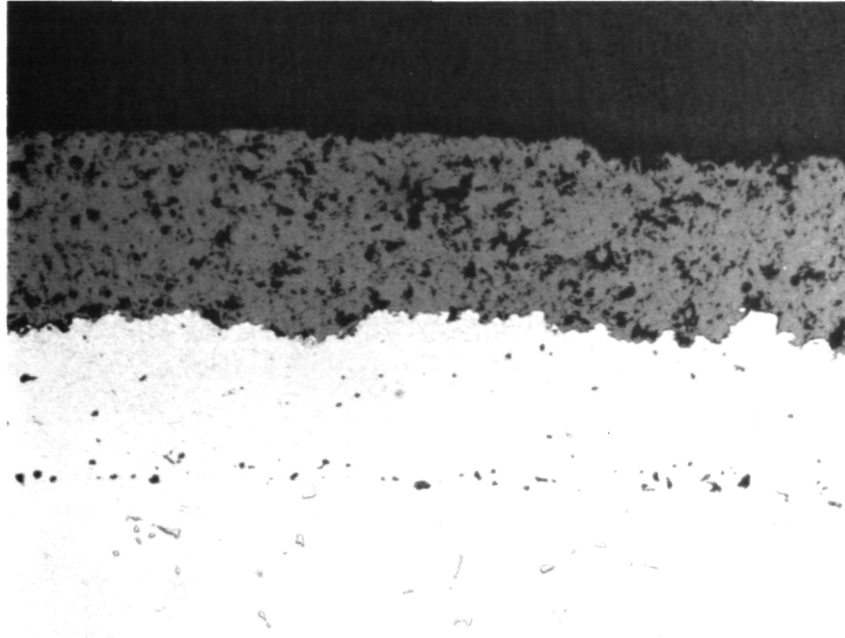
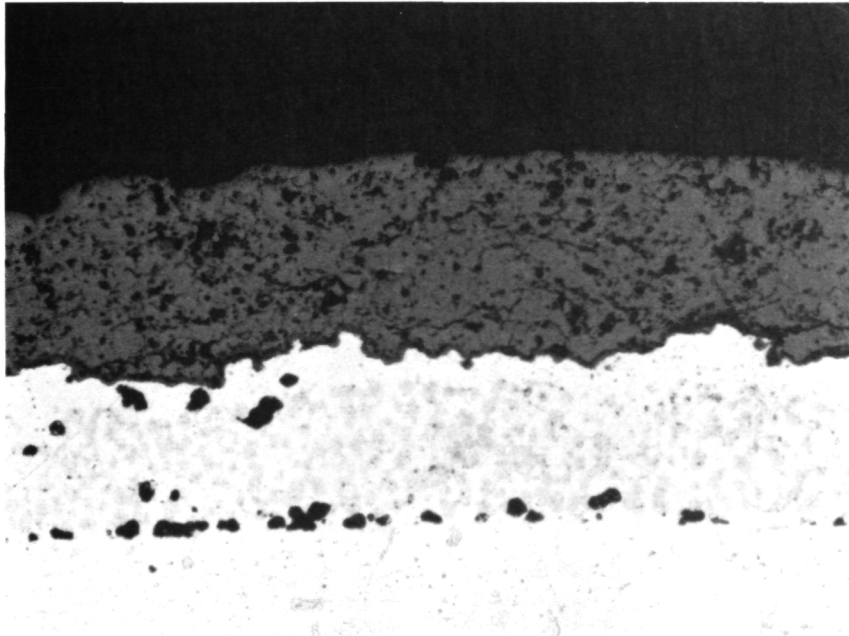
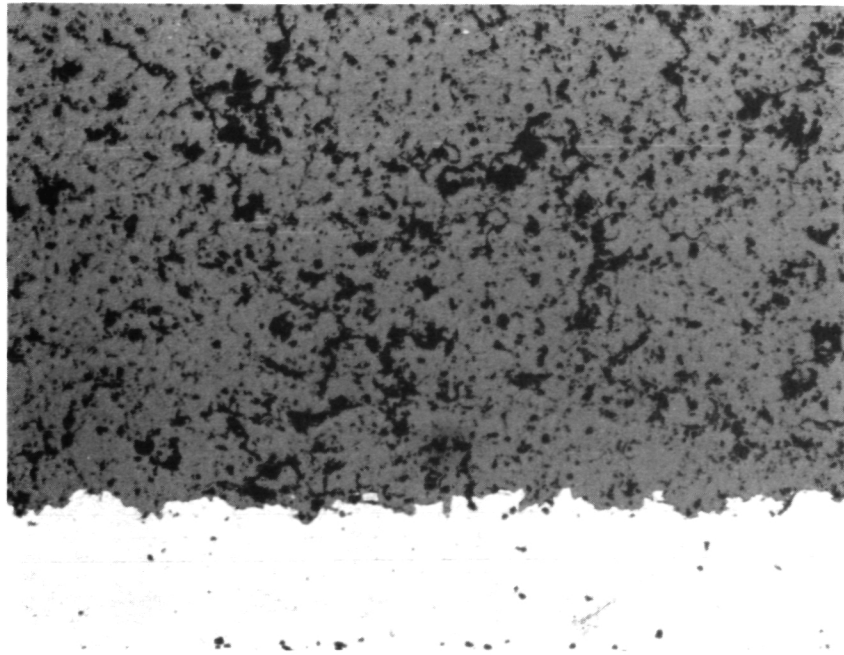


Figure 26a Light Photomicrograph of Pre-Test Microstructures for Thin Specimens, D1 Test 200X



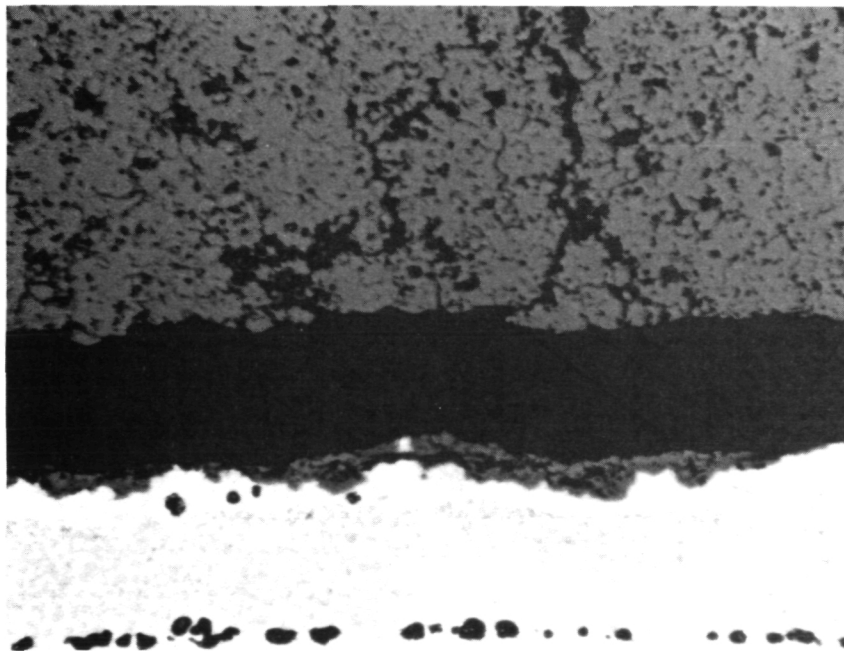
200X

Figure 26b Light Photomicrograph of Post-Test Microstructures of Thin Specimens, D1 Test After 243 hrs at 2100°F/Short Cycle/Fast Heatup



200X

Figure 27a Light Photomicrograph of Pre-Test Microstructures for Thick Specimen, D1 Test



200X

Figure 27b Light Photomicrograph of Post Test Microstructures for Thick Specimen, D1 Test, After 160 hrs at 2100°F/Short Cycle/ Fast Heatup

ORIGINAL PAGE IS
OF POOR QUALITY

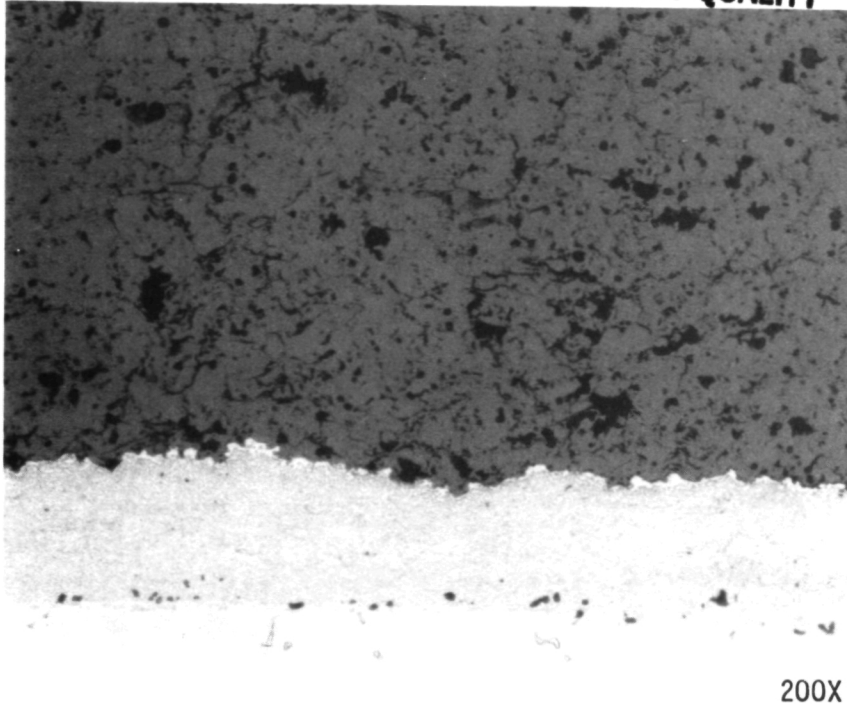


Figure 28a Light Photomicrograph of Pre-Test Microstructure for Thick Ceramic Specimen, D2 Test

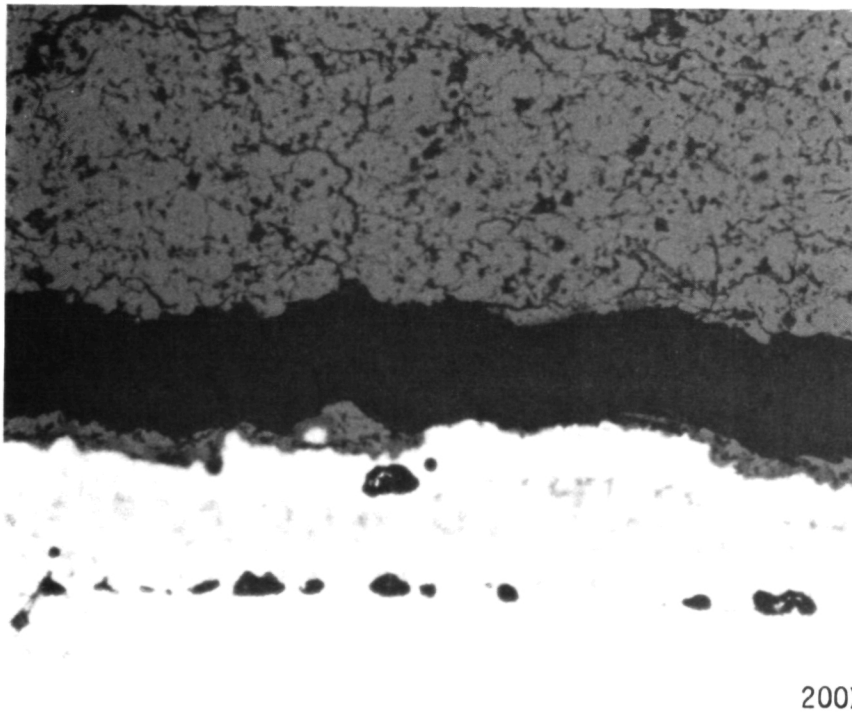
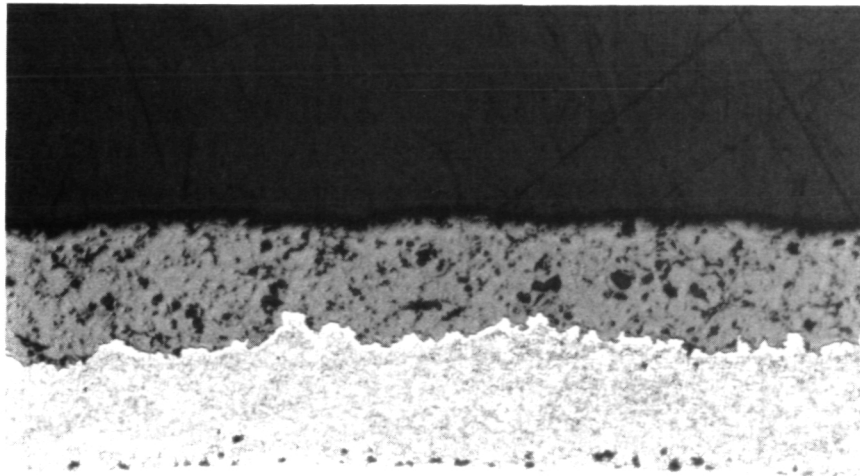
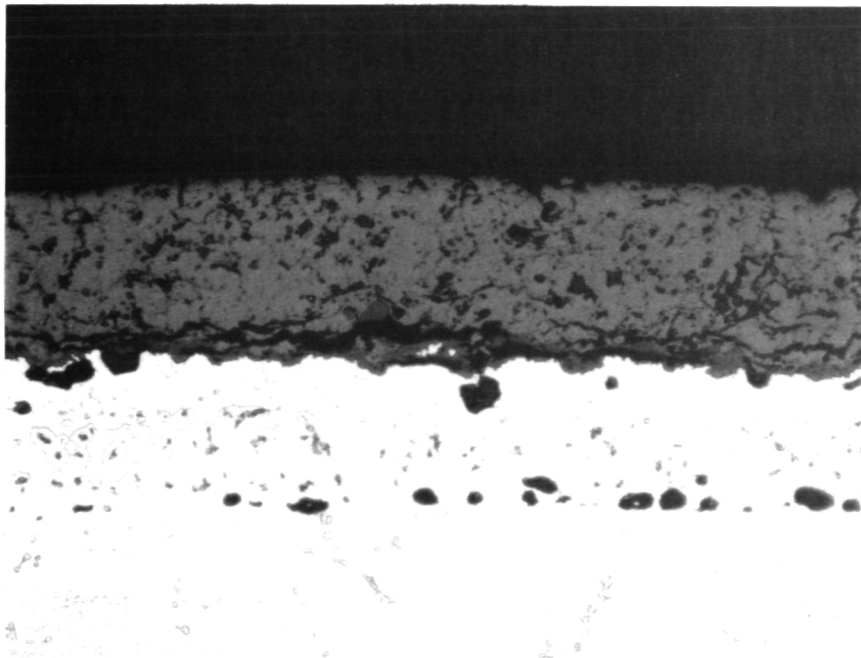


Figure 28b Light Photomicrograph of Post-Test Microstructure for Thick Ceramic Specimen, D2 Test After 454 hrs at 2000°F/Short Cycle/Fast Heatup



200X

Figure 29a Light Photomicrograph of Pre-Test Microstructure for Thin Ceramic Specimen, D2 Test



200X

Figure 29b Light Photomicrograph of Post-Test Microstructure for Thin Ceramic Specimen, D2 Test After 492 hrs at 2000°F/Short Cycle/Fast Heatup

3.1.2.3 Cyclic Hot Corrosion Testing

This subtask was to determine the relative importance of hot corrosion as a thermal barrier coating failure mechanism and provide test data from which a preliminary life prediction model might be developed. A minimum of six specimens was exposed at two different corrodent levels (three specimens minimum per level). A minimum of twenty additional specimens is being exposed to various cyclic life fractions. A maximum of three ducted burner rig tests each of 1000 hours maximum duration is being conducted to test these specimens.

The test method involves ducted burner rig testing as described in Appendix B. To maximize the potential for hot corrosion damage, these tests are being conducted at a maximum specimen surface temperature of 1650°F. A partial factorial test program is shown in Figure 28. Testing to spallation failure was conducted at a "high" corrodent level; 35 ppm synthetic sea salt, condition "H" in Figure 30, and at a lower corrodent level; 10 ppm synthetic sea salt identified as "J" in Figure 30. To provide information concerning the nature and rate of accumulation of hot corrosion damage, a fractional exposure test, identified as "K" in Figure 30, will be conducted. In this test, specimens exposed to decile fractions of the high corrodent level hot corrosion life will be examined metallographically to identify and characterize progressive damage mode(s) which cause thermal barrier coating hot corrosion failure. A minimum of two specimens will be cycled to each of the approximately 10%, 20%, 30%, 40%, 50%, 60%, 70%, 80%, and 90% fraction of the average cyclic failure life defined in the "H" test. A minimum of two additional specimens will be cycled to failure to verify prior failure life data.

The designed cyclic hot corrosion test program is nearing completion. The high corrodent level and low corrodent level tests have been completed. The fractional corrosion test (K) is in progress.

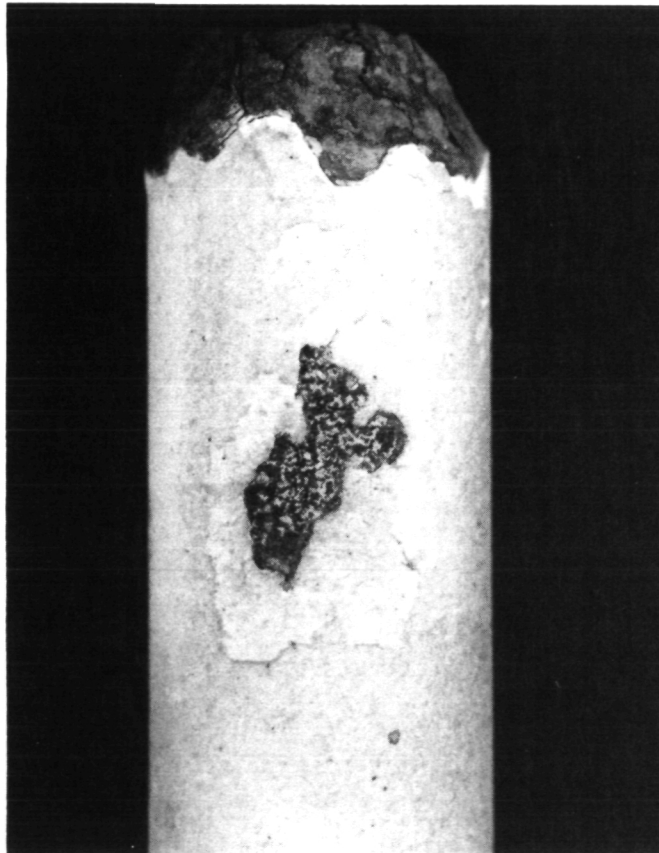
The high corrodent level test (H) was run out to 1000 hrs as required by the work plan at these conditions: 1650°F, 35 ppm artificial sea salt, 1.3%SO₃, 1 hour cycle (57 minutes in the flame + 3 minutes FAC). The test results are presented in Table XIII.

	LOW CORRODANT LEVEL, 10 PPM	HIGH CORRODANT LEVEL, 35 PPM
CYCLE TO FAILURE	(25) J	(26) H
FRACTIONAL EXPOSURE	(27) 	(28) K

Figure 30 Task I Hot Corrosion Test Program

TABLE XIII
CYCLIC HOT CORROSION TEST RESULTS (CONDITION H):
1650°F, Long Cycle (57 minutes in the flame + 3 minutes FAC)/
35 ppm Artificial Sea Salt/1.3% SO₃

<u>Failure Time (Hrs)</u>	
693	} Avg = 618
693	
638	
615	
1000	} No Failure Observed
1000	



4X

Figure 31 Cyclic Hot Corrosion Test Specimen Showing Multi-level Flaking of the Ceramic

The failure criteria is 50% of the hot zone area (for ducted tests the entire length of the exposed portion of the bar acts as the hot zone). Failures occurred well above the ceramic-metallic interface with large amounts of ceramic remaining adherent. Small cracks grew in length and depth as testing continued until discrete patches of ceramic spalled around the bar, favoring leading edge locations. Evaluation of post-test specimens revealed a multi-level failure mode; i.e., flaking as seen in Figure 31. Some additional specimens were tested in which the failure criteria was not met after 1000 hours of test time.

Figures 32 - 33(a and b) show the pre-test and post-test microstructures of specimens tested 693 and 1000 hours respectively. Ceramic spallation; i.e., multi-level flaking is clearly different from clean fuel burner rig test failures.

Figures 34(a-c), and 35(a-d) show post-test surface structure and transverse microstructure for a test specimen exposed for 450 hrs in the high corrosive level test (Condition H). The EMP results as seen in the X-ray maps clearly show the infiltration of sodium and sulfur in the pores and microcracks.

Further post corrosion test specimen evaluations have confirmed infiltration of sodium and sulfur in localized areas of porosity and microcracking throughout the width of the ceramic coating. Increased exposure time shows increased infiltrant concentration in these areas. Magnesium, contained in synthetic sea salt as $MgCl_2$ (see Table XIV), was generally not detected in the ceramic coating but was found concentrated in the oxide layer between the ceramic/bond coat interface. As shown in Figures 36(a-g), X-ray maps for Al and Mg may suggest the predominance of the formation of $MgAl_2O_4$ spinel.

TABLE XIV
ARTIFICIAL SEA SALT COMPOSITION

NaCl	58.4%
MgCl ₂	26.4
Na ₂ SO ₄	9.7
CaCl ₂	2.7
KCl	1.6
NaHCO ₃	.4
KBr	.23
H ₃ BO ₃	.07
SrCl ₂	.007

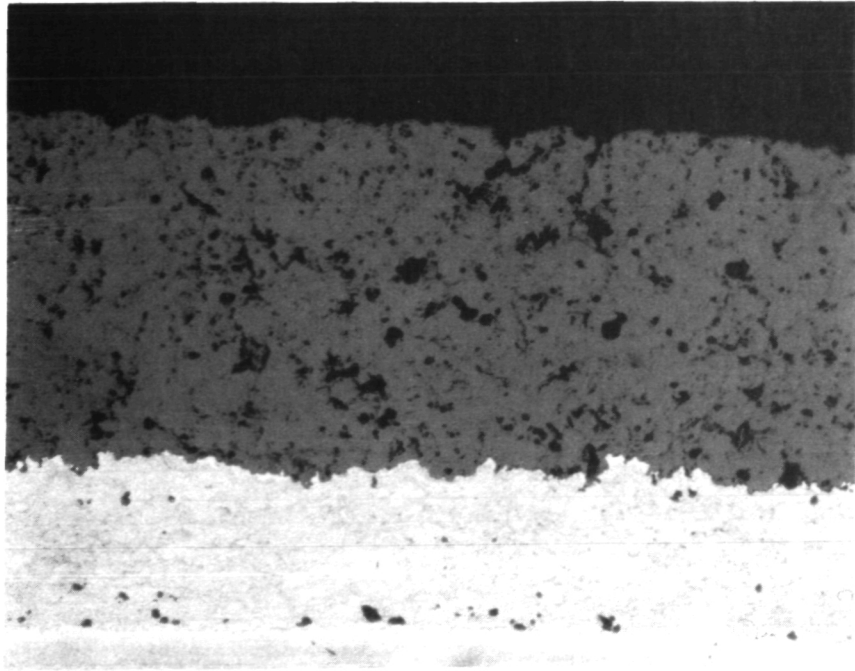


Figure 32a Pre-Test Hot Corrosion Test Specimen; 35 ppm Artificial Sea Salt/
1650°F/1 Hour Cycle

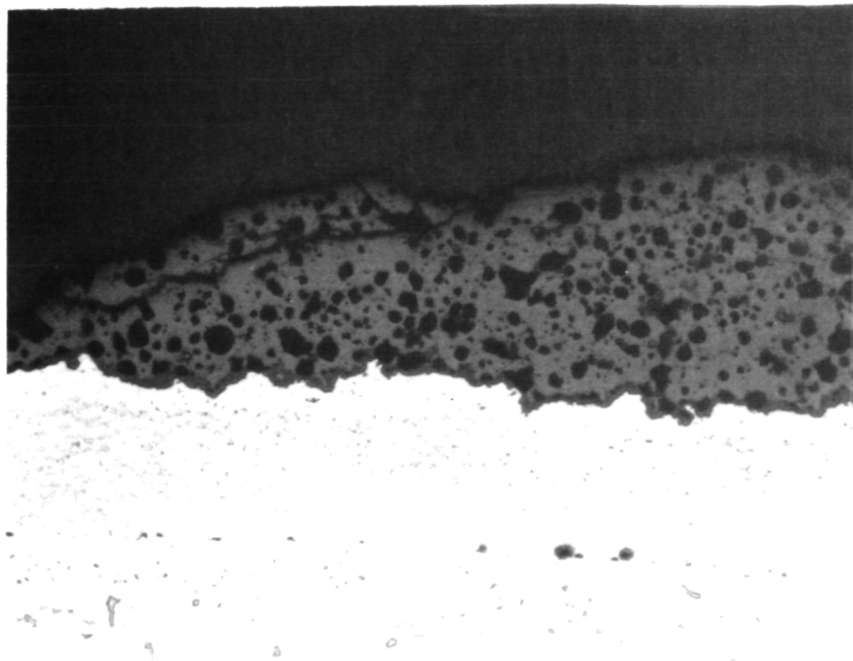


Figure 32b Post-Test Hot Corrosion Test Specimen Showing In-Plane Ceramic
Cracking in Central and Upper Portion of Ceramic Layer After 693
hrs at 35 ppm Artificial Sea Salt/1650°F/1 Hour Cycle

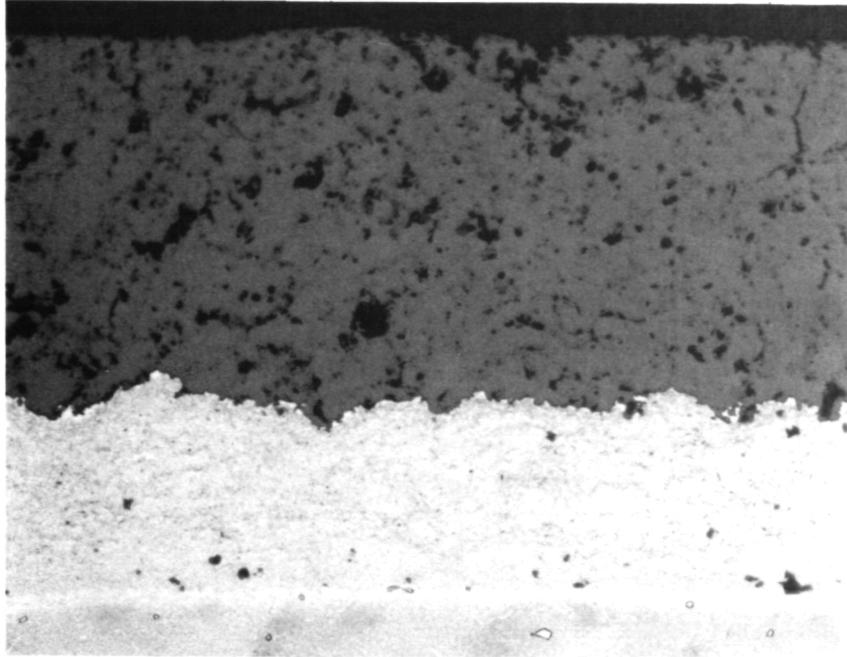


Figure 33a Pre-Test Hot Corrosion Test Specimen; 35 ppm Artificial Sea Salt/
1650°F/1 Hour Cycle

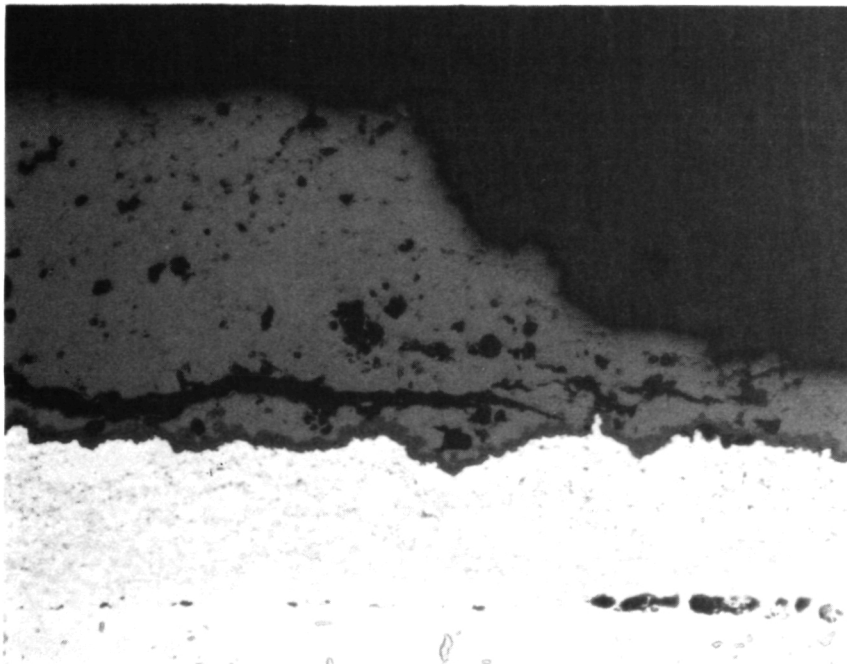
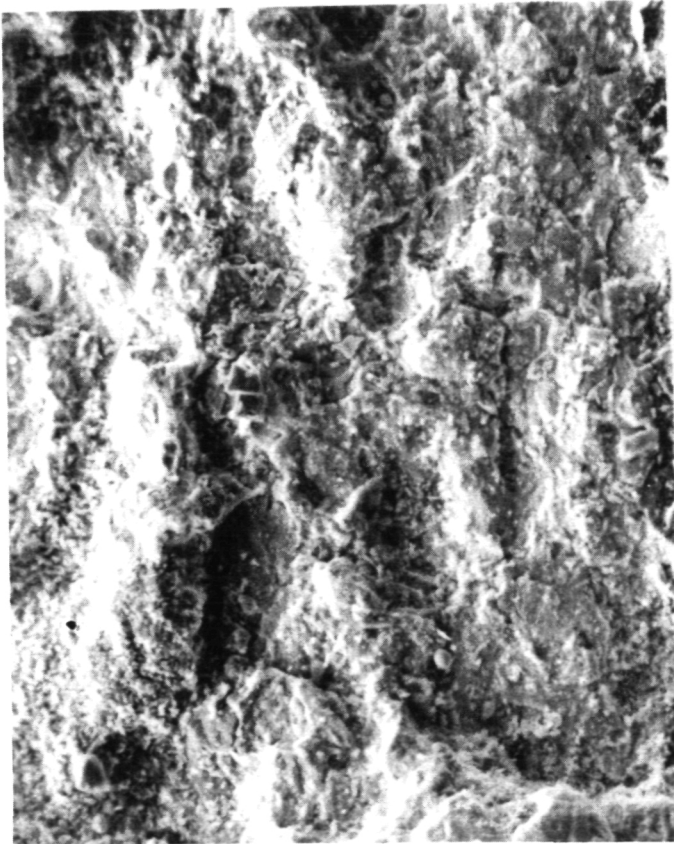


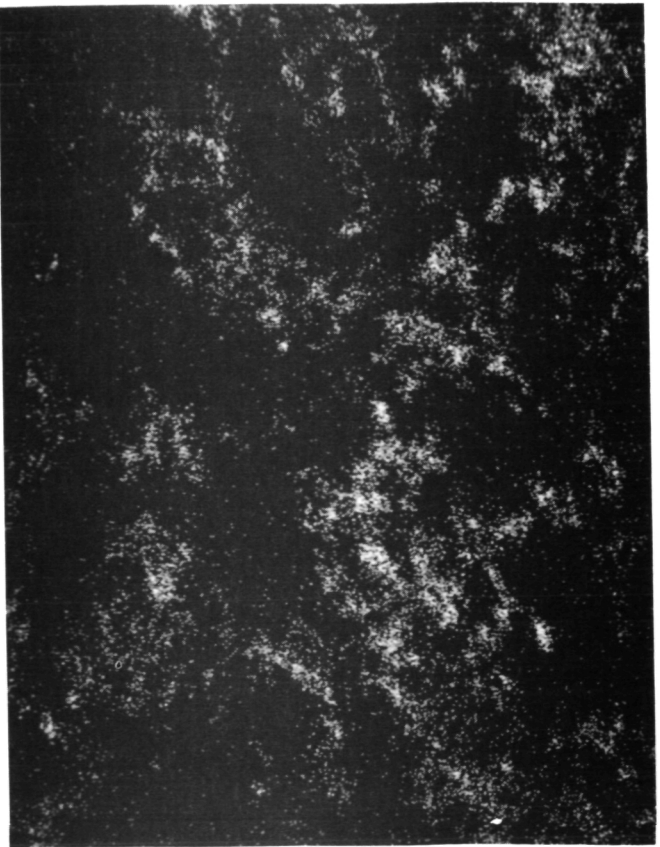
Figure 33b Post-Test Hot Corrosion Test Specimen After 1000 hrs at 35 ppm
Artificial Sea Salt/1650°F/1 Hour Cycle

ORIGINAL PAGE IS
OF POOR QUALITY

Figure 34 Cyclic Hot Corrosion Test
Specimen Surface (HST 086)
After 450 Hrs./1650°F - High
Corrodent Level Test



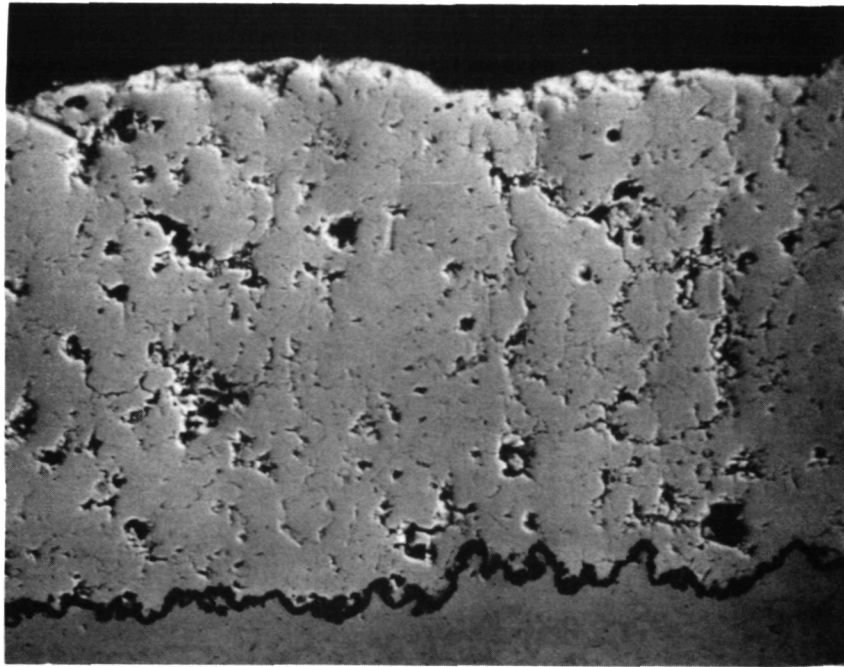
a) SEI Detailed Image Of Coating On Test
Bar Surface 800X



b) Sulfur X-Ray Map 800X

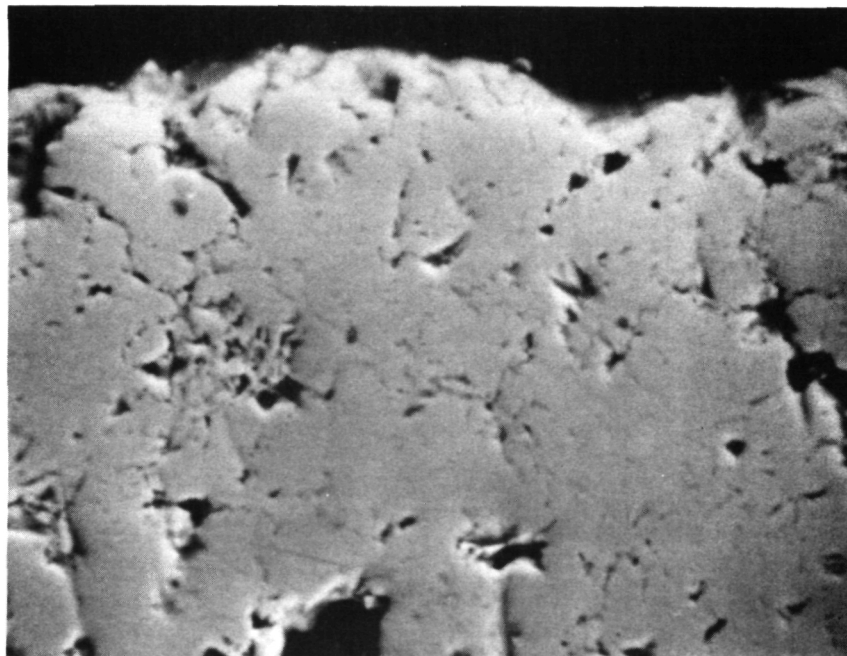


c) Sulfur X-Ray Map 800X



a) BEI

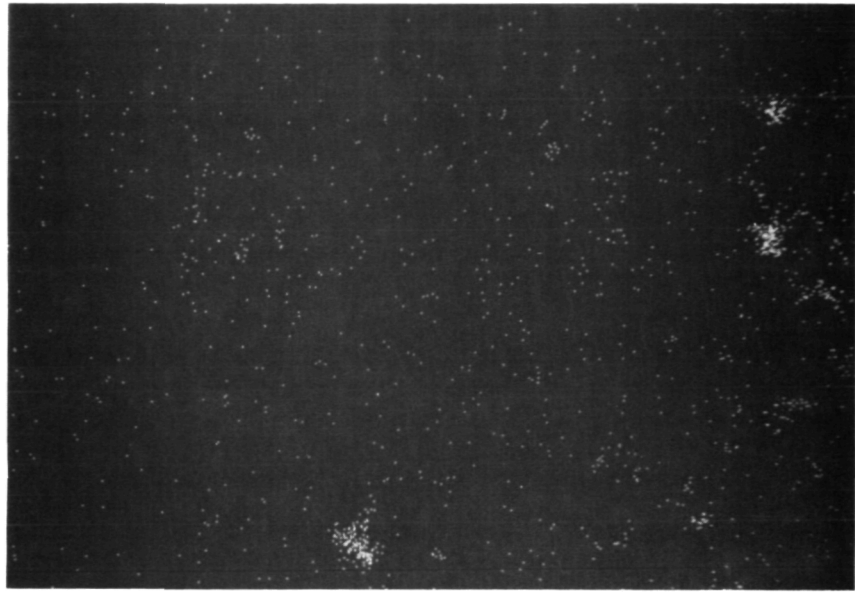
300X



b) BEI Detailed Image Of Outer Surface Of
Coating

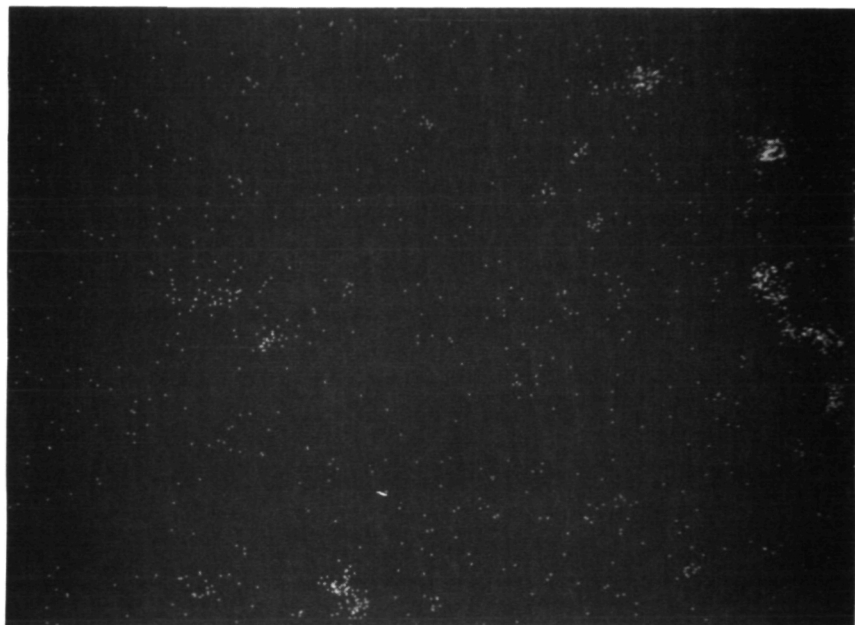
1000X

Figure 35 Cyclic Hot Corrosion Test Specimen After 450 Hrs at 1650°F. High
35 ppm Corrodent Level in Area Near Failure.



c) Na X-Ray Map

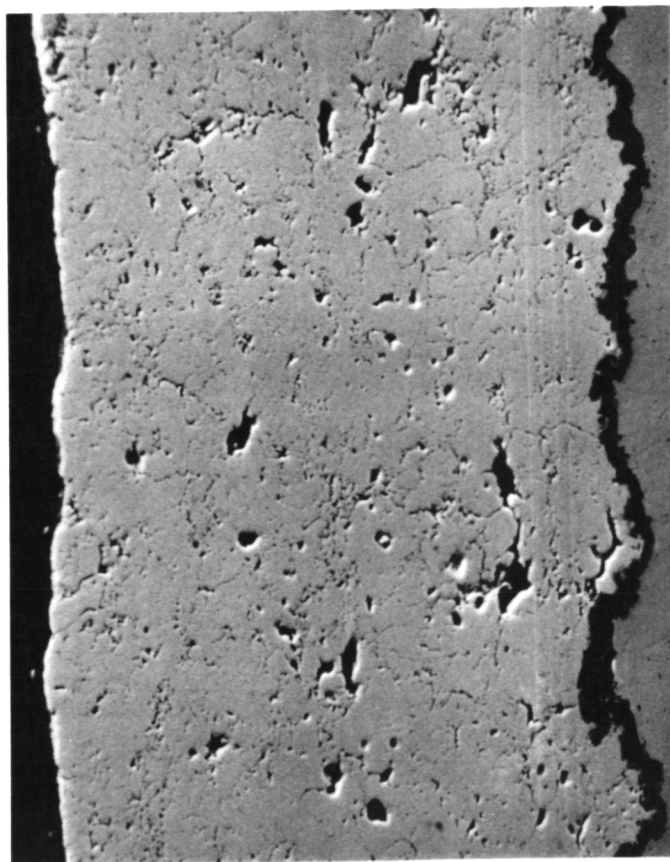
1000X



d) Sulfur X-Ray Map

1000X

(continued)
Figure 35 Cyclic Hot Corrosion Test Specimen After 450 Hrs at 1650°F. High Corroderent Level in Area Near Failure.



a) BEI

300X



b) BEI

Detailed Image of Oxide Layer

2000X



c)

Al X-Ray Map

2000X



d)

Mg X-Ray Map

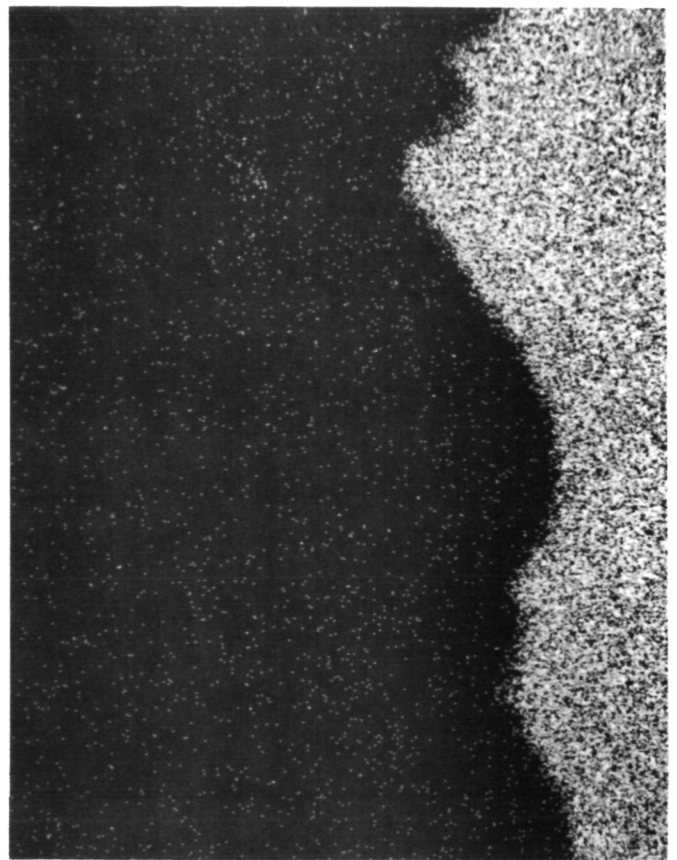
2000X

Figure 36 Cyclic Hot Corrosion Post-Test Specimen After 1000 hrs at 1650°F/
Long Cycle/35 ppm Artificial Sea Salt/1.3% SO₃

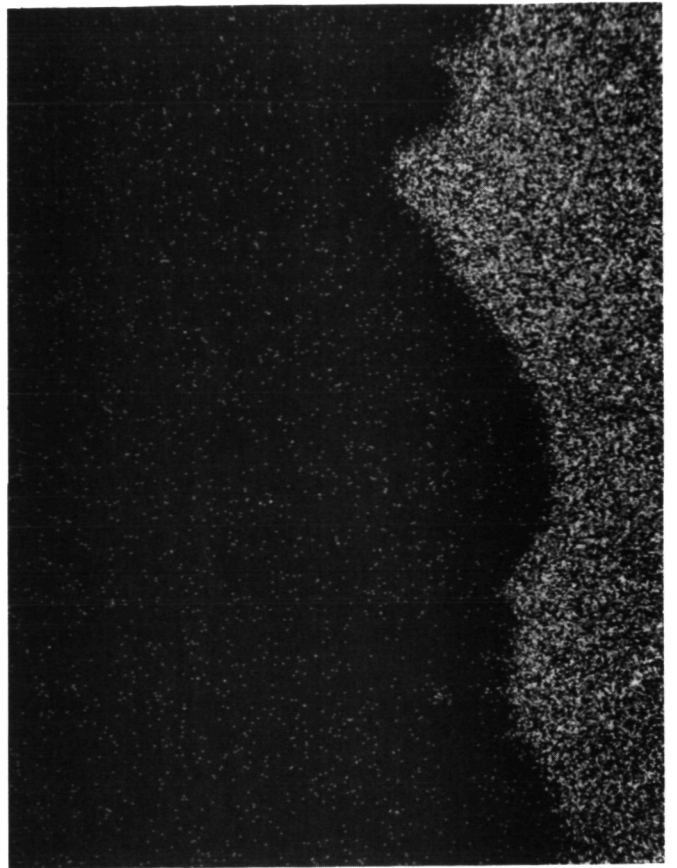
Figure 36 (Continued)
Cyclic Hot Corrosion Post-Test
Specimen After 1000 hrs at 1650°F/
Long Cycle/35 ppm Artificial Sea
Salt/1.3% SO₃



e) Cr X-Ray Map 2000X



f) Ni X-Ray Map 2000X



g) Co X-Ray Map 2000X

Table XV shows X-ray diffraction analysis for representative high corrodent level test specimens (condition H). It is noted that "higher" time specimens show a significant increase in v/o monoclinic and also up to 10 v/o of other phases; i.e., fcc NiO, or the orthorhombic NiCrO₄, Ca₂SiO₄. This increase in monoclinic phase (destabilization of ZrO₂) has been reported to influence coating life.

TABLE XV
X-RAY DIFFRACTION ANALYSIS FOR SOME REPRESENTATIVE CYCLIC
HOT CORROSION POST-TEST SPECIMENS
(High Corrodent Level)

Specimen/ Location	v/o fcc ZrO ₂	v/o Tetragonal ZrO ₂	v/o Monoclinic ZrO ₂	Other	Failure Time (hrs)
(HST #086) Spalled Area	60-65	35-40	5	1 v/o Unidentified	450
(HST #088) Spalled Area	50	25-35	15-10	10 v/o fcc and /or MgO 1 v/o orthorhombic NiCrO ₄	615
(HST #091) Spalled Area	45-50	45-50	10	1 v/o fcc NiO, MgO and/or Ca ₂ SiO ₂	693

The low corrodent level test (Condition J) 10 ppm artificial sea salt, 1.3% SO₃, was terminated after completing 1000 hrs of test time. None of the specimens showed any sign of coating degradation. The specimens did show, however, a dark brown surface appearance as seen in Figure 37.

Table XVI presents X-ray diffraction data for two representative low corrodent level samples. The phase distribution as shown is not consistent for these two specimens exposed for the same length of time. There may have been some experimental error in determining the v/o phases presents, one key point to make is that for at least one specimen a high v/o monoclinic ZrO₂ was detected. However, no failures occurred. Thus, the thermomechanical failure mode; i.e., thermal expansion difference between infiltrated synthetic sea salt and the TBC may be more critical than thermochemical interactions in determining ceramic coating life.

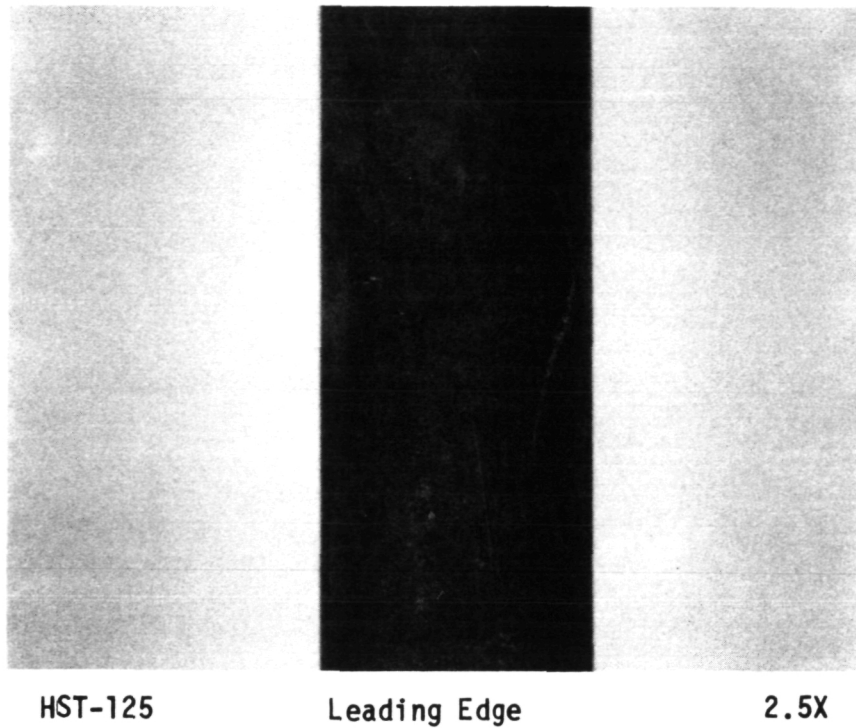


Figure 37 Light Photomicrograph of Test Specimen After 1000 hrs at 1650°F/
Long Cycle/10 ppm Synthetic Sea Salt/1.3% SO₃ - Condition J

TABLE XVI
X-RAY DIFFRACTION ANALYSES OF SOME REPRESENTATIVE POST-TEST SPECIMENS,
CYCLIC HOT CORROSION TEST (Low Corrodent Level)

Specimen ID/ Exposure Time	FCC ZrO ₂	Tetragonal ZrO ₂	Monoclinic ZrO ₂	Other
HST 113/ 1000 hrs	42-45	32-35	5	10-7 fcc NiCr ₂ O ₄ and/or NiFe ₂ O ₄ spinel), 5 fcc NiO and and/or MgO, 3-1 hexagonal NiS, 2-1 bcc Y ₂ O ₃ , 1 tetra- gonal TiO ₂ , and possibly 1 hexagonal α - Al ₂ O ₃
HST 131/ 1000 hrs	30-35	25-20	25-20	5 fcc NiFe ₂ O ₄ and/or NiFe ₂ O ₄ (spinel), 5 hexagonal NiS, 10-15 fcc (Fe,Ni)S ₂

The high corrosive level; i.e., 35 ppm, fraction test (Condition K), is continuing with no failures having occurred after several hundred hours. Duplicate specimens were cycled to each of the 10%, 20%, 90% fractions of total anticipated test life and are being metallographically examined to identify and characterize accumulated damage. The test will continue until failure of the 100% specimens or until 1000 hours is reached.

3.1.3 Task IB.2 Determine Physical/Mechanical Properties

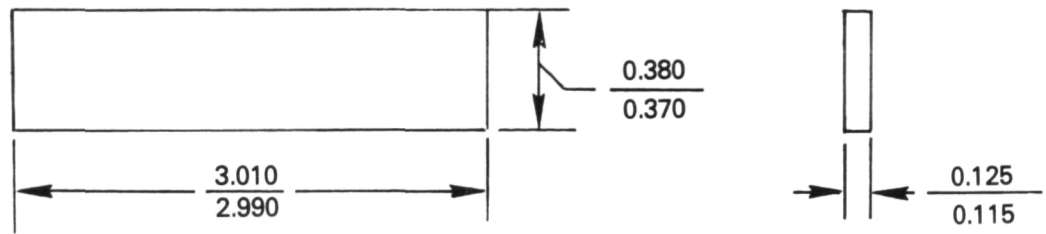
The objective of this subtask is to conduct key mechanical and thermo-mechanical physical property testing to acquire data required for thermal and stress analysis.

Coating physical and mechanical properties listed in Table XVII are being measured to permit structural analysis of the thermal barrier coating system. Figures 38, 39, 40 show the bulk ceramic specimen geometries being used. Coating specimens have been fabricated to obtain these properties. All required substrate properties currently are available.

TABLE XVII
COATING PROPERTY TESTS

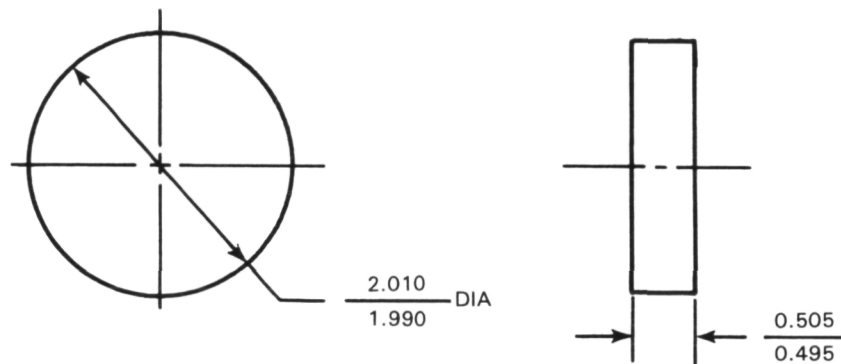
	<u>Virgin Ceramic (Bulk Specimen)</u>	<u>Virgin Bond Coat (Bulk Specimen)</u>
o Elastic Constants	4 Tests: 1000°F, 1300°F, 1600°F, 2100°F	-
o Creep (4 pt. bend)	9 Tests (3 stress levels): 1000°F, 1600°F, 2100°F	-
o Thermal Conductivity	3 Tests: 1000°F, 1600°F, 2100°F	3 Tests: 1000°F, 1600°F, 2100°F
o Thermal Expansion	2 Tests: 1000°F, 2100°F	2 Tests: 1000°F, 2100°F
o Specific Heat	3 Tests: 1000°F, 1600°F, 2100°F	3 Tests: 1000°F, 1600°F, 2100°F
o Isothermal LCF		9 Tests: 1000°F, 1400°F, 2100°F

Total number of tests is 42.



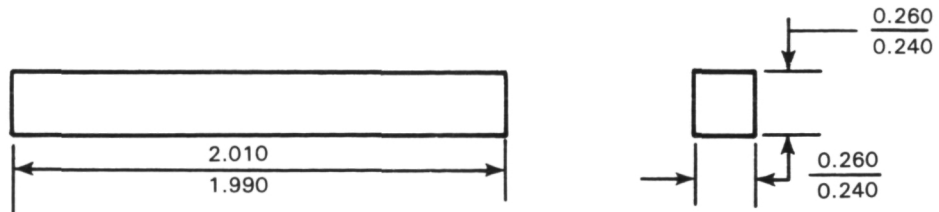
All Dimensions Shown In Inches

Figure 38 Bulk Four Point Bend Specimen Geometry Utilized for Determination of Elastic Constants, Stress Rupture, Creep, and Isothermal LCF Tests



All Dimensions Shown In Inches

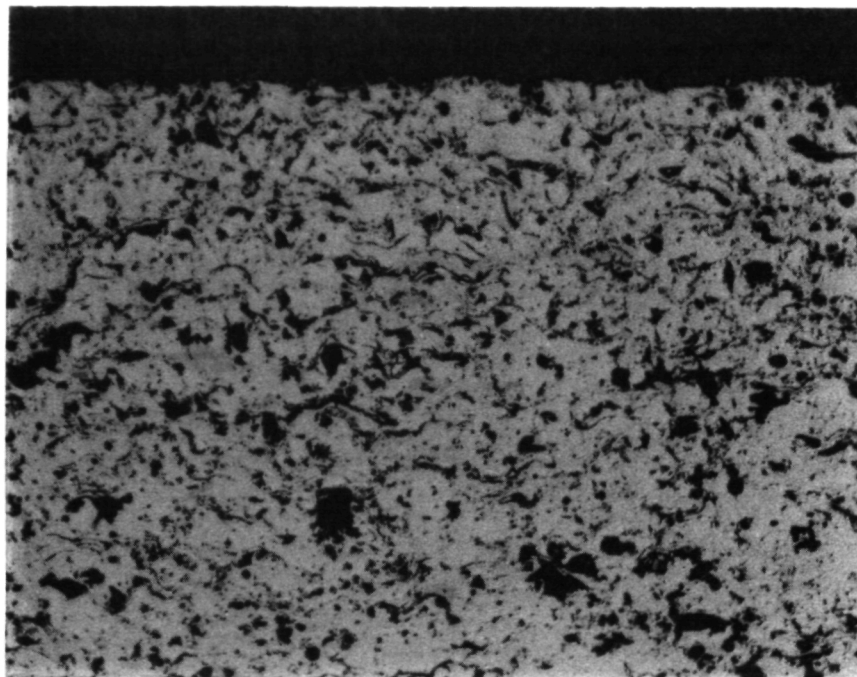
Figure 39 Thermal Conductivity Test Specimen



All Dimensions Shown In Inches

Figure 40 Thermal Expansion Test Specimen Geometry

Bulk ceramic and metallic specimens for physical/mechanical property tests were air plasma sprayed and low pressure plasma sprayed, respectively, using standard conditions. Coating thickness of up to 1/4 - 1/2 inch were built up on mill steel panels and then the test specimens were machined off and ground to test specification dimensions. Figure 41 shows that the bulk ceramic microstructure simulates the microstructure of the 10 mil coating quite closely.



200X

Figure 41 Bulk Ceramic Microstructure Used for Physical/Mechanical Property Tests

Thermal conductivity, thermal expansion and specific heat tests for bulk ceramic specimens have been completed and the data is presented in Tables XVIII, XIX and XX respectively. Procedures used to obtain this data for these tests were conducted by Dynatech, Cambridge Mass.; test procedures are described in subsequent paragraphs. Physical property tests for bulk metallic specimens is nearing completion.

TABLE XVIII
CERAMIC THERMAL CONDUCTIVITY*

Temperature (°C/°F)	Thermal Conductivity	
	W/mK	Btu in/h ft ² F
538/1000	0.645	4.47
871/1600	0.675	4.68
1100/2012	0.660	4.58

*Tolerance: $\pm 8 - 10\%$

TABLE XIX
CERAMIC SPECIFIC HEAT

Temperature (°C/°F)	Specific Heat	
	J/g C	cal/g C (Btu/lb F)
538/1000	0.582	0.244
871/1600	0.593	0.248
1149/2100	0.603	0.253

TABLE XX
CERAMIC THERMAL EXPANSION

Temperature (°C/°F)	Coefficient of* Thermal Expansion TE x 10 ⁴	Thermal Expansion x 10 ⁶ (°C ⁻¹)
25/77	0	-
100/212	7.26	9.68
200/392	17.53	10.02
300/572	27.00	9.82
400/752	36.39	9.70
500/932	45.77	9.64
600/1112	56.25	9.78
700/1292	66.72	9.88
800/1472	77.64	10.02
900/1652	89.15	10.19
1000/1832	100.82	10.34
1100/2012	110.64	10.29
1175/2147	116.12	10.10

*Average-from ambient temperature to temperature indicated

3.1.3.1 Experimental Procedure for Physical Property Tests

Physical property tests were conducted at DYNATECH R/D COMPANY, located in Cambridge, Massachusetts. Procedures used for these tests are described below.

Thermal Conductivity - A comparative method was used to determine thermal conductivity. The sample was instrumented with thermocouples and placed between two instrumented reference standards of identical geometry to the sample. The composite stack was fitted between an upper heater and lower heater and the complete system placed on a liquid cooled heat sink. A load was applied to the top of the system and a thermal guard which could be heated or cooled was placed around the system.

A temperature gradient was established in the stack; radial heat loss was minimized by establishing a similar gradient in the guard tube. The system reached equilibrium after which successive readings of temperatures at various points were averaged and evaluated. From this data, heat flux was determined and specimen thermal conductivity calculated. The results are shown in Table XVIII.

Specific Heat - The specific heat was determined using a high temperature calibrated copper drop calorimeter. The sample was attached to a 3mm platinum support wire and suspended vertically at the center of a three-zone controlled temperature furnace with the sample resting upon the receiver below it. Thermocouples were attached such that junctions touched the sample near the top and bottom.

The sample was allowed to attain a selected equilibrium temperature for a period of time on the order of 1-2 hours then regular readings of the thermocouple were taken. At a given time, the radiation shields moved to allow the sample to fall and come to rest in the receiver. When the sample came to rest, these shields returned to the original position to reduce any radiation heat transfer from the furnace to the receiver or convective and radiant heat transfer from the receiver to the outside. The temperature of the copper receiver was taken regularly. Following a drop the receiver system was allowed to come to equilibrium for the order of two hours. The specific heat was calculated at selected temperature by differentiation and substitution and is shown in Table XIX.

Thermal Expansion - The room temperature length of each specimen was measured before the test. The specimen was then placed in an electronic automatic recording dilatometer and a thermocouple placed in contact with the center of the sample. An environmental chamber which controlled the temperature at constant rates surrounded the system. The dilatometer was allowed to run with length and the temperature recorded continuously and autographically. The results for the specimens tested are given in Table XX.

Bulk ceramic mechanical property testing had been initiated. Room temperature, four point bent tests were conducted to aid in understanding future test results. Four point bend specimens were cycled at 1 KSI and 3 KSI. The results are as follows:

- 1) 85% dense bulk 7YSZ ceramic exhibits nonlinear behavior which is proportional to the stress level and the number of cycles. Some data for monolithic (dense ZrO_2) ceramics found in the literature suggested that this nonlinearity is not observed.
- 2) The modulus appears to decrease with increasing loading and increasing number of cycles.
- 3) Similar behavior is noted in compression and tension. This suggests cracking occurred in random directions other than the transverse direction.
- 4) First cycle behaves differently from the second and subsequent cycles which may suggest the elimination of residual stresses and cracking occurring. Based on this result, all specimens for static testing will be cycled once prior to testing.

After cycling, one specimen was taken out to failure. The outer fiber tensile stress at fracture was 6.89 KSI with an apparent modulus of 5.84×10^6 psi, Poissons ratio of 0.0909 and an effective percent strain of 0.255. These results are on the order of the data documented in the literature. The psuedo-ductility present in the form of nonlinear behavior is believed due to cracks opening up.

It must be noted that all specimens were somewhat bowed and skewed due to residual stresses. Measurements of this nature were carefully documented for every specimen.

3.1.4 Task IC - Predominant Mode Determinations

Based on the information generated in Tasks 1A and 1B, the relative importance of the thermomechanical and thermochemical failure modes will be determined and three failure mode confirmation tests will be conducted to determine the limits of each mode. An empirically based correlative life prediction model will be developed to independently predict life for the predominant failure mode.

The thermal cycle failure correlation model will constitute plots of thermally induced loading (stress or strain range) vs. number of cycles to failure. Values of thermally induced loading for the various test conditions investigated in Task 1B will be calculated using the transient asymmetrical temperature distribution for each test condition. These data will be obtained for each test condition during the course of Task 1B testing by a combination of thermocouple data and thermal analysis. Temperature-dependent material properties, i.e., elastic moduli and thermal expansion coefficient, for each constituent of the TBC system will be used together with the calibrated transient temperature distribution to carry out a uniaxial (one dimensional) thermoelastic stress analysis. The transient thermoelastic analysis will include the axial and the thermal bending effects produced by the asymmetrical temperature distribution.

The proposed test method to be used for failure mode confirmation testing will involve clean fuel and/or ducted cyclic burner rig testing as appropriate to the predominant mode determined above. The burner rig apparatus to be used for this testing will be as described for the subtask 1B failure mode determination tests. To allow more precise instrumentation and control of thermal environment, only a single specimen will be tested in each rig. This specimen will be located in the center of the rotating spindle, so that it rotates about its own axis and thus has a uniform circumferential temperature distribution. Figure 42 shows the specimen. To improve the simulation of airfoil conditions, the specimen will be hollow and will incorporate internal cooling to provide a steady state thermal gradient across the TBC. Three sets of test parameters, different from those employed in Task 1B, will be recommended to simulate typical airfoil mission cycles.

3.1.4.1 Task 1C.1 Development Preliminary Life Prediction System

The objective of this subtask is to determine the relative importance of various failure modes through the development of empirically based correlative life prediction models. Specific failure modes to be addressed in this model development include cyclic stress induced cracking, thermal exposure and hot corrosion. Using a typical engine mission cycle, these life prediction models will be used to independently predicted mission cycle coating life for each failure mode.

In order to accurately characterize key coating life driving parameters such as temperature, stress and strain throughout a test cycle, thermocouple measurements from the instrumented specimen were obtained. The temperatures obtained from the instrumented specimens served as boundary conditions for transient thermal-structural analyses employing a general purpose finite element computer program designed for the linear and nonlinear static and dynamic analysis of structures. To execute this analysis, a specimen analysis mesh has been generated (Figure 43) that includes detail of the thermal barrier coating metallic bond coat and substrate. Currently available material properties are being used for the initial calculations. Material property data developed under this program will be used to update the computations as it becomes available. Detailed output from these computations along with failure mode observations will form the basis for the formulation of life prediction models.

A MARC finite element break up for the Figure 3 test specimen was completed and is shown in Figures 44 and 45, and a test case having an analytical solution was executed. Imposed conditions for this test case were constant material properties and a uniform convective environment externally, making a radially dependent transient conduction problem. This was compared to the classic analytic solution found in Conduction of Heat in Solids by Carslow and Jaeger. MARC results compared favorably with the classical analysis. Discrepancy between the two solutions remained very small throughout the entire transient as illustrated in Figure 46. The greatest difference occurred at about 20 seconds into the transient. Total transient time to steady state temperature determined by both approaches were in agreement as were results early in the transient where interest is great. Disagreement between the two analyses can be reduced if required by lowering the allowable time step at the cost of running time.

ORIGINAL PAGE IS
OF POOR QUALITY

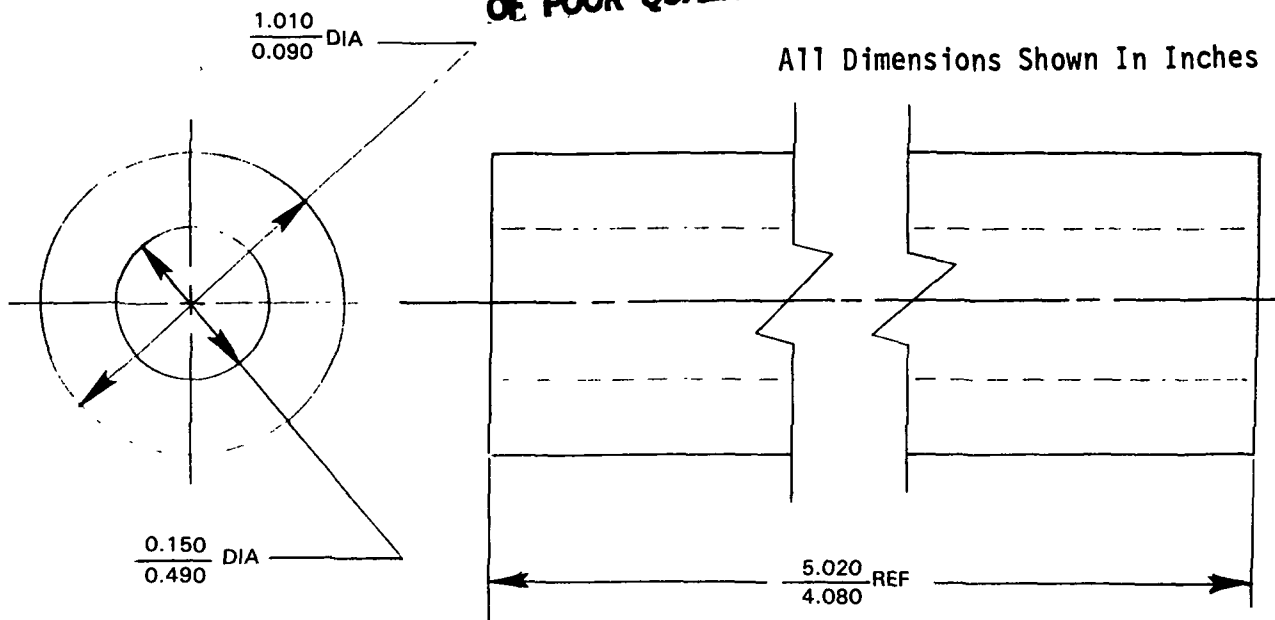


Figure 42 Single Rotating, Internally-Cooled Tube Tests Specimen Geometry

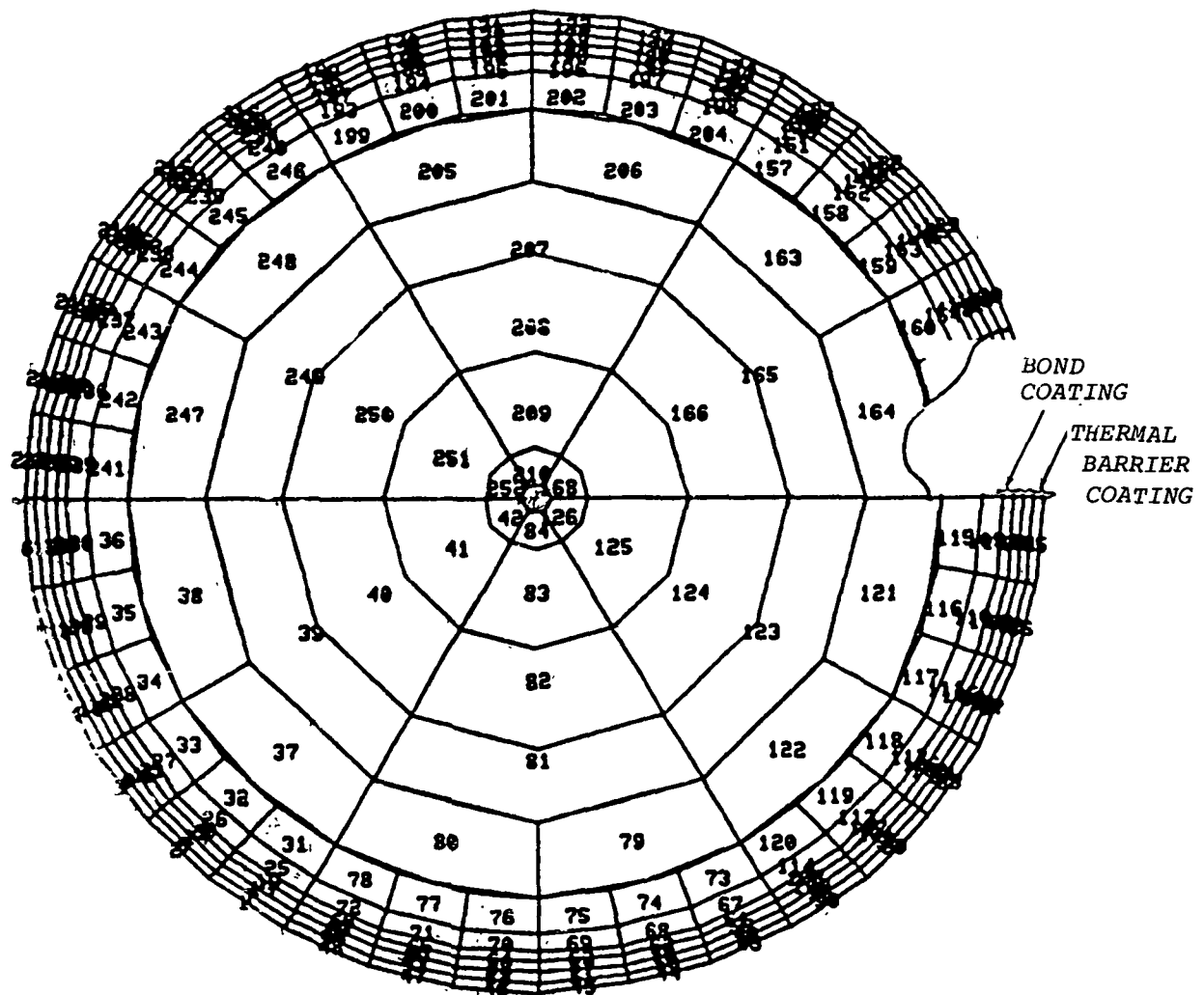


Figure 43 Thermal Barrier Coating Thermal Analysis Mesh

ORIGINAL PAGE IS
OF POOR QUALITY

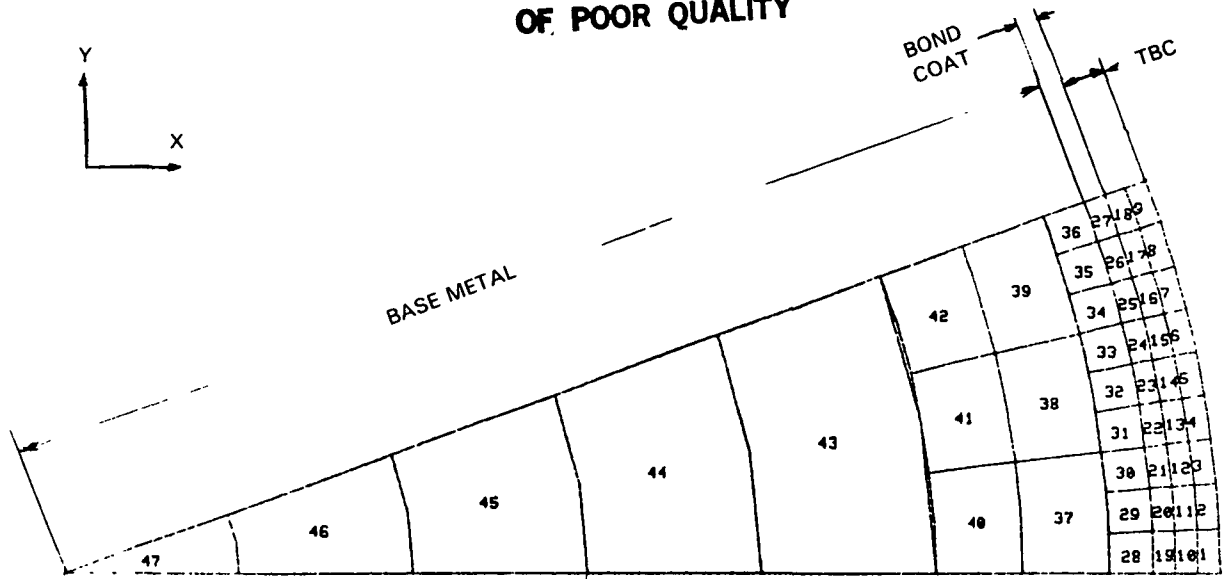


Figure 44 Modified Thermal Barrier Coating Life Model

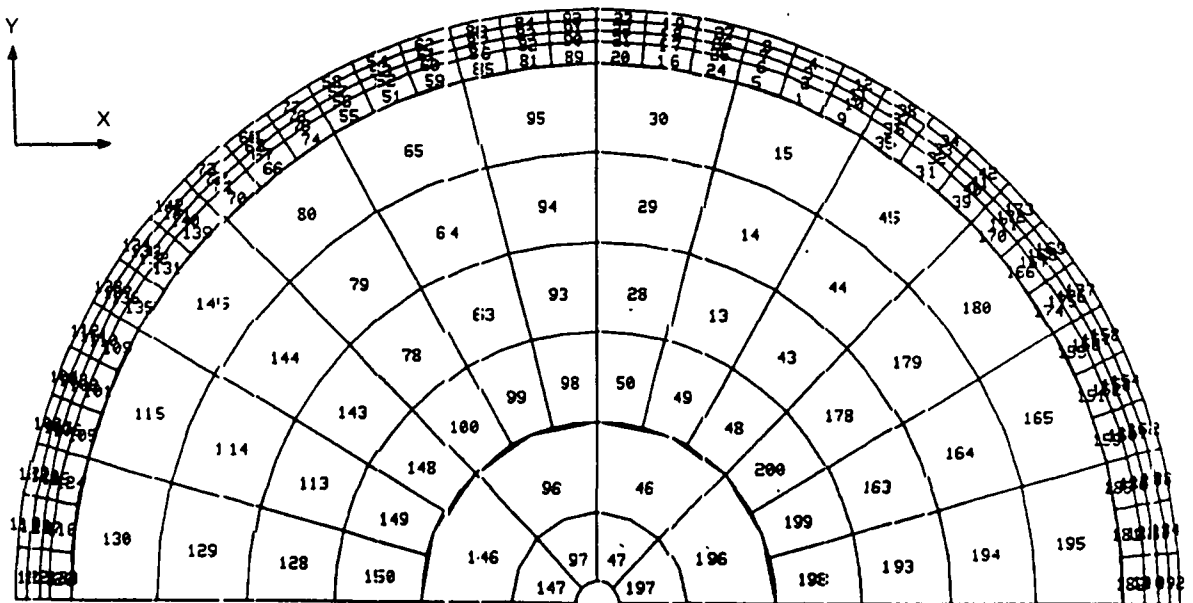


Figure 45 Finite Element Breakup

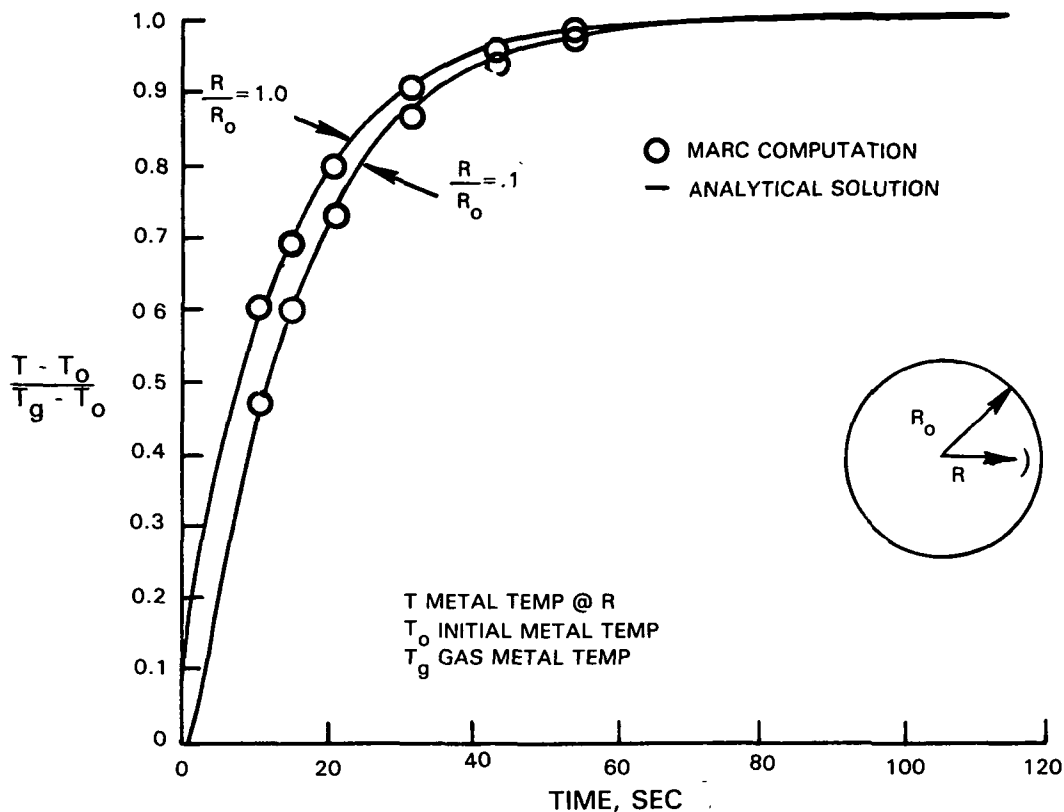


Figure 46 Results from Initial Marc Finite Element Heat Transfer Analysis Conducted on Test Specimen

Design of the instrumented specimen, used to obtain experimental transient temperature data is shown in Figure 47. Eight grooves were cut, aligned with the axis of the specimen to accommodate the thermocouple sensors and leads. The leads were routed along "isotherms", reducing conduction errors. In addition, the T.C. sensors were welded in place to eliminate any differences between sensor readings and actual metal readings. After installation of the sensors the grooves were filled with a material having thermal properties similar to the base metal and then machined to the original contour. Thermocouples were placed every 45°, from 0° to 180°, where 180° is inside the carousel where spallation is normally first observed (failure zone).

Two specimens were instrumented; one with and one without the ceramic coating layer. The uncoated specimen enabled determination of the surface convective boundary. The same derived convective boundary conditions will be imposed on the coated specimens. The difference in sensor readings will be due to the insulating effect of the ceramic coating. As time and temperature increase, radiation effects occur. This was monitored by having a band of material with known emissivity on the ceramic surface enabling temperatures to be read optically. Once the surface conditions were determined the entire temperature and corresponding thermal stress fields could be established.

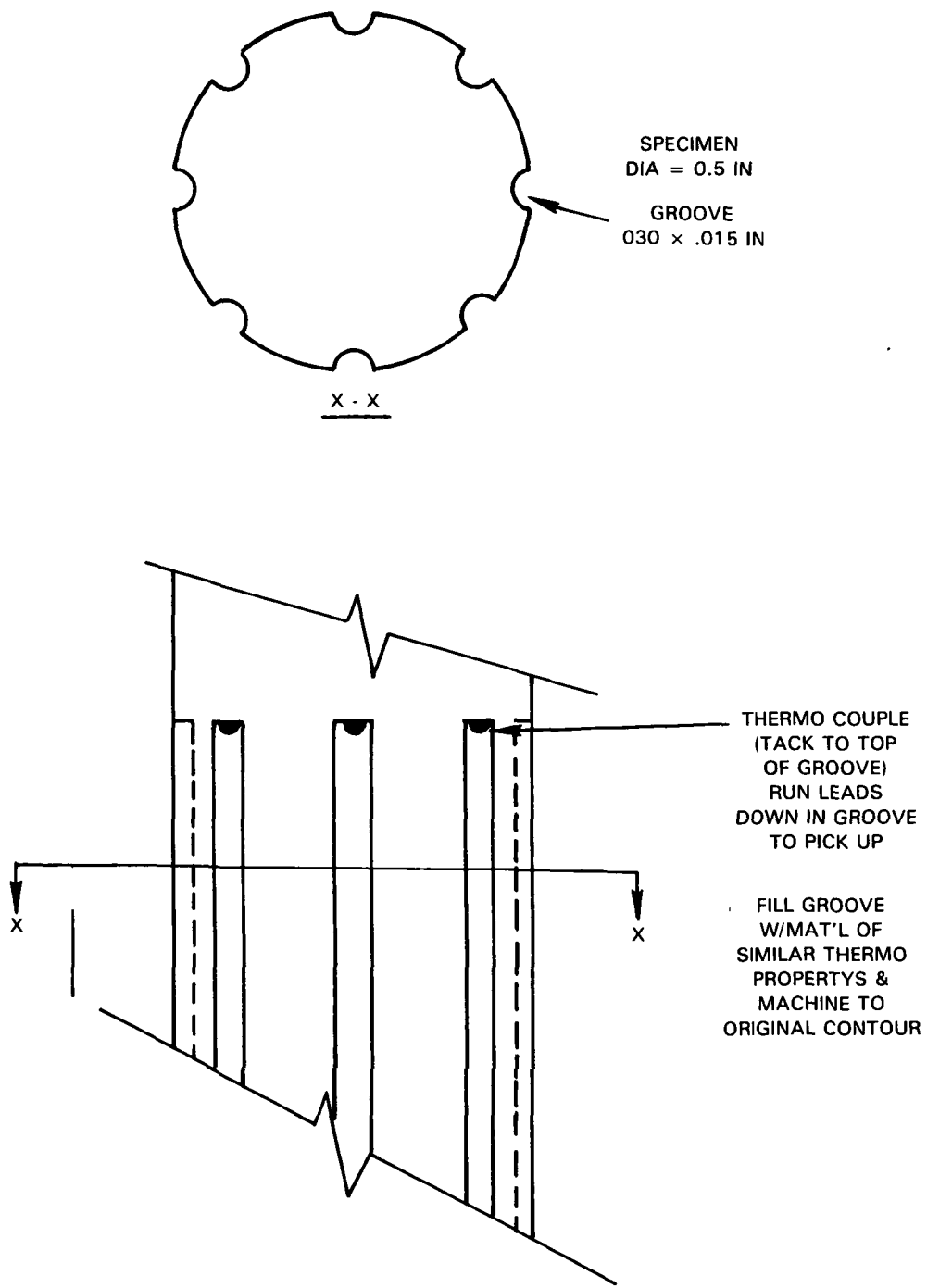


Figure 47 Instrumented Test Specimen

Figure 48 presents the test results for the thermocouples located at 180° on both specimens. Figures 49 and 50 show the results for the heatup portion of the cycle of all the thermocouples. Location of the thermocouples is shown in Figures 49 and 50 with the numbers corresponding to channels on the data collection equipment. For both specimens the circumferential variation in temperature is insignificant in the spallation zone. These results show that the dominant temperature gradients are in the radial direction.

Effort was completed to model analytically the measured temperature data in the failure zone of the uncoated specimen during the heatup portion of the 2100°F, short cycle, fast heatup rate test (Condition D1). The analysis was done on a nominal specimen and it is anticipated that accounting for actual specimen diameters and coating thicknesses will yield good agreement.

This analysis considered the following steps:

- I. The measured temperature of the specimen surface at the end of the heatup time was taken to be equal to the local gas temperature.
- II. Known burner exit conditions (temperature, mass flow and fuel/air ratio) used with the local gas temperature taken at the end of the heatup allowed the mass of test cell air entrainment to be established.
- III. Holding the entrained air constant, local gas temperature was determined as a function of burner fuel/air ratio and the gas temperature vs. time was established (see Figure 51).
- IV. "MARC" was run using the T_{gas} vs. time obtained previously, iterating on the heat transfer coefficient until data was matched on the uncoated specimen. "MARC" results were within 2° (average) of the data and are presented in Figure 52.
- V. Using T_g and the heat transfer coefficient vs. time of step IV above, "MARC" was on the coated model to predict temperature vs. time at the coating substrate interface. Using the test data available for thermal barrier coating properties (K , C_v) and 10 mil coating thickness, "MARC" results were hotter by an average of 45° than the data.

The MARC, 2100°F, short cycle, fast heatup rate (Condition D1) test cycle data match made for the coated specimen is shown in Figure 53. Since the MARC match is good for approximately the first 30 seconds of transient heatup time, thermal-stress analysis can be initiated for this part of the cycle.

A detailed analysis of the burner rig data which has been obtained has yielded an acceptable temperature prediction scheme. As a consequence a transient thermal analysis for each characterized test cycle is presently being conducted using previously generated temperature data and updated material property data. A transient thermoelastic analysis for each test cycle is also currently being executed employing the temperatures generated by above discussed thermal analysis. The best currently available material properties are being utilized for this analysis with an update being planned when the material property data currently being developed under this contract becomes available. Based on results of these thermal and stress analyses, empirically based life prediction models will be developed for the predominant observed modes of damage.

3.1.4.2 Task IC.2 Verification Tests

The objective of this subtask is to verify the relative importance of various failure modes based on the information generated in Tasks IA and B, and to determine the limits of each failure mode as applicable. The basis for the confirmation tests shall be preliminary life prediction model(s).

The test method to be used for failure mode verification testing will involve either clean fuel and/or ducted cyclic burner rig testing as appropriate to the predominant mode determined in Tasks IA, B, and C.1. To allow more precise instrumentation and control of the thermal environment, only a single specimen will be tested in each rig. The one-inch diameter specimens to be used for this task have been cast, machined and coated. Due to the fabrication complexity of the original design for the thermocoupled, instrumented, one-inch diameter specimen, the design is being re-assessed.

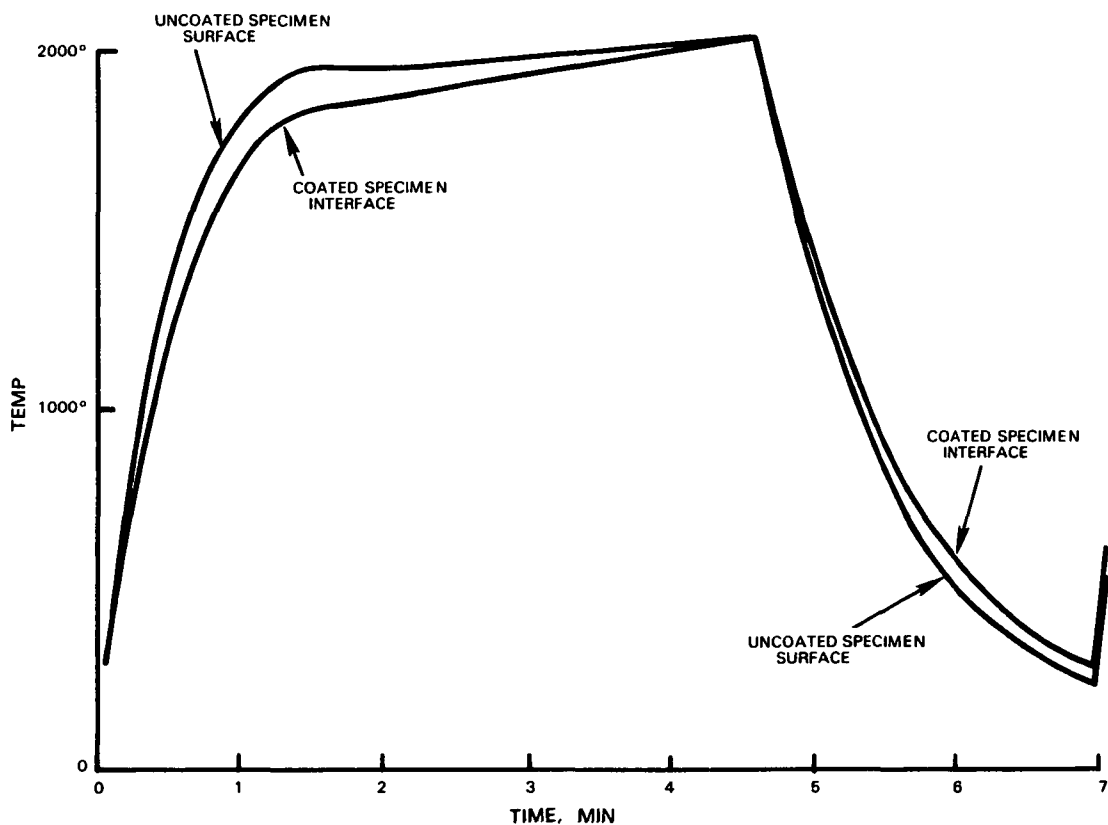


Figure 48 D1 Cycle Thermocouple Data

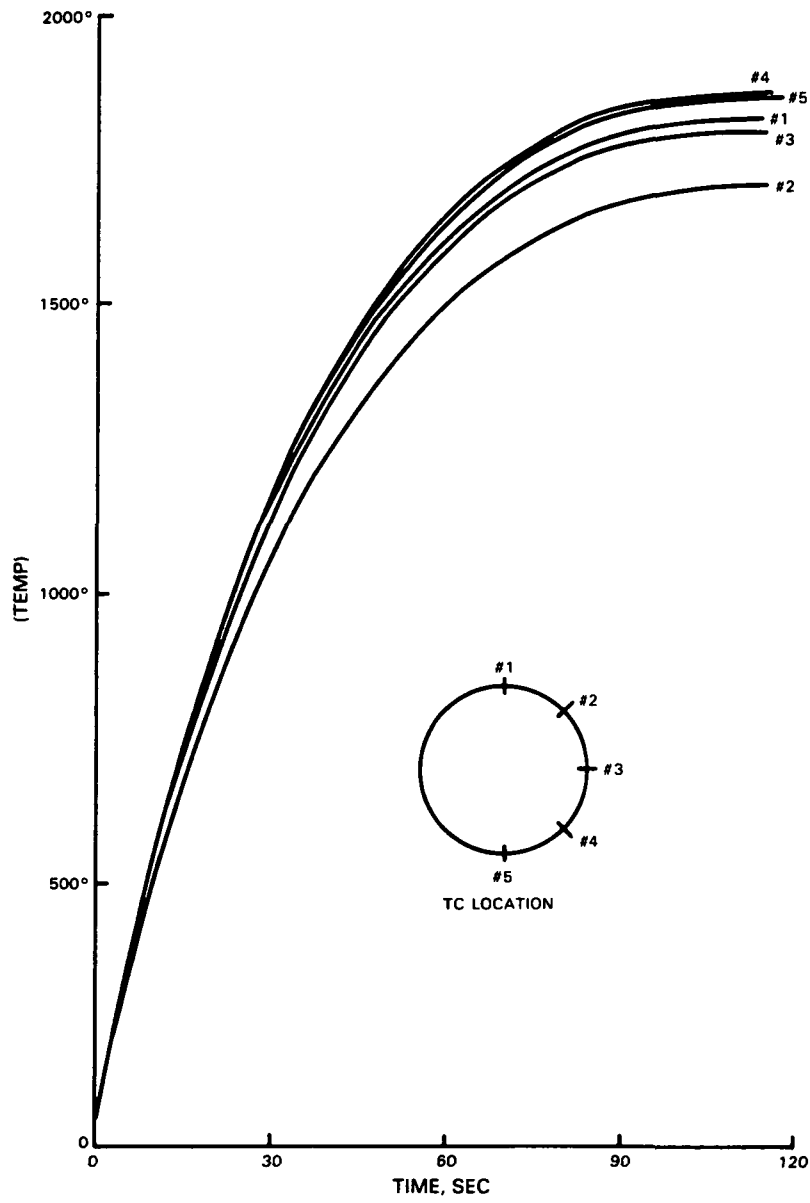


Figure 49 D1 Test, Coated Specimen Temperature at Interface

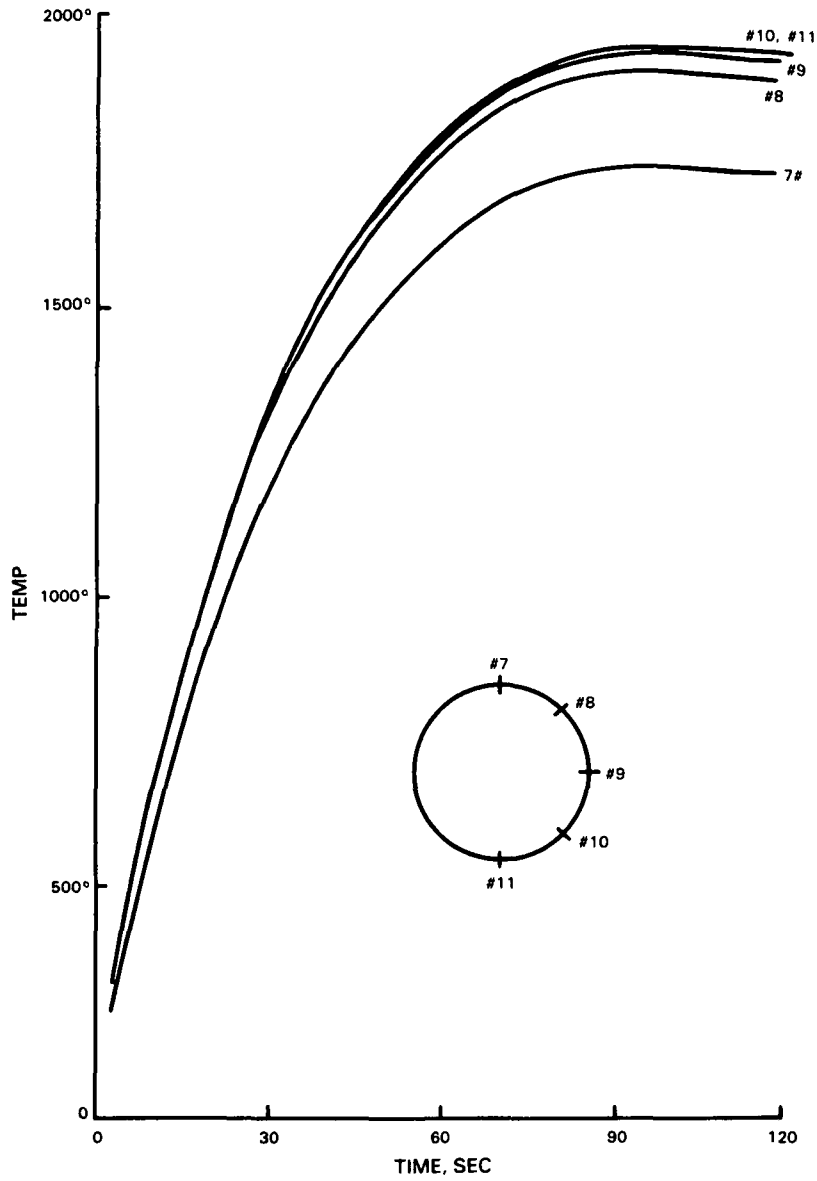


Figure 50 D1 Test, Specimen #2: Uncoated Specimen Surface Temperature

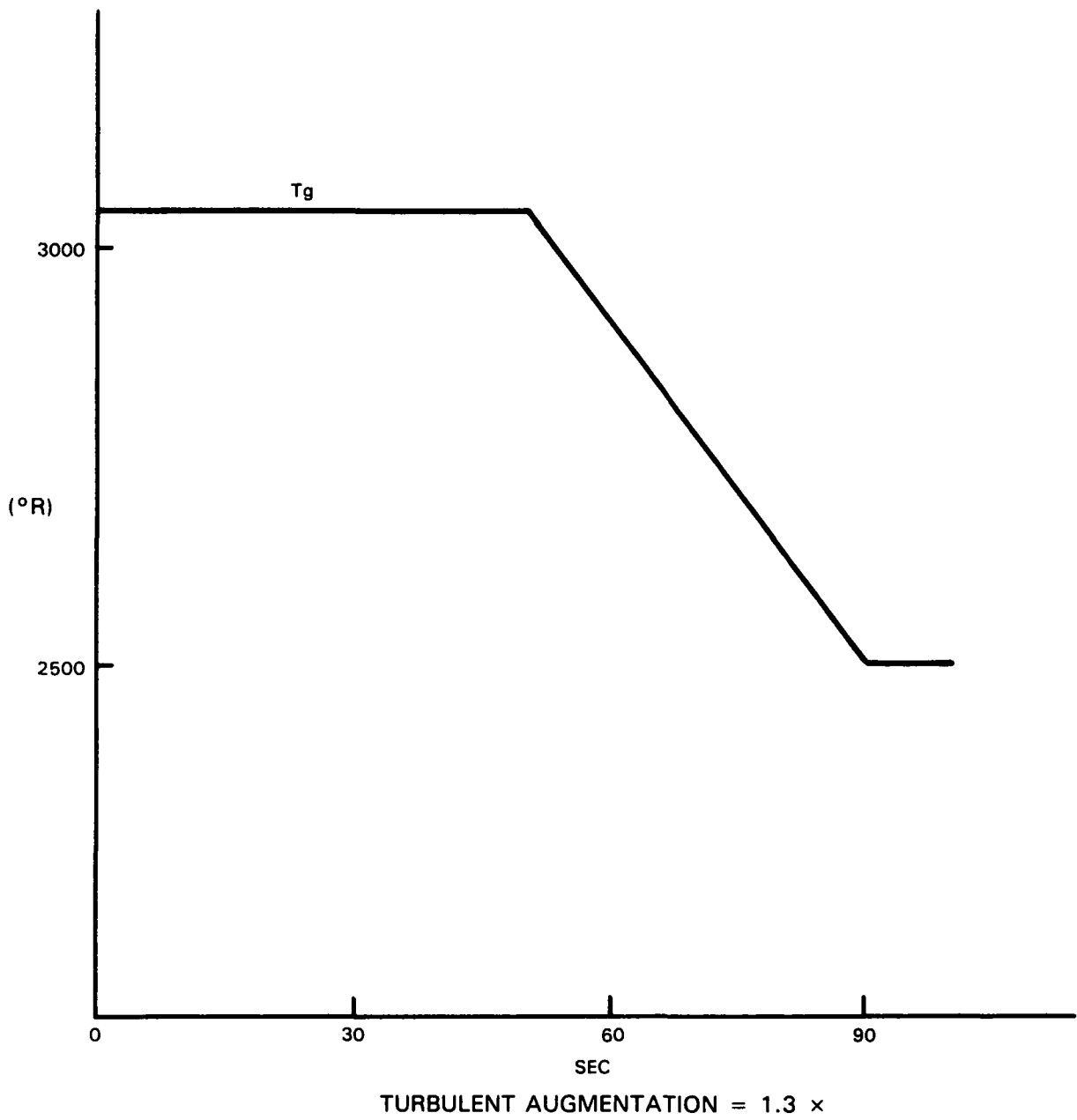


Figure 51 Cyclic Burner Rig Test at 2100°F, Short Cycle, Fast Heatup Rate (Condition D1) Data Match - Boundary Conditions in Marc Analysis

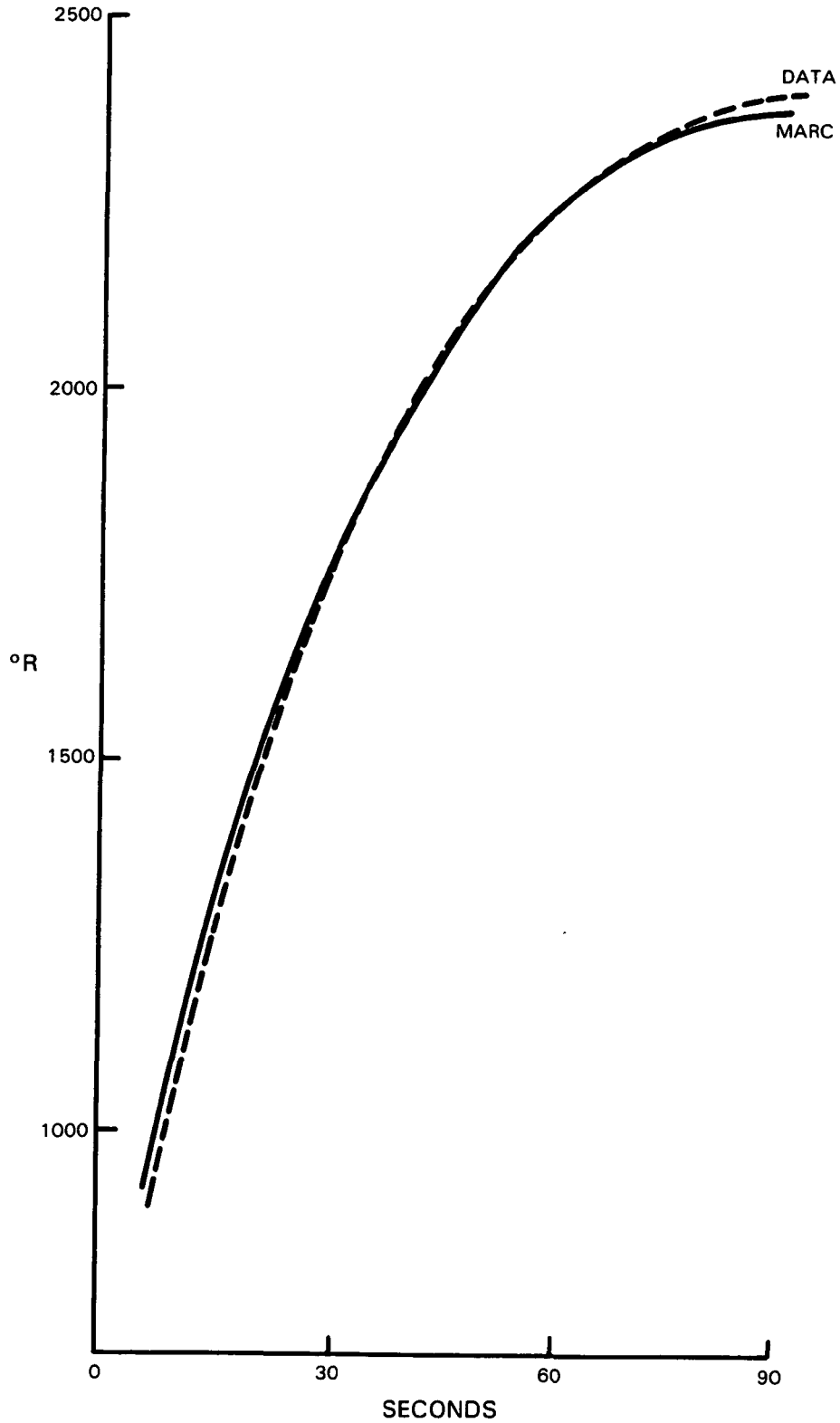


Figure 52 Cyclic Burner Rig Test at 2100°F, Short Cycle, Fast Heatup Rate (Condition D1) Data Match - Uncoated Specimen Surface

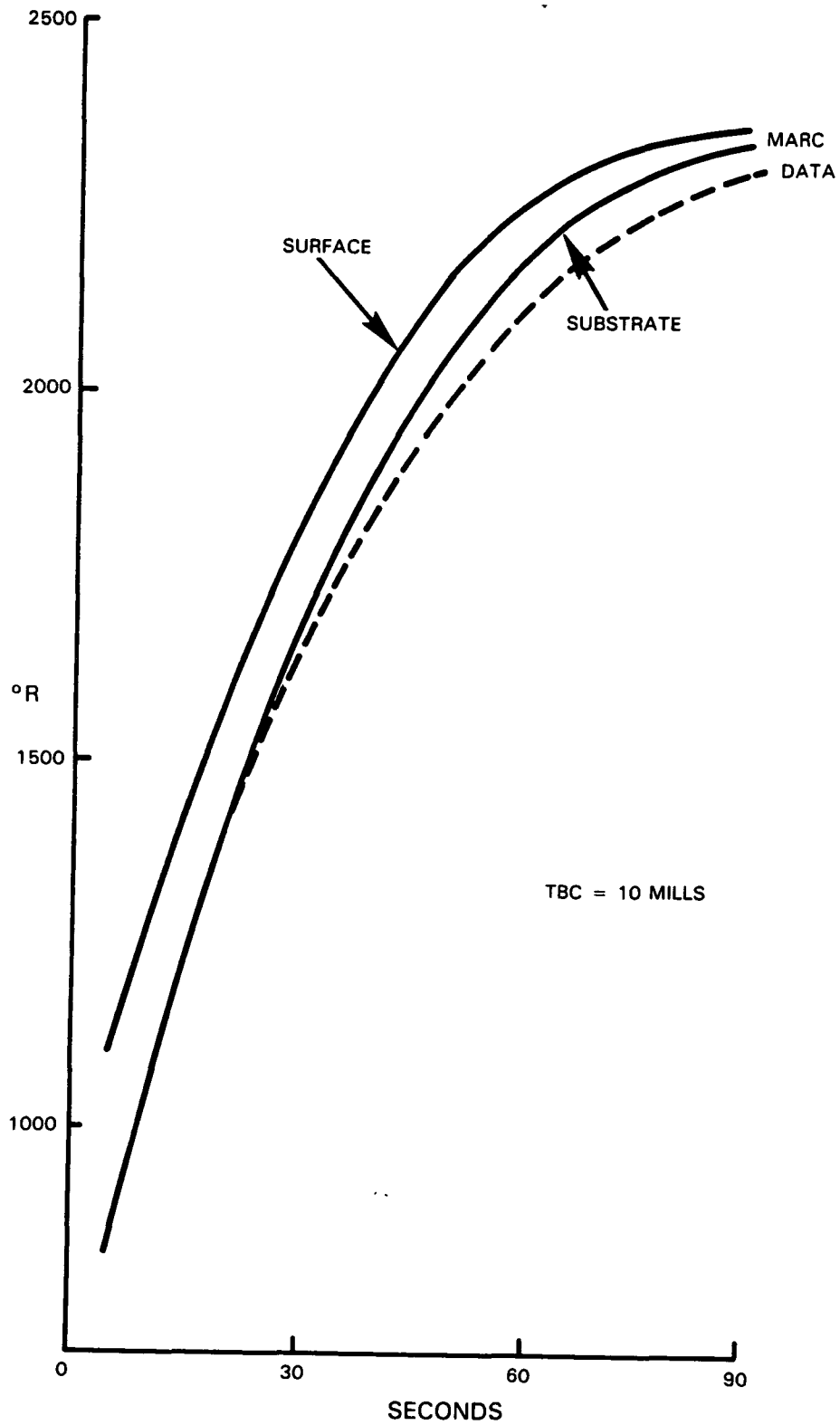


Figure 53 Cyclic Burner Rig Test at 2100°F, Short Cycle, Fast Heatup Rate (Condition D1) Data Match - Coated Specimen

4.0 CONCLUSIONS

The Task I program approach was designed to assess the predominant TBC failure mechanisms. The laboratory test program included the study of the influence of driving forces such as interface temperature, thermal cycle frequency, environment and coating thickness on ceramic spalling life. The predominant failure mode was determined to be thermomechanical ceramic spallation occurring near the interface and influenced by oxidation.

The Task I initiative included furnace exposure tests in air and argon, clean fuel cyclic burner rig tests, cyclic hot corrosion testing and physical/mechanical property testing of the bulk ceramic and metallic bond coat materials.

In the Task I testing conducted to date, coating life was found not only to be driven by interfacial temperature but is also a function of cyclic content such that shorter thermal cycles with larger transients will spall the coating before its equivalent full furnace (long cycle) life is achieved. Also for all tests a thermal transient was required to spall the ceramic; i.e., furnace tests specimens failed upon cool down during a particular thermal cycle. Consistent with the hypothesis that bond coat oxidation is an important factor effecting coating durability, it was found that thermal exposure in an inert environment limits coating degradation while pre-exposure in air reduces coating durability significantly.

Ceramic thickness effects were also found to play a role in coating longevity. Thin ceramic coatings, nominal 5 mils thick, showed an increase in coating spalling life as compared to the baseline 10 mil coating, while 15 mil thick ceramic spalled earlier than the baseline.

Cyclic hot corrosion is considered to be a secondary failure mode. As indicated by the engine exposed part evaluation, the characteristic "multi-level" type failure mode is generally not observed. In laboratory testing, TBC failures due to hot corrosion were only observed at high corrosive levels (35 ppm) in which the TBC failure life is considered to be more a function of thermomechanical damage than thermochemical interactions.

APPENDIX A CYCLIC BURNER RIG TEST DETAILS

The uncooled burner rig test employed in Task I involves cyclic flame heating and forced air cooling of coated cylindrical test specimens. A set of 12 specimens are installed on a spindle per test set at one time. These bars are rotated in the exhaust gases of a jet fuel burner rig to provide a uniform temperature for all specimens. The exhaust gases are the combustion products of Jet A fuel and air, with a velocity of Mach 0.3. Specimen temperature is controlled using an optical pyrometer and automatic feedback controller.

During rig operation the fuel pressure is regulated automatically to maintain the desired temperature. To provide cyclic cooling, the burner is automatically moved away from the specimens for the cool-down portion of the cycle, during which a compressed air blast is applied to the specimens. The test rig is shown in Figure A-1. Testing is interrupted approximately every 20 hours to allow for visual examination of the specimens. Failure is considered to have occurred when spallation occurs over approximately 50 percent of the "test" zone of the bar. The "test" zone includes an area which is approximately 2.5 cm (1 inch) long at the center of the exposed portion of the bar, having a uniform temperature during testing. This failure criterion recognizes that some ceramic loss may occur without severe degradation of the protective nature of the ceramic. It should be noted that once initiated, spallation failure propagates relatively rapidly, so that the stated coating life is not highly sensitive to end point definitions.

In order to further maintenance of reliable test temperatures with good repeatability, one of the twelve 0.5" diameter test bars was replaced with a coated specimen with two internal passages for the routing of thermocouple sensors. One passage was an axial hole 0.170" diameter through the entire length of the specimen. The other hole also penetrated the bar parallel to the axis, but located 50% of the distance between the circumference of the aforementioned 0.170" hole and the outside diameter of the specimen. This passage extended approximately 1.25" down from the tip of the bar and was of 0.040" diameter to accept a 0.032" thermocouple sensors. The specimen geometry is shown in Figure A-2. This specimen is installed in the test cluster with the sensor located in the trailing edge or inside diameter wall of the bar. Thermocouple leads are routed down the specimen drive unit through a slip-ring and finally to a recording device.

By correlating optical pyrometer values with thermocouple readings, optical controller set points are established daily with the thermocouple, thus avoiding drift of test specimen temperature resulting from gradual ceramic emissivity changes.

An alternate specimen was also designed and has seen limited application. Essentially, this specimen is utilized similar to the previously described type, except there is no 0.170" I.D. center hole, and there are three, rather than one, thermocouple holes, each terminating within different longitudinal points in the specimen/cluster hot zone.

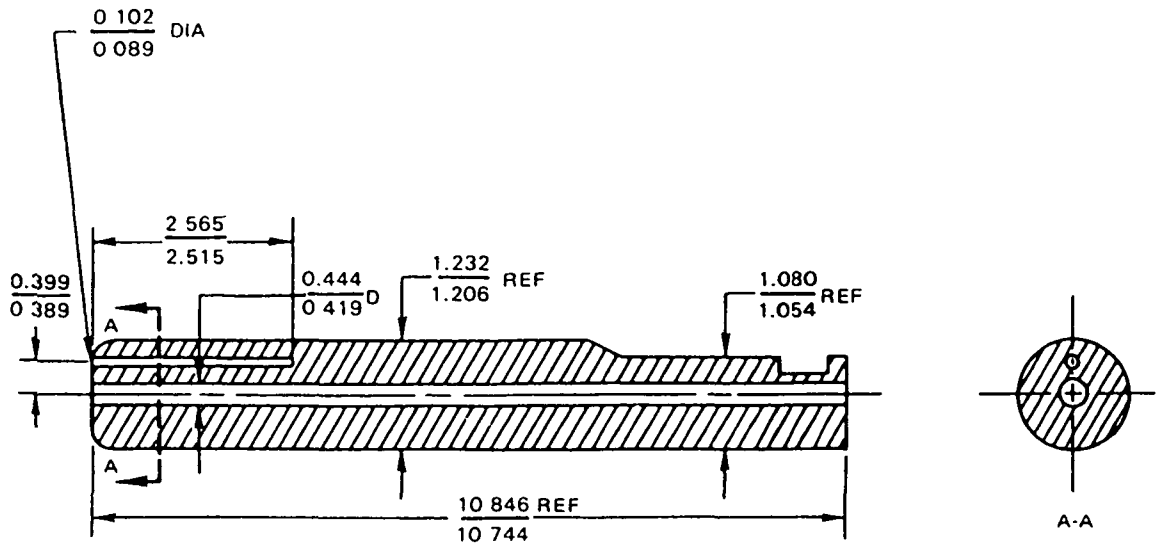


Figure A-1 Diagram of Thermocoupled Specimen Used for Burner Rig Testing. Dimensions are expressed in centimeters.

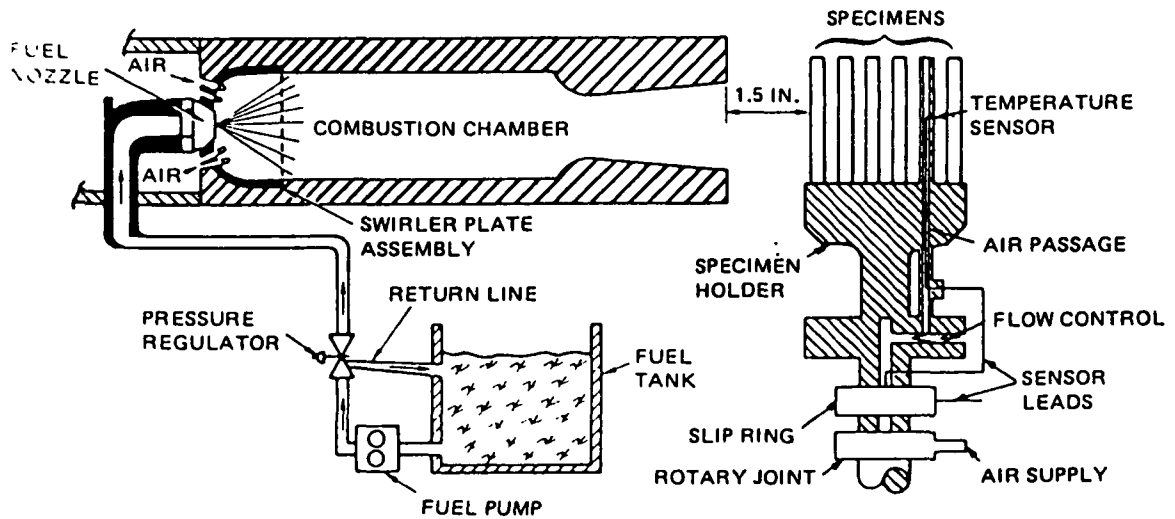


Figure A-2 Schematic Diagram of Cyclic Burner Rig Test Apparatus for Task I

APPENDIX B CORROSION BURNER RIG TEST

A cyclic hot corrosion test was utilized in Task I to aid in defining the capability of the coating system under simulated field service conditions. Specific test conditions were selected to model a mixed oxidation-hot corrosion type of exposure encountered in relatively high temperature aircraft turbine exposure with "clean" fuels and moderate atmospheric contaminants.

Intensive study of hot corrosion phenomena at Pratt & Whitney has shown that the primary contaminants responsible for hot corrosion attack in aircraft turbine engines operating on clean fuels are sea salt from near ground level air (ingested during take-off) and sulfur trioxides from the combustion gases. A comprehensive analysis of hot corrosion mechanisms has shown conclusively that acidification of contaminant salt deposits by sulfur trioxide is critically related to turbine hot corrosion and that meaningful laboratory hot corrosion testing requires that the activity of SO_3 be maintained at levels characteristic of turbine operation. Accordingly, the hot corrosion test rig used in Task I provides for control of both salt contaminant loading and for control of combustion gas composition by effectively limiting excess dilution air.

The test rig used in the hot corrosion exposure evaluation was specifically designed for evaluation of turbine materials in contaminated environmental conditions. The rig is similar to that previously described in Appendix A for oxidation test evaluation in that it maintains full automatic control of test temperature and cooling cycles and features a special rotating specimen mounting fixture with internal specimen cooling air. This fixture provides for simultaneous test of twelve air-cooled specimens. There is also provision for metered injection of contaminants to allow accurate simulation of aircraft turbine environments. Temperature control of the hot corrosion test rig is conducted in the same manner as previously discussed for oxidation test rigs.

The major modification in the hot corrosion test rig is that the cooled specimen cluster is operated inside a burner exhaust gas duct as shown schematically in Figure B-1. This duct exhaust allows specific restriction of ambient air dilution and consequently provides for optimum control of the level of exhaust gas sulfur and air contaminants.

The hot corrosion test conditions used in Task I simulate typical hot corrosion conditions encountered in near ground aircraft engine operation. Selection of the 899°C (1650°F) ceramic surface temperature were based on conditions that exist where major salt loading from atmosphere contamination occurs. The test cycle was the same as that used for cyclic oxidation testing, i.e., 57 minutes in the flame and three minutes for air cooling.

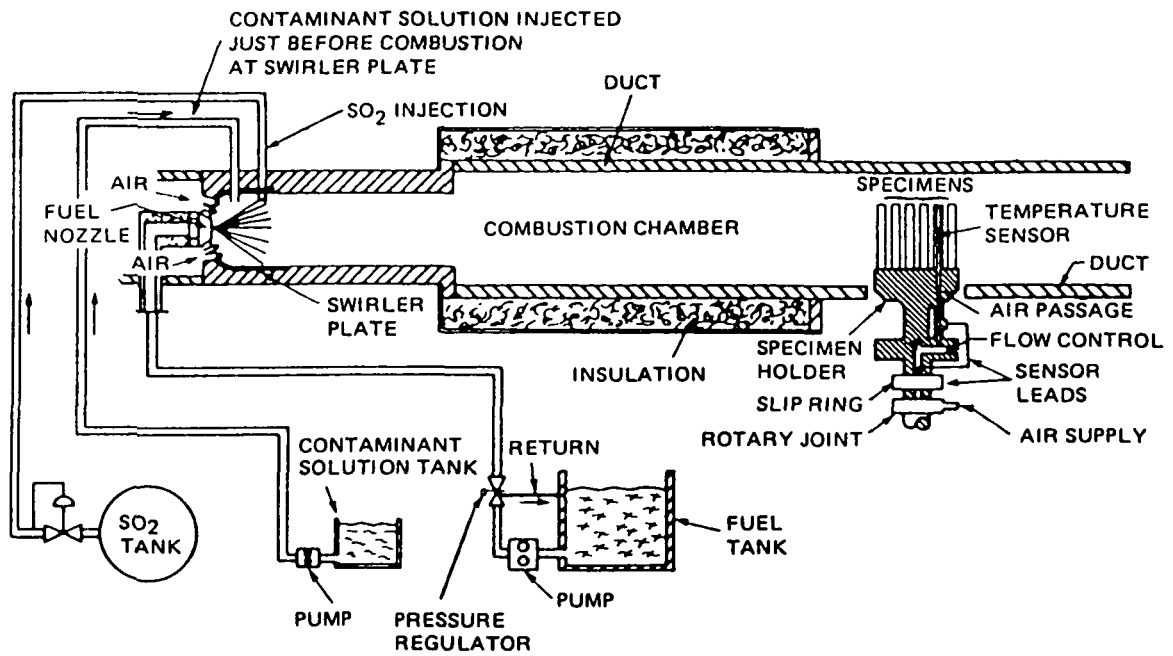


Figure B-1 Schematic Diagram of Ducted Burner Rig Test Apparatus for Task I Hot Corrosion Exposure. Test specimens are enclosed to allow precise control of SO_3 and other contaminants.

REFERENCES

1. Stecura, S., "Effects of Plasma Spray Parameters on Two-Layer Thermal Barrier Coating System Life", NASA TM 81724, 1981.
2. Summer, I. E., "Development of Improved-Durability Plasma Sprayed Ceramic Coatings for Gas Turbine Engine", AIAA/SAE/ASME 16th Joint Propulsion Conference, AIAA-80-1193, 1980.
3. Cassenti, B. N., Brickley, A. M., "Thermal and Stress Analysis of Thermal Barrier Coatings", AIAA-81-1402, 1981.
4. Grot, A. S., Martin, J. K., "Behavior of Plasma Sprayed Ceramic Thermal Barrier Coating for Gas Turbine Engines", American Ceramic Society Bulletin, Vol. 60 No. 8, pp. 807-811, 1981.
5. Anderson, N. P., Sheffler, K. D., "Development of Stain Tolerant Thermal Barrier Coating Systems" Final Report, Tasks I-III, Contract No. NAS3-22548, NASA CR-168251, PWA-5777-29, 1983.
6. Miller, R. A., Levine, S. R., Stecura, S., "Thermal Barrier Coatings for Aircraft Gas Turbines", AIAA 80-0302, 1980.
7. Sheffler, K. D., Graziani, R. A., Sinko, G. C., "JT9D Thermal Barrier Coated Vanes," Final Report, Contract No. NAS3-20630, NASA CR 167964, 1982.
8. Becher, P. F., Rice, R. W., Wu C. Cm., Jones, R. L. "Factors in the Degradation of Ceramic Coating for Turbine Alloys" Thin Solid Films 53, pp. 225-232, 1978.
9. Gladden, H. J., "Thermal Performance of a Ceramic Coated Turbine Vane Under Transient Gas Conditions" SAE preprint N810205, presented Feb. 23-27, 1981.
10. Duvall, D. S., Ruckle, D. L., "Ceramic Thermal Barrier Coatings for Turbine Engine Components" ASME, International Gas Turbine Conference and Exhibit ASME Paper 82-GT-322, 27th, London, England, Apr. 18-22, 1982.
11. Ruckle, D. L., "Plasma-Sprayed Ceramic Thermal Barrier Coatings for Turbine Vane Platforms" Thin Solid Films 73, pp. 455-461, 1980.
12. Stecura, S., "Two-Layer Thermal Barrier Coating for Turbine Airfoils - Furnace and Burner Rig Test Results", NASA TM X-3425, Sept. 1976.
13. Stecura, S., "Two-Layer Thermal Barrier Coating for High Temperature Components" American Ceramic Society Bulletin, Vol. 56, No. 12, pp. 1082-1089, 1977.
14. Levine S. R., Miller, R. A., Hodge, P. E., "Thermal Barrier Coatings for Heat Engine Components" SAMPE Quaterly, pp. 20-26, 1980.

15. Miller, R. A., Lowell C. E., "Failure Mechanisms of Thermal Barrier Coatings Exposed to Elevated Temperatures", Thin Solid Films, 95, pp. 265-273, 1982.
16. Stecura, S., "Effects of Yttrium, Aluminum and Chromium Concentrations in Bond Coatings on the Performance of Zirconia-Yttria Thermal Barriers" Thin Solid Films, 73, pp. 481-489, 1980.
17. Andersson, C. A., Lau, S. K., Bratton, R. J., Lee, S. Y., Rieke, K. L., "Advanced Ceramic Coating Development for Industrial/Utility Gas Turbine Applications", Final Report DOE/NASA 0110-1, NASA CR-165619, 1982.
18. Miller, R. A., "Oxidation - Based Model for Thermal Barrier Coating Life" Ceramic Journal, 1, pp. 83-87, 1984.
19. McDonald, G., Hendricks R. C., "Effects of Thermal Cycling on ZrO_2 - Y_2O_3 Thermal Barrier Coatings" Thin Solid Films, 72, (2), pp. 491-496, 1980.
20. Gedwill, M. A., "Burner Rig Evaluation of Thermal Barrier Coating Systems for Nickel Base Alloys", NASA-TM 81685, Feb. 1981.
21. Andersson, C. A., "Thermal Stress Fracture of Ceramic Coatings", Fracture Mechanics of Ceramics, Vol. 6, Measurements, Transformation, and High Temperature Fracture, N.Y., Plenum Press, pp. 497-509, 1983.
22. Miller, R.A., Berndt, C.C., "Performance of Thermal Barrier Coatings in High Heat Flux Environments," Thin Solid Films, 119, pp. 195-202, 1984.
23. Harding, A. G., Adam, T. "Thermal Stress in Ceramics Applied as Thermal Barrier Layers to Turbine Blades", British Ceramic Society Transactions, Vol. 65, No. 5, pp. 289-307, 1965.
24. Miller, R. A., Smialek, J. L., Garlick, R. G., "Phase Stability in Plasma Sprayed Partially Stability in Plasma Sprayed Partially Stabilized Zirconia-Yttria" Advances in Ceramics, Vol.3, pp. 241-253, 1981.
25. Miller, R. A., Garlick, R. G., Smialek, J. L., "Phase Distributions in Plasma Sprayed Zirconia-Yttria" American Ceramic Society Bulletin, Vol. 62, No. 12, pp. 1355-1358, 1983.
26. Rice, R. W., Pahanke, R. C., McDonough, W. J., "Effect of Stresses from Thermal Expansion Anisotropy, Phase Transformation and Second Phases on the Strength of Ceramics", J. Am. Cer. Soc., 63, No. 11-12, pp. 703-710, 1980.
27. Berndt, C. C., Herman, H., "Anisotropic Thermal Expansion Effects in Plasma Sprayed ZrO_2 -8% Y_2O_3 Coatings", Ceramic Engineering and Science Proceedings, Vol. 4, pp. 792-801, 1983.

28. Stecura, S., "Two-Layer Thermal Barrier Systems for Ni-Al-Mo Alloy and Effects of Alloy Thermal Expansion on System Life", American Ceramic Society Bulletin, Vol. 61, No.2, pp. 256-262, 1982.
29. Bevan, C. E., "Development of Advanced Plasma Sprayed Ceramic Coatings for Industrial Gas Turbine Engines" Final Report, DOE/Batelle Subcontract B-A0747-A-Z, PWA 5906, 1982.
30. Miller, R. A., "Analysis of the Response of a Thermal Barrier Coating to Sodium and Vanadium Doped Combustion Cases", DOE/NASA 2593-79/7, NASA TM-79205, 1979.
31. Hodge, P. E., Stecura, S., Gedwell, M. A., Zaplatynsky, I., Levine, S. R., "Thermal Barrier Coating: Burner Rig Hot Corrosion Test Results", J. Materials for Energy Systems, 1, pp. 47-58, March 1980.
32. Hodge, P. E., Miller, R. A., Gedwill, M. A., "Evaluation of Hot Corrosion Behavior of Thermal Barrier Coatings", Thin Film Solids, 73, pp. 447-453, 1980.
33. Pettit, F. S., Goward, G. W., "High Temperature Corrosion and use of Coatings for Protection", Metallurgical Treatises, Metallurgical Society of AIME, pp. 603-619, 1983.
34. Lau, S. K., Bratton, R. J., "Degradation Mechanisms of Ceramic Thermal Barrier Coatings in Corrosion Environments", High Temperature Protective Coatings Proceedings of the Symposium, Atlanta, Georgia, March 7, 8, 1983 Metallurgical Society of AIME, pp. 305-317, 1984, .
35. Barkalow, R. H., "Hot Corrosion of Ceramic Coating Materials for Industrial/Utility Gas Turbines", DOE No.DE-AC-03-78ET15236, Ref. No. 81-200-7003-FR, Jan. 1981.
36. Hamilton, J. C., Nagelberg, A. S., "In Situ Raman Spectroscopic Study of Yttria-Stabilized Zirconia Attack by Molten Sodium Vanadate", J. Am. Cer. Soc., 67, No. 10, pp. 686-690, Oct. 1984.
37. Shankar, R. N., Berndt, C. C., Herman, H., "Phase Analysis of Plasma Sprayed Zirconia-Yttria Coatings", Ceramic Engineering and Science Proceedings, Vol. 4, pp. 784-787, 1983.

DISTRIBUTION LIST

NASA Scientific and Technical
Information Facility
Attn: Acquisition Branch
P.O. Box 8757
Baltimore Washington Inter. Airport
Baltimore, MD 21240

D. L. Alger (301-2)
NASA Lewis Research Center
21000 Brookpark Road
Cleveland, OH 44135

L. F. Aprigliano
D. Taylor Shipyard
R&D Center
Annapolis, MD 21402

M. M. Bailey (77-6)
NASA Lewis Research Center
21000 Brookpark Road
Cleveland, OH 44135

Michael Bak (5-16)
Williams International
P.O. Box 200
Walled Lake, MI 48088

H. Beale
Applied Coatings, Inc.
775 Kaderly Drive
Columbus, OH 43228

Robert Beck
Teledyne - CAE
1330 Laskey Road
Toledo, OH 43612

Biliyar N. Bhat (EH-23)
NASA Marshall Space
Flight Center
Huntsville, AL 35812

Donald H. Boone
University of California
Bldg. 62, Room 351
Berkeley, CA 94720

David Bott
Muscle Shoals Mineral Company
1202 East 2nd Street
Muscle Shoals, AL 35661

R. J. Bratton
Westinghouse Electric R&D
1310 Buelah Road
Pittsburgh, PA 15235

Sherman D. Brown
Chemical Engineering Dept.
University of Illinois
Urbana, IL 61801

Walter Bryzik (RGRD)
U.S. Army Tank-Auto. Command
Diesel Engine Research RMSTA
Warren, MI 48397

R. F. Bunshah
University of California
6532 Boelter Hall
Los Angeles, CA 90024

George C. Chang (MC 219)
Cleveland State University
Cleveland, OH 44115

Jerry Clifford
U.S. Army Applied Tech. Lab.
SAVDL-ATL-ATP
Fort Eustis, VA 23604

DISTRIBUTION LIST (cont'd)

Dave Clingman
Detroit Diesel Allison - GMC
Engineering Operations
Indianapolis, IN 46206

J. W. Glatz
NAPTC R&D Division
Naval Air Prop. Test Center
Trenton, NJ 08628

Arthur Cohn
E P R I
3412 Hillview Avenue
Palo Alto, CA 94303

G. W. Goward
Coatings Technology Corp.
2 Commercial Street
Branford, CT 06405

Thomas A. Cruse
Southwest Research Institute
P.O. Box 28510
San Antonio, TX 78284

M. A. Greenfield (RM)
NASA Headquarters
600 Independence Avenue
Washington, DC 20546

Keith Duframe
Battelle Labs.
Columbus, OH 43216

S. J. Grisaffe (49-1)
NASA Lewis Research Center
21000 Brookpark Road
Cleveland, OH 44135

Mrityunjoy Dutta
U.S. Army AMSAV-EAS
4300 Goodfellow Blvd.
St. Louis, MO 63120

D. K. Gupta
Pratt & Whitney Group
400 Main Street
East Hartford, CT 06108

D. S. Engleby
Naval Air Rework Facility
Mail Drop 9, Code 017
Cherry Point, NC 28533

William K. Halman
Temescal
2850 Seventh Street
Berkeley, CA 94710

John Fairbanks (FE-22)
Department of Energy
Office of Fossil Energy
Washington, DC 20545

D. Hanink
Detroit Diesel Allison-GMC
Engineering Operations
Indianapolis, IN 46206

N. Geyer
AFWAL/MLLM
Wright Patterson AFB
Dayton, OH 45433

Doug Harris
APS - Materials Inc.
153 Walbrook
Dayton, OH 45405

DISTRIBUTION LIST (cont'd)

Harold Herman
Argonne National Lab.
9700 South Cass Avenue
Argonne, IL 60439

Larry A. Junod
Allison Gas Turbine Division
P.O. Box 420, Plant 8-T12
Indianapolis, IN 46206

H. Herman (W-8)
Detroit Diesel Allison-GMC
P.O. Box 894
Indianapolis, IN 46206

C. Kortovich
TRW Inc.
23355 Euclid Avenue
Cleveland, OH 44117

M. Herman
Dept. of Materials Science
State Univ. of New York
Stonybrook, NY 11794

Propulsion Laboratory (302-2)
U.S. Army Res. & Tech. Lab.
21000 Brookpark Road
Cleveland, OH 44135

Frank Hermanek
Alloy Metals, Inc.
501 Executive Drive
Troy, MI 48084

Sylvester Lee
AFWAL-MLTM
Wright Patterson AFB
Dayton, OH 45433

R. Hillery (M-85)
General Electric Company
MPTL
Cincinnati, OH 45215

A. V. Levy
Lawrence Berkely Lab.
University of California
Berkely, CA 94720

J. Stan Hilton
University of Dayton
300 College Park
Dayton, OH 45469

C. H. Liebert (77-2)
NASA Lewis Research Center
21000 Brookpark Road
Cleveland, OH 44135

Richard R. Holmes (EH-43)
Marshall Space
Flight Center
Huntsville, AL 35812

E. L. Long, Jr.
Oak Ridge National Lab.
P.O. Box X, Bldg. 4508
Oak Ridge, TN 37831

Lulu Hsu
Solar Turbines, Inc.
2200 Pacific Highway
San Diego, CA 92138

Frank N. Longo
Metco, Inc.
1101 Prospect Avenue
Westbury, L.I., NY 11590

DISTRIBUTION LIST (cont'd)

Richard Martin (9W-61)
Boeing Commercial Airplane Co.
P.O. Box 3707
Seattle, WA 98124

Gopal Revanton
Deer & Company
3300 River Drive
Moline, IN 61265

R. A. Miller (105-1)
NASA Lewis Research Center
21000 Brookpark Road
Cleveland, OH 44135

David Rigney (D-83)
General Electric Company
Cincinnati, OH 45215

T. E. Mitchell
Case Western Reserve Univ.
10900 Euclid Avenue
Cleveland, OH 44106

Joseph Scricca
AVCO-Lycoming Division
550 South Main Street
Stratford, CT 06497

S. Naik
AVCO-Lycoming Division
550 South Main Street
Stratford, CT 06497

Keith Sheffler
Pratt & Whitney Group
400 Main Street
East Hartford, CT 06108

Dr. J. A. Nesbitt (105-1)
NASA Lewis Research Center
21000 Brookpark Road
Cleveland, OH 44135

T. P. Shyu
Caterpillar Tractor Company
100 N.E. Adams
Peoria, IL 61629

J. W. Patten
Cummins Engine Company
Box 3005
Columbus, IN 47202

R. W. Soderquist (165-03)
Pratt & Whitney Group
400 Main Street
East Hartford, CT 06108

Ronne D. Proch
Corning Glass Works
31501 Solon Road
Solon, OH 44139

D. E. Sokolowski (49-7)
NASA Lewis Research Center
21000 Brookpark Road
Cleveland, OH 44135

R. J. Quentmeyer (500-220)
NASA Lewis Research Center
21000 Brookpark Road
Cleveland, OH 44135

C. A. Stearns (106-1)
NASA Lewis Research Center
21000 Brookpark Road
Cleveland, OH 44135

DISTRIBUTION LIST (cont'd)

S. Stecura (105-1)
NASA Lewis Research Center
21000 Brookpark Road
Cleveland, OH 44135

F. C. Toriz
Rolls Royce, Inc.
1985 Phoenix Blvd.
Atlanta, GA 30349

T. E. Strangman
Garrett Turbine Engine Co.
111 South 24th Street
Phoenix, AZ 85034

Donald Whicker
GM Research Laboratory
GM Technical Center
Warren, MI 48090

T. N. Strom (23-2)
NASA Lewis Research Center
21000 Brookpark Road
Cleveland, OH 44135

Volker Wilms
Chromalloy R&T
Chromalloy Amer. Corp.
Orangeburg, NY 10962

T. A. Taylor
Linde Division
Union Carbide Corporation
Indianapolis, IN 46224

I. Zaplatynsky (105-1)
NASA Lewis Research Center
21000 Brookpark Road
Cleveland, OH 44135

Robert P. Tolokan
Brunswick Corporation
2000 Brunswick Lane
DeLand, FL 32724